SIMULATION OF SINGLE AND MANY PARTICLE GAUGE THEORIES WITH ULTRACOLD ATOMIC GASES

Matthew James Edmonds

Submitted for the Degree of Doctor of Philosophy

Heriot-Watt University
Institute of Photonics and Quantum Sciences
Quantum Optics and Cold Atoms Group
Edinburgh, November 2013.

Abstract

The study of systems formed from ultracold atomic gases has emerged to become one of the most active research fields within the condensed matter landscape. These highly controllable macroscopic systems amalgamate ideas from many sub disciplines of physics, including the study of low temperatures, quantum optics and quantum information theory as well as the seemingly disparate field of high energy physics. The central concept of this thesis is gauge theories as applied to systems of bosonic atoms, which at temperatures close to absolute zero form Bose-Einstein condensates. To simulate the mathematical structure of a gauge theory, the geometric (Berry) phase formalism is adopted. This is in turn accomplished by considering the adiabatic following of the eigenstates of the light-matter coupling for an ensemble of atoms forming a Bose-Einstein condensate. These concepts are then applied to show how one can generate a spin-orbit coupling in a one-dimensional condensate, which additionally features a random mass term that allows us to study the physics of Anderson localization in an intriguing "quasi" relativistic regime. One of the features of light induced gauge potentials is that they are static; in the sense that there is no feedback between the light-matter interaction and the matter field. In the second part of this thesis it is demonstrated how such a feedback mechanism can be induced by the appropriate modification of the light-matter interaction. The consequences this has for the condensate are then described at the mean-field level, including the expected experimental signatures of the resulting 'interacting' gauge theory, in terms of the expansion of the condensate and also the structure of the solitons of this nonlinear system. Finally, this nonlinear model is applied to a double well system, from which the associated Bose-Hubbard model is derived and analysed; and the nonlinear Josephson problem studied.

Acknowledgements

There are many people to whom I wish to extend my gratitude towards for the guidance, friendship and support they have shown me during the course of my doctoral studies. The most important person is my supervisor, Patrik, whose guidance, expertise and encouragement throughout the course of my PhD has been first class. The groups PostDoc, Manuel has also been key in guiding my understanding of difficult concepts and ideas. I would also like to thank the other students in our group both past and present, Michael, Chaitanya, Daniel, Zhi Hao, Fritz, Lawrence and Yvan have all made the course of my studies a more enjoyable and beneficial experience.

My friends in the University have also been an important part of my PhD, in particular I wish to thank Peter, Will, Jean-Cristophe, Natalia, Nadezhda, Ashleigh, Sebastian, Adam, Robert, Wolf, Jack and Vishal for providing distraction and a pleasant atmosphere to work in.

I wish to also thank my family both in Scotland and Sussex for their support during my studies, especially my parents for their love and encouragement over the extended course of my education. In Sussex, I also wish to thank Jeremy and Chris, who have also followed my academic progress with great interest. In Scotland, my gratitude lies with my Aunt and Uncle, Katherine and John MacMillan, to whose hospitality over the many years of my studies I am indebted.

I would like to recognise the support I have received from the Scottish Doctoral Training Centre in Condensed Matter Physics, which has given me the opportunity to attend scientific meetings all over the world. As well as this, I would like to thank Prof. Andy MacKenzie and Dr Chris Hooley for all of their hard work. Last, but certainly not least, two very important people must be thanked, Dr Simon Gardiner and Dr Sabrina Maniscalco for examining this thesis.

Contents

List of publications

This thesis is based on the following three publications

- M. J. Edmonds, J. Otterbach, R. G. Unanyan, M. Fleischhauer, M. Titov and P. Öhberg "From Anderson to anomalous localization in cold atomic gases with effective spin-orbit coupling" *New. J. Phys.* **14**, 073056 (2012).

  Abstract: We Study the dynamics of a spin-orbit (SO)-coupled Schrödinger particle with two internal degrees of freedom moving in a one-dimensional random potential. Numerical calculation of the density of states reveals the emergence of a Dyson-like singularity at zero energy when the system approaches the quasi-relativistic limit of the random-mass Dirac model for large SO coupling. Simulation of the expansion of an initially localized wave packet shows a crossover from an exponential (Anderson) localization to an anomalous power-law behaviour reminiscent of the zero-energy (mid-gap) state of the random-mass Dirac model.

- M. J. Edmonds, M. Valiente, G. Juzeliūnas, L. Santos and P. Öhberg "Simulating an interacting gauge theory with ultracold Bose gases" *Phys. Rev. Lett.* **110**, 085301 (2013).

  Abstract: We show how density dependent gauge potentials can be induced in dilute gases of ultracold atoms using light-matter interactions. We study the effect of the resulting interacting gauge theory and show how it gives rise to novel topological states in the ultracold gas. We find in particular that the onset of persistent currents in a ring geometry is governed by a critical number of particles. The density-dependent gauge potential is also found to support chiral solitons in a quasi-one-dimensional ultracold Bose gas.

- M. J. Edmonds, M. Valiente and P. Öhberg "On the Josephson effect in a Bose-Einstein condensate subject to a density dependent gauge potential" *J. Phys. B: At. Mol. Opt. Phys.* **46**, 134013 (2013).

  Abstract: We investigate the coherent dynamics of a Bose-Einstein condensate in a double well, subject to a density-dependent gauge potential. Further, we derive the nonlinear Josephson equations that allow us to understand the many-body system in terms of a classical Hamiltonian that describes the motion of a nonrigid pendulum with an initial angular offset. Finally we analyse the phase-space trajectories of the system, and describe how the self-trapping is affected by the presence of an interacting gauge potential.

Chapter 1

Quantum simulation

The ability to manipulate individual quantum particles has caused a landslide of fascinating discoveries that have substantially increased our understanding of both the microscopic and macroscopic world. Of principal interest are condensed matter systems where it is now possible to realise Feynman's vision of quantum simulation: the emulation of one system of interest with another [1]. Atomic condensates formed of bosons and fermions have been utilised to study a plethora of ideas due to the experimental and theoretical control they afford. One prominent example that has been the subject of intense study over the last few years is the ability to create artificial gauge potentials in ensembles of ultracold matter [2–4]. The ability to study gauge theories in this context has heralded new directions in the ultracold-atoms landscape such as spin-orbit coupling [5], Hall physics [6, 7] and even relativistic effects [8, 9]. The experimental control achievable over these systems means that one has the ability to study single and many-body physics with a sophisticated level of control.

There are many reasons why the simulation of gauge theories with systems comprised of ultracold atoms is interesting to purseue. Primarily, the experimental study of condensates has reached maturity; as such the control possible over these many-particle systems is formidable, in particular one can control both the sign and magnitude of the inter-particle interactions. Further, these systems are naturally very clean, so one can investigate many different external effects.

One can naturally divide ultracold atom systems into lattice and continuum schemes. Optical lattices formed from standing waves of laser light have become an extremely

useful tool for investigating the transport, binding and scattering properties of systems of few to many particles [10]. Early work in this field showed how a quantum phase transition can occur from a Mott insulating phase to a superfluid phase for bosons trapped in an optical lattice [11], and has opened the path toawrds studying effects such as magnetic frustration [12], and even strongly correlated physics such as the Kondo effect.

On the other hand, one can study continuum effects with ultracold atoms. Very recently the field of quantum information has emerged, which brings the classical theory of information into the quantum domain [13]. As such, cold atoms can be used to answer fundamental questions about how we will communicate quantum information in the future, as for instance the Qubit - which is the fundamental unit of quantum information is represented by a superposition of two quantum states. Cold atom systems naturally allow one to mimic a Qubit and perform operations on it. It is also possible to simulate the physics of gravitationally massive objects such as black holes with cold atom based systems [14], here the analogy is drawn by considering how quasiparticles in positive and negative energy states annihilate in a similar way to how real black holes have been predicted to behave.

The main focus throughout this thesis will be understanding how one can generate gauge potentials using the dressed states of different configurations of shaped laser light interacting with multi-level ultracold atoms. In particular, the Born-Oppenheimer (BO) approximation will play a central role. By studying gauge theories with cold atoms, an immediate link can be drawn with the fundamental forces of particle physics [15], although the primary focus in this thesis is not directly the simulation of such theories, some time will be spent discussing some of the building blocks of particle physics, such as the Dirac equation [16]. The notion of quantum simulation has found wide spread application with systems comprised of ultracold atoms, and it is expected that these systems will continue to provide fundamental insight into new and existing theories across a broad range of subjects within the condensed matter landscape.

Chapter 2

Cold Atoms

2.1 Spin and statistics

Statistics plays a fundamental role in the everyday world, from the tossing of a coin to decide how a sporting event begins, to the pricing of stocks and shares on the stock market, our world is shaped by statistical events, which in turn affect the course of our lives in both subtle and considerable ways. In this thesis, the concept of statistics as applied to systems of quantum particles called bosons plays a central role. A discussion of the statistics of many particle quantum systems begins naturally with the notion of spin. The spin of a quantum particle has no classical analogue, and plays a fundamental role in determining the physical characteristics of few and many particle systems. Particles can be grouped into either bosons or fermions, having integral and half-integral spin respectively.

The consequence of the indistinguishability of quantum particles is that we cannot place labels on two identical particles. Hence, if we exchange them one expects to measure the same physical quantities. In quantum mechanics measurement entails explicit knowledge of the wave function of the system. By denoting two identical particles with co-ordinates $\mathbf{r}_i$ and spin projection σ_i, this condition can be expressed for two particles as [17]

$$\Psi(\mathbf{r}_1\sigma_1, \mathbf{r}_2\sigma_2) = \pm\Psi(\mathbf{r}_2\sigma_2, \mathbf{r}_1\sigma_1). \tag{2.1.1}$$

Equation (2.1.1) demonstrates how the interchange of two identical particles has introduced a sign into the many-body wave function, this sign depends on the spin

of the particles. The + sign applies for all particles of integral spin, bosons, while the − sign indicates particles of half-odd-integral spins, fermions. In this thesis, we are primarily interested in bosons. Although there are many examples of elementary particles which are bosons, for condensed matter systems such particles are composites, but still obey the same fundamental rule, equation (2.1.1).

Consider an ensemble of non-interacting bosons (fermions) in thermodynamic equilibrium at temperature T and with chemical potential μ, then the average occupation function can be shown to be given by

$$f_{\pm}(E) = \frac{1}{\exp(E-\mu)/kT \pm 1}, \tag{2.1.2}$$

where the − and + in equation (2.1.2) are for bosons and fermions respectively. The sign difference in the denominator shows that these two classes of particles will display quite different behaviour at low temperatures. On the one hand, no two spin one-half particles can have the same set of quantum numbers. Consequenly one can only place one spin-up and one spin-down fermion into the same momentum state. Bosons however behave quite differently, and according to equation (2.1.2) there is no limit on the number of these particles that can be placed into the same state. Now, if the total number of particles is N, and there are fewer than this number of particles in excited states, then these other particles must occupy the single particle ground state, and the system is said to exhibit Bose-Einstein condensation (BEC) [18, 19]. The Bose condensation temperature, T_c is defined as the highest temperature at which the condensate exists. As such, Bose-Einstein condensation is an example of a phase transition that directly depends on the statistics of the particles.

2.2 Criterion for BEC

In the previous section, the concept of Bose-Einstein condensation was introduced for non-interacting particles. This is defined as the macroscopic occupation of the single particle ground state of the system. Insight into when the transition occurs can be obtained from comparing the thermal de Broglie wavelength with the mean inter particle separation. For particles of mass m at temperature T the thermal de Broglie wavelength λ_{T} is given by

$$\lambda_{\mathrm{T}} = \left(\frac{2\pi\hbar^2}{mk_BT}\right)^{1/2}. \tag{2.2.1}$$

When the inter particle spacing given by $n^{-1/3}$ is comparable to λ_{T}, the quantum nature of the particles is manifest. A further quantity can be defined from equation

2.2.1 to characterise the transition to the condensed state, namely the phase-space density. The dimensionless phase-space density n_{PS} is defined as the number of particles whose volume is given by the cube of the de Broglie wavelength, equation (2.2.1), hence

$$n_{\mathrm{PS}} = n\left(\frac{2\pi\hbar^2}{mk_BT}\right)^{3/2}. \tag{2.2.2}$$

Typically one finds that the phase-space density needs to be of order one to achieve condensation. This indicates the necessity of low temperatures combined with large particle densities that are the requirement for BEC. A more detailed treatment must include interactions between particles. At the single particle level a comprehensive description of a non-interacting quantum system is achieved with the density matrix, which can be defined in terms of the creation and annihilation operators $\hat{\psi}^\dagger$ and $\hat{\psi}$ by

$$\rho(\mathbf{r}, \mathbf{r'}) = \langle\hat{\psi}^\dagger(\mathbf{r'})\hat{\psi}(\mathbf{r})\rangle, \tag{2.2.3}$$

where $\langle\cdots\rangle$ represents the quantum mechanical average if the particle is in a pure state, and equation (2.2.3) is interpreted as the amplitude associated with removing a particle at $\mathbf{r}$ and creating a particle at $\mathbf{r'}$. The condition for BEC can then be defined as equation (2.2.3) having an eigenvalue that is of order N, where N is the number of particles. The diagonal terms of the density matrix $\rho(\mathbf{r}, \mathbf{r})$ define the particle density at $\mathbf{r}$. To proceed, we define the momentum distribution in terms of the operator $\hat{\psi}(\mathbf{r})$ as

$$\hat{a}_{\mathbf{p}} = \frac{1}{\sqrt{V}}\int d\mathbf{r}e^{-i\mathbf{p}\cdot\mathbf{r}/\hbar}\hat{\psi}(\mathbf{r}), \tag{2.2.4}$$

and by substituting equation (2.2.4) into equation (2.2.3), one obtains the expression

$$\rho(\mathbf{r}, \mathbf{r'}) = \frac{1}{V}\sum_{\mathbf{p}} N_{\mathbf{p}}e^{i\mathbf{p}\cdot(\mathbf{r}-\mathbf{r'})/\hbar}. \tag{2.2.5}$$

To write equation (2.2.5) the relation $\langle\hat{a}^\dagger_{\mathbf{p}}\hat{a}_{\mathbf{p'}}\rangle = \delta_{\mathbf{p},\mathbf{p'}}N_{\mathbf{p}}$ has been used. We wish to understand under what conditions the density matrix (equation (2.2.5)) obtains a macroscopic eigenvalue. Now, for large $|\mathbf{r} - \mathbf{r'}|$, the only term that contributes will be the $\mathbf{p} = 0$ one, as all $\mathbf{p} \neq 0$ will average to zero due to the interference between different momentum states. Hence one finds

$$\lim_{|\mathbf{r}-\mathbf{r'}|\to\infty}\rho(\mathbf{r}, \mathbf{r'}) = \frac{N_{\mathbf{p}=0}}{V}. \tag{2.2.6}$$

We are able to write equation (2.2.6) because for a non-interacting system the number operator for the zero momentum state commutes with the underlying single particle Hamiltonian. However, to generalise to an interacting system, the eigenstates will generally speaking not be eigenstates for the number of zero momentum

particles, so instead one defines

$$\lim_{|\mathbf{r}-\mathbf{r}'|\to\infty} \rho(\mathbf{r},\mathbf{r}') = \frac{\langle \hat{N}_{\mathbf{p}=\mathbf{0}} \rangle}{V}. \tag{2.2.7}$$

The quantity $\langle \hat{N}_{\mathbf{p}=\mathbf{0}} \rangle$ denotes the average number of particles in the zero momentum state for the interacting system. If we consider a finite system, then taking the limit $|\mathbf{r}-\mathbf{r}'| \to \infty$ makes little sense. Instead, one expands the density matrix in terms of the single particle eigenfunctions $\chi_j(\mathbf{r})$ which satisfy the equation $\int d\mathbf{r}' \rho(\mathbf{r},\mathbf{r}')\chi_j(\mathbf{r}') = \lambda_j \chi_j(\mathbf{r})$. Again, for the interacting system the condition for BEC is that one of the λ_j becomes of order N, while the others remain finite in the thermodynamic limit [20].

2.3 Experiments and applications

In the previous two sections a purely theoretical description was given of the phenomena of Bose-Einstein condensation. It was realised early on that Bose-Einstein condensation explains the low temperature behaviour of He [21] and many of the theoretical tools used to study atomic condensates were originally introduced to treat the Helium liquids [22]. The idea of Bose-Einstein condensation was also important in the development of the microscopic theory of superconductivity. Here, pairs of highly delocalized electrons forming a Cooper pair undergo the BCS phase transition which involves simultaneous pairing and condensation of Cooper pairs [23]. The quest to achieve condensation with a gas of atoms would however take longer to achieve, as the techniques required for the experimental preparation of these systems did not exist for many years. Unlike the Helium liquids, most atoms remain in the solid phase down to absolute zero, thus one needs clever techniques to keep the atoms in the gas form in order to produce BEC.

The quest for atomic condensates principally required two main ingredients:

i The ability to trap the atoms in a region of space for a length of time,

ii A method for cooling the atoms into the ground state.

The breakthrough came in the 1970s with the development of laser cooling, which made it possible to optically cool atoms below cryogenic temperatures [24,25]. Spin-polarized hydrogen was proposed as an early candidate for atomic condensation, as its low mass meant that it would have a higher condensation temperature than other atoms, further the attraction between two hydrogen atoms with their spins aligned was estimated to be very weak [26].

The first generation of experiments were performed on vapours formed from trapped atoms of rubidium [27], sodium [28] and lithium [29]. Since then a range of other atomic species have been condensed, as well as bosonic molecules of Li_2 [30]. This achievement in particular highlights the utility of the Feshbach resonance, where an external magnetic field can be used to alter the scattering properties of the atoms. Crucually for these experiments, the use of this technique [31] meant that two-particle bound states (dimers) could be produced. Finally, solid state systems have also been used to study BEC. Here, bosonic quasiparticles called polaritons are formed from the coupling of light and matter, and are condensed to form a BEC [32].

2.4 Trapping and cooling of atoms

In this section a schematic description will be given of the process by which a Bose-Einstein condensate of a gas of atoms can be produced, including the important cooling mechanisms that are used to bring the atoms into the ground state.

A simplified picture can be used to describe the process required to reach quantum degeneracy, which principally involves four steps,

1. The atoms enter the gas phase by heating in an 'oven'.
2. The atoms are slowed to a thermal velocity of $\approx 1K$ using a Zeeman slower.
3. The atoms are trapped in a Magneto-optical trap where they are further cooled.
4. Finally the atoms are evaporatively cooled to produce a BEC.

When the atoms enter the gas phase they are at temperature $\approx 600K$. The Zeeman slower consists of a laser directed oppositely to and resonant with the atoms as they leave the oven. However, due to the doppler effect the atomic transition frequencies are shifted. This can be accounted for by applying an inhomogeneous magnetic field that cancels this effect.

After the atoms have left the Zeeman slower, they can be captured by a magneto-optical trap (MOT) where they are further cooled to a temperature $\approx 100\mu K$. To reach the ground state, evaporative cooling is used. Here, the trapping potential is lowered so that the most energetic atoms can escape, thereby lowering the average energy of the atoms remaining in the trap. Thus, the remaining atoms enter the lowest energy state to form a Bose-Einstein condensate.

2.5 Many-body aspects

For a number of reasons, the study of systems of interacting ultracold quantum particles is a burgeoning area of interest. Many particle systems of bosons and/or fermions can now be manipulated with a sophisticated level of experimental dexterity. Moreover, from a theoretical perspective such systems represent a highly attractive tool to study a plethora of fundamental ideas; indeed the coherent nature of the ground state allows one to draw an immediate analogy with the classical theory of electromagnetism of Maxwell. If we consider a system of N bosons interacting via an effective potential $V(\mathbf{r}_i - \mathbf{r}_j)$ that depends on the difference of the i^{th} and j^{th} particles coordinates, then one can write the Hamiltonian for such a system as

$$\hat{H} = \int d\mathbf{r} \left\{ \frac{\hbar^2}{2m} \nabla\hat{\Psi}^\dagger(\mathbf{r}) \cdot \nabla\hat{\Psi}(\mathbf{r}) + \frac{1}{2} \int d\mathbf{r}' \hat{\Psi}^\dagger(\mathbf{r}) \hat{\Psi}^\dagger(\mathbf{r}') V_{\text{int}}(\mathbf{r}' - \mathbf{r}) \hat{\Psi}(\mathbf{r}) \hat{\Psi}(\mathbf{r}') \right\}, \quad (2.5.1)$$

where the bosonic field operators $\hat{\Psi}^\dagger(\mathbf{r})$ and $\hat{\Psi}(\mathbf{r})$ create and destroy particles at position $\mathbf{r}$ respectively. The equation of motion for $\hat{\Psi}(\mathbf{r}, t)$ is obtained from the corresponding Heisenberg picture, the celebrated Gross-Pitaevskii equation [33, 34]

$$i\hbar \frac{\partial}{\partial t} \hat{\Psi}(\mathbf{r}, t) = \left\{ -\frac{\hbar^2}{2m} \nabla^2 + \int d\mathbf{r}' \hat{\Psi}^\dagger(\mathbf{r}', t) V_{\text{int}}(\mathbf{r}' - \mathbf{r}) \hat{\Psi}(\mathbf{r}', t) \right\} \hat{\Psi}(\mathbf{r}, t). \quad (2.5.2)$$

Equation (2.5.2), the Gross-Pitaevskii equation, allows us to study the many particle interacting condensed state at $T = 0$ in terms of an effective single particle equation of motion. The Gross-Pitaevskii equation is written assuming quantum and thermal fluctuations can be ignored. The field operator $\hat{\Psi}(\mathbf{r}, t)$ can be written as $\hat{\Psi}(\mathbf{r}, t) = \langle \hat{\Psi}(\mathbf{r}, t) \rangle + \hat{\delta}(\mathbf{r}, t)$, where $\hat{\delta}(\mathbf{r}, t)$ is the operator that describes fluctuations. For a system of identical atomic bosons, two-body collisions will give the dominant contribution to the scattering of particles. This is explained by considering the typical densities of experimental systems, which lie in the range 10^{12}-10^{15}cm^{-3}, consequentially the average spacing between particles $n^{-1/3}$ will be 0.1-1μm [10]. On the other hand, the scattering length for these atoms are of the order of nanometers, thus interaction effects are small. The table below provides a summary of the

Atom	**Scattering length** a_t, [a.u.]	$\boldsymbol{C_6}$
H	1.2	6.5
^{23}Na	85	1556
^{87}Rb	106	4691
^{7}Li	-27	1389

Figure 2.1: Table contrasting the scattering length a_t with the dimensionless van der Waals constant C_6 for different atoms. The scattering lengths are for scattering between atoms of the same type. The data is taken from [35]

scattering lengths and van der Waals constants for several atomic species. One can calculate an order of magnitude value of the scattering length a by equating the kinetic energy and the van der Waals energy of an atom, which results in the relation $a \approx (C_6 m/m_e)^{1/4} r_0$, where m is the atomic mass and r_0 the atomic radius. The electron mass m_e enters this expression through the definition of atomic radius. The two-body contact interaction appearing in equation (2.5.2) (in three dimensions) can be written as

$$V_{\text{int}}(\mathbf{r}' - \mathbf{r}) = \frac{4\pi\hbar^2 a}{m}\delta(\mathbf{r}' - \mathbf{r}). \tag{2.5.3}$$

Equation (2.5.3) contains the atomic mass m for a particular atomic species as well as the delta function that describes the hard sphere scattering between the atoms.

2.6 Superfluidity

One of the most remarkable features of the condensed phase is the possibility for dissipation-less flow, which for charge neutral systems is referred to as superfluidity, the analogous effect in charged systems being superconductivity. From a phenomenological perspective, the properties of a superfluid system can be understood by two quantities, namely the density $\rho(\mathbf{r}) = |\Psi(\mathbf{r})|^2$ and the phase, $\theta(\mathbf{r})$. The gradient of the phase defines the velocity of condensate, with $\vec{\mathbf{v}} = \frac{\hbar}{m}\nabla\theta(\mathbf{r})$ [36]. The fact that the velocity field of the condensate is the gradient of a scalar means in turn that $\nabla \times \vec{\mathbf{v}} = \vec{0}$. The velocity field $\vec{\mathbf{v}}$ is irrotational, which places restrictions on the allowed motion of the condensate. As the wave function of the condensate has to be a single-valued function, it follows that a change in the phase must be an integer multiple of 2π. Hence we can write

$$\Delta\theta = \oint \nabla\theta \cdot d\mathbf{l} = 2\pi l, \tag{2.6.1}$$

where l is an integer. The connection between Bose-Einstein condensation and superfluidity originated with the study of Helium [21]. However, it is not generally the case that the existence alone of the condensed state means that one has a superfluid carrying currents without dissipation. In fact, the ideal Bose gas is not a superfluid. To understand these effects, one treats the system as being comprised from two interpenetrating components. The first of these is the superfluid component, which is identified with the condensate, whilst the second is the normal component, which refers to the excitations.

Under rotation vortices can enter the condensate. Only the normal component will be brought into rotation, and at low angular velocities the superfluid component remains instead at rest. To understand this behaviour, consider the energy

in the rotating frame $E_r = E - \mathbf{\Omega} \cdot \mathbf{L}$, where Ω is the angular velocity and L the angular momentum. As Ω is gradually increased, a point will be reached where it will become thermodynamically favourable for the condensate to enter a rotating state such that $L \neq 0$. The prediction of vortices was made by Onsager [37] and independently by Feynman [38].

The superfluid state can only exist in these systems in the presence of interactions. This can be understood by considering the Landau criterion for the superfluid state. This states that below a minimum velocity v_c, it is impossible to create excitations within the fluid, hence the motion of the fluid cannot be degraded. For the ideal Bose gas, this velocity is identically zero, hence there is no superfluid state. On the other hand, calculation of the excitation spectrum for the interacting fluid with a uniform density gives $\epsilon_k = \sqrt{(\epsilon_k^0)^2 + 2ng\epsilon_k^0}$, which is gapped at $k = 0$. Hence, there is a non-zero critical velocity v_c.

2.7 Summary

In this chapter the concept of Bose-Einstein condensation was introduced. It was described how a system of interacting bosons can undergo a transition to a state where a single particle state becomes macroscopically occupied. The criterion for this was given in terms of the density matrix. It was then explained how laser cooling and trapping can be employed in order to obtain a Bose-Einstein condensate for a gas of atoms. Finally, one of the most prominent effects associated with the condensate, namely superfluidity was described.

It is the purpose of this thesis to describe how atomic Bose-Einstein condensates can be used to simulate gauge theories. As such, chapter three gives the background to this field and introduces the mathematics required to construct these theories. Following on from this, chapter four is concerned with the simulation of pseudo-spin, in particular the role that disorder plays for such a condensate. The two chapters after this detail how one can create an 'interacting' gauge theory, and what consequences this has for a one-dimensional many-body system of bosons. The final chapter gives a Summary and Outlook for the thesis.

Chapter 3

Simulating Gauge Theories

3.1 Introduction

In order to create artificial vector potentials, one can for instance stir the condensate with a laser, a technique which has been used to realise the vortex lattice of a condensate [39]. This has its limitation in that we can only create a constant magnetic field in the rotating frame. Alternately; one can use optical couplings that lead to dark state dynamics [40] or Raman transitions [41, 42]. Further, one also has the option to study gauge potentials on a lattice. To induce gauge potentials in the discrete setting, laser assisted tunnelling can be used in order to prepare the required phases for the tunnelling amplitudes between individual sites that constitute the lattice [43, 44]. This has led to the experimental realisation of an effective magnetic field in a lattice [45], where Raman-induced tunneling between lattice sites gives rise to an induced Aharonov-Bohm phase.

Creating gauge potentials in the continuum requires shaped laser light interacting coherently with an ensemble of multi level atoms. This methodology has been studied extensively, with early work focussed on the study of slow light [46,47] which results from the interference of two lasers coupling to a common excited state in the electromagnetically induced transparency (EIT) configuration [48,49] for a Λ atom. It has also been shown how optically coupling a third state to the common excited state can lead to an equation of motion whose solutions are spinors [9]. The resulting vector potential can then have a non-abelian symmetry, yielding an immediate connection to the physics of relativistic particles.

Subsequent work focussed on studying scenarios where relativistic effects became tractable; including the quantum simulation of the Dirac equation [50] which naturally leads onto the study of effects such as Zitterbewegung [8,51], the Klein paradox and exotic effects like negative refraction [52]. Although it seems at first counter-intuitive to study the models of high energy physics in the ultracold, low momentum regime, there are distinct advantages that ultracold atoms provide. Firstly, observing physics associated with single relativistic charged particles such as Zitterbewegung is essentially inacessable experimentally, due to the mass of the electron and the speed of light giving an oscillation frequency of order $m_e c^2/\hbar \sim 10^{20}$ Hz. One could for example use solid state systems to simulate these effects, however this also presents problems as the electrons in solids are in eigenstates of the Dirac equation; and further one does not have any control over the particle interactions, making simulating single particle effects of the Dirac equation difficult.

Another important tool in the quantum simulation toolbox is the optical lattice [53]. Lattices formed from standing waves of laser light have been used to study models such as the celebrated Hubbard model [11] to more exotic systems that mimic the field theories of relativistic particles [54]. Ultracold atoms on lattices form a natural system with which to study gauge theories. For example, the theories of high energy physics are formulated within the path integral formulation of quantum mechanics. There are only a handful of these integrals that can be evaluated exactly; hence one must resort to approximations to gain insight, indeed it is by discretising the path integral [55] that they can be evaluated using powerful numerical techniques such as Monte Carlo [56]. The emulation of gauge theories with condensed matter systems is however disjoint from this, here one is interested in for example the simulation of the symmetries of high energy physics, such as the non-abelian situation [57]. Recently, it has become experimentally possible to control individual atoms within the lattice [58], a situation which in the future will have important applications for the simulation of a variety of condensed matter effects.

The generation of gauge potentials for neutral atoms on a lattice can be achieved in a number of ways, for instance one can 'shake' the lattice by oscillating one of the mirrors employed in generating the standing wave [59, 60], resulting in a modified hopping parameter for the associated Hubbard model that depends directly on the rate of oscillation of the mirror. Alternately, laser-assisted tunnelling can be used. Here, a state dependent lattice is required, such that when a particle transverses an elementary cell an overall phase is acquired [40]. Recently, there has been interest in studying quantum hall physics with optical lattices [61], as these systems are very clean it is expected that many outstanding questions can be addressed. However,

reaching the quantum hall regime requires large magnetic fluxes, which are not easily achievable as the acquired flux scales with the length of the system. To address this, optical flux lattices have been proposed [62]. Here, the particles acquire a phase when they traverse both co-ordinate directions (x and y for a 2D lattice), hence the total acquired flux depends on the area of the cloud.

This work will focus primarily on ensembles of ultracold atoms interacting in the continuum with spatially shaped laser fields. The underlying methodology is the adiabatic theorem, which states that a quantum system will remain in an eigenstate when subject to a perturbation if the perturbation is small enough, and is a generalisation of the concept of a stationary state. The corollary to this is that the system will acquire an additional phase, known as the Mead-Berry connection [63] or simply Berry phase [64].

3.2 Rotating gases

The simplest method for generating a static magnetic field for a condensate is to stir the gas, such that in the rotating frame a term appears such that it is as if the condensate feels a homogeneous magnetic field [35]. To understand this, consider the microscopic Hamiltonian for the N body system, which can be written as

$$\hat{H}_{\mathrm{rot}} = \sum_{i=1}^{N} \left(\frac{1}{2m} \hat{\mathbf{p}}_i^2 + V(\mathbf{r}_i) - \boldsymbol{\Omega} \cdot (\mathbf{r}_i \times \mathbf{p}_i) \right) + g \sum_{i<j} \delta(\mathbf{r}_i - \mathbf{r}_j), \tag{3.2.1}$$

which can also be written in the form

$$\hat{H}_{\mathrm{rot}} = \sum_{i=1}^{N} \left(\frac{1}{2m} (\mathbf{p}_i - m\boldsymbol{\Omega} \times \mathbf{r}_i)^2 + V(\mathbf{r}_i) - \frac{m}{2} (\boldsymbol{\Omega} \times \mathbf{r}_i)^2 \right) + g \sum_{i<j} \delta(\mathbf{r}_i - \mathbf{r}_j), \tag{3.2.2}$$

where in equation 3.2.1 the angular momentum of particle i is $\mathbf{L} = \mathbf{r}_i \times \mathbf{p}_i$. Equation (3.2.2) shows that stirring the condensate produces a microscopic Hamiltonian which couples to the vector potential $m\boldsymbol{\Omega} \times \mathbf{r_i}$. When the rotation frequency Ω exceeds a critical value, vortices enter the condensate. If the vortices are given time to equilibrate, they arrange themselves into a triangular lattice known as the Abrikosov lattice [65], such that the vortices' repulsive interactions are minimised. The appearance of vortices can be understood by considering the allowed rotational motion of the superfluid. For a classical fluid, the total energy can be minimised by taking $\mathbf{v} = \boldsymbol{\Omega} \times \mathbf{r}$, however this is not permissible for the quantum fluid as one must have $\nabla \times \mathbf{v} = \mathbf{0}$. This situation is circumvented by the presence of vortices, the phases of which have a singularity at their cores.

3.3 Adiabaticity and the Berry phase

Let us consider for concreteness a simple example that demonstrates the connection between the adiabatic theorem and the Berry phase. Consider the Schrödinger equation $i\hbar\dot{\psi} = \hat{H}(\mathbf{R})\psi(t)$, where $\hat{H}(\mathbf{R})$ is a Hamiltonian that depends on the time dependent parameter $\mathbf{R} \equiv \mathbf{R}(t)$, and the associated state vector $|\psi(t)\rangle$ can be written in terms of the eigenstates of $\hat{H}(\mathbf{R})$ as

$$|\psi(t)\rangle = \sum_m c_m(t)|m;\mathbf{R}(t)\rangle. \tag{3.3.1}$$

Then, the adiabatic theorem is valid if all but one of the $c_m(t)$, say n appearing in equation (3.3.1) are identically zero[1], i.e. one has [66]

$$|\psi(t)\rangle \overset{\text{adiabatic}}{=} c_n(t)|n;\mathbf{R}(t)\rangle. \tag{3.3.2}$$

To understand this situation better, we substitute equation (3.3.2) into the Schrödinger equation defined above, yielding the expression

$$\left(\frac{d}{dt}c_n(t) + iE_n(\mathbf{R}(t))c_n(t)\right)|n;\mathbf{R}(t)\rangle \overset{\text{adiabatic}}{=} -c_n(t)\frac{d}{dt}|n;\mathbf{R}(t)\rangle, \tag{3.3.3}$$

which can be written as a differential equation for the amplitude $c_n(t)$ as

$$\frac{dc_n(t)}{dt} = -c_n(t)\left[iE_n(\mathbf{R}(t)) + \langle n;\mathbf{R}(t)|\frac{d}{dt}|n;\mathbf{R}(t)\rangle\right]. \tag{3.3.4}$$

Integrating equation (3.3.4) gives the following expression for the amplitude $c_n(t)$

$$\int_{c_n(0)}^{c_n(t)} \frac{dc_n(t)}{c_n(t)} = -i\int_0^t dt' E_n(\mathbf{R}(t')) + i\int_0^t dt'\ i\langle n;\mathbf{R}(t')|\frac{d}{dt'}|n;\mathbf{R}(t')\rangle. \tag{3.3.5}$$

With the initial condition $c_n(0) = 1$ equation (3.3.5) can be solved, giving

$$c_n(t) = \exp\left(-i\int_0^t dt' E_n(\mathbf{R}(t')) + i\gamma_n(t)\right), \tag{3.3.6}$$

[1]The situation where more than one state is occupied is considered later, the details presented here draw out the essential features that we are interested in.

where the geometric Berry phase $\gamma_n(t)$ is defined as

$$\gamma_n(t) = \int_0^t dt' i\langle n; \mathbf{R}(t')|\frac{d}{dt'}|n; \mathbf{R}(t')\rangle. \tag{3.3.7}$$

Equations (3.3.6) and (3.3.7) show that the adiabatic condition given by equation (3.3.2) has an extra consequence: there is an additional phase factor $\gamma_n(t)$ that is acquired along with the dynamical phase when the state $|\psi(t)\rangle$ explores the parameter space $\mathbf{R}(t)$. This idea will form the basis of subsequent chapters, where it will be this formalism that will be utilised in order to generate geometric phases for neutral atoms.

3.4 The Born-Oppenheimer method

It was demonstrated in the previous section how a quantum system prepared initially in an eigenstate of its Hamiltonian can acquire a non-dynamical phase that depends on the geometric nature of the particular eigenstate. This methodology will be developed further by considering a quantum system whose state space can be partitioned into slow and fast degrees of freedom. Let us consider a quantum particle whose state vector can be written as

$$|\psi\rangle = \sum_{j=1}^{N} \psi_j(\mathbf{r}, t) \otimes |\chi_j(\mathbf{r})\rangle, \tag{3.4.1}$$

where $|\chi_j\rangle$ is the j^{th} eigenstate of the Hamiltonian $\hat{H}$, which can be written as

$$\hat{H} = \frac{1}{2m}\hat{\mathbf{p}}^2 + V(\mathbf{r}). \tag{3.4.2}$$

The equation of motion for the state ψ_l is obtained from the matrix elements of equation (3.4.2) with the eigenstates $|\chi_j\rangle$, which can be shown to be $i\hbar\dot{\psi}_l = \langle\chi_l|\hat{H}|\psi\rangle$. Hence we obtain

$$i\hbar\dot{\psi}_l = \frac{1}{2m}\sum_{j,k=1}^{N}\left[\delta_{l,k}\hat{\mathbf{p}} - \mathbf{A}_{l,k}\right]\cdot\left[\delta_{k,j}\hat{\mathbf{p}} - \mathbf{A}_{k,j}\right]\psi_j(\mathbf{r}) + \sum_{j=1}^{N} V_{l,j}\psi_j(\mathbf{r}), \tag{3.4.3}$$

where the matrix elements of the gauge potential arise from the spatial variation of the states $|\chi_j\rangle$ and are defined by $\mathbf{A}_{n,m} = i\hbar\langle\chi_n|\hat{\nabla}\chi_m\rangle$ and the external potential $V(\mathbf{r})$ possesses the matrix elements $V_{l,j} = \langle\chi_l|V(\mathbf{r})|\chi_j\rangle$. Equation (3.4.3) defines the equation of motion for the amplitude $\psi_l(\mathbf{r}, t)$ per equation (3.4.1). We are specifically interested in a subset of these equations, such that a Born-Oppenheimer approximation can be used.

The Born-Oppenheimer method [67] has applications in many different areas of physics [68–70], here we will wish to partition the eigenstates $\{|\chi_1\rangle, ..., |\chi_N\rangle\}$ into 'fast' and 'slow' degrees of freedom. To proceed, we define the column vector formed from the coefficients ψ_l as $\mathbf{\Psi}^T = (\psi_1, \psi_2, ...\psi_N)$, which from equation (3.4.3) obeys the Schrödinger equation

$$i\hbar\frac{\partial \mathbf{\Psi}}{\partial t} = \left[\frac{1}{2m}(\hat{\mathbf{p}} - \hat{\mathbf{A}})^2 + V(\mathbf{r})\right]\mathbf{\Psi}, \tag{3.4.4}$$

and it will prove convenient to write the vector potential as

$$\hat{\mathbf{A}} = \frac{i\hbar}{2}\sum_{j=1}^{N}\Big\{|\hat{\nabla}\chi_j\rangle\langle\chi_j| - |\chi_j\rangle\langle\hat{\nabla}\chi_j|\Big\}. \tag{3.4.5}$$

In what follows we can assume that the full Hilbert space of $\hat{H}$, equation (3.4.2) possesses $n < N$ states that are degenerate. As such we can use the adiabatic theorem to construct a Schrödinger equation that describes the motion of the quantum particle within this manifold. The projection operator that projects into this space (this will be the 'fast' degree of freedom) is defined as

$$\hat{\mathcal{P}}_{\text{fast}} = \sum_{l=1}^{n}|\chi_l\rangle\langle\chi_l|. \tag{3.4.6}$$

Then, one can use equations (3.4.4) and (3.4.5) to obtain the Schrödinger equation for the truncated 'fast' space, by projecting with equation (3.4.6) in order to obtain an equation of motion in the truncated space $\hat{\mathcal{P}}_{\text{fast}}\mathbf{\Psi} = (\psi_1, \psi_2, ...\psi_n) = \tilde{\mathbf{\Psi}}$, which leads to the Schrödinger equation

$$i\hbar\frac{\partial \tilde{\mathbf{\Psi}}}{\partial t} = \left[\frac{1}{2m}(\hat{\mathbf{p}} - \hat{\mathbf{A}})^2 + \tilde{V}(\mathbf{r}) + \mathbf{\Phi}\right]\tilde{\mathbf{\Psi}}. \tag{3.4.7}$$

Equation (3.4.7) differs from equation (3.4.4) as we have effectively reduced the original $N \times N$ Hamiltonian matrix to a $n \times n$ one. Further, the projection has given rise to the scalar potential $\mathbf{\Phi}$, which can be derived using the projection operator form of the gauge potential, equation (3.4.5)

$$\langle\chi_l|\hat{\mathbf{A}}^2|\chi_m\rangle = \sum_{j=1}^{n}\mathbf{A}_{l,j}\cdot\mathbf{A}_{j,m} + \underbrace{\sum_{j=n+1}^{N}\mathbf{A}_{l,j}\cdot\mathbf{A}_{j,m}}_{\mathbf{\Phi}_{l,m}}. \tag{3.4.8}$$

The second term on the right hand side of equation (3.4.8) above defines the matrix elements $\mathbf{\Phi}_{l,m}$ of the scalar potential, while the first term gives the matrix elements

of the square of the gauge potential $\mathbf{A}$ in the fast space. The physical meaning of the scalar potential is the kinetic energy associated with the fast internal degree of freedom, as explained by [71].

3.5 Light-matter couplings for multi-level atoms

Let us consider the methodology by which a multi-level atomic system interacts coherently with an incident radiation field. Principally there are a number of ways that one can describe this interaction. Here, we will treat the matter quantum mechanically and the light classically, so that we are interested only in theories consistent with the classical theory of Maxwell. As such, consider the form of minimal coupling that accounts for N charges coupled to a gauge field, given by [72]

$$\hat{\mathcal{H}}(t) = \sum_{\alpha} \frac{1}{2m}(\hat{\mathbf{p}}_\alpha - q_\alpha A(\mathbf{R}_0, t))^2 + V_{\text{Coulomb}}(\mathbf{r}), \tag{3.5.1}$$

From an experimental point of view the wavelength of the incident radiation will be much larger than the size of the atoms, hence one can ignore the spatial variation of $A(\mathbf{r}, t)$. Then the point $\mathbf{R}_0$ is chosen as the origin of the system. The next step is to transform to a frame which translates the operator $\hat{\mathbf{p}}_\alpha$ by an amount $q_\alpha A(\mathbf{r}, t)$. Such a frame is defined by the unitary operator

$$\hat{U}(t) = \exp\left(-\frac{i}{\hbar} \sum_{\alpha} q_\alpha \mathbf{r}_\alpha \cdot A(\mathbf{R}_0, t) \right). \tag{3.5.2}$$

To calculate the transformed Hamiltonian, we note that in the rotated frame the Hamiltonian now becomes $\mathcal{H}'(t) = \hat{U}(t)\mathcal{H}(t)\hat{U}^\dagger(t) + i\hbar\dot{\hat{U}}(t)\hat{U}^\dagger(t)$. Hence, the Hamiltonian in the rotated frame is given by[2]

$$\mathcal{H}'(t) = \sum_{\alpha} \frac{1}{2m}\hat{\mathbf{p}}_\alpha^2 - \mathbf{d} \cdot \mathbf{E}(\mathbf{R}_0, t), \tag{3.5.3}$$

where the electric dipole moment of the distribution of charges is given by $\mathbf{d} = \sum_\alpha q_\alpha \mathbf{r}_\alpha$. Equation (3.5.3) shows how the rotation has transformed the original Hamiltonian (3.5.1) into a form that accounts for the light-matter interaction in terms of the electric field $\mathbf{E}(\mathbf{R}_0, t)$ coupling to the dipole moment of the charges. This form of interaction is called the electric dipole Hamiltonian, and is the foundation for the work described in what follows. This argument only holds for a charge neutral system, for systems of particles with a net charge, e.g. ions, extra terms

[2]This is aided by the use of the relation $\hat{U}(t)\hat{\mathbf{p}}_\alpha\hat{U}^\dagger(t) = \hat{\mathbf{p}}_\alpha + q_\alpha A(\mathbf{R}_0, t)$.

appear in equation (3.5.3).

Let us consider the situation whereby a system of such charges interacts with a classical field with optical frequency ω that couples the internal states $|a\rangle$ and $|b\rangle$. The electric dipole Hamiltonian is given by

$$\mathcal{H}_d(t) = -\mathbf{d} \cdot \mathbf{E}(\mathbf{R}_0, t). \tag{3.5.4}$$

Then, the matrix elements of equation (3.5.4) can be easily calculated with the definition of the electric field

$$\mathbf{E}(\mathbf{R}_0, t) = E_0 \left\{ \hat{\boldsymbol{\epsilon}} e^{i(\omega t - \mathbf{k}\cdot\mathbf{R}_0)} + \hat{\boldsymbol{\epsilon}}^* e^{-i(\omega t - \mathbf{k}\cdot\mathbf{R}_0)} \right\}, \tag{3.5.5}$$

where $\hat{\boldsymbol{\epsilon}}$ is the polarization vector of the light and the matrix elements are given by $\mathbf{d}_{ab} = \langle a|\mathcal{H}_d(t)|b\rangle = \sum_\alpha q_\alpha \langle a|\mathbf{r}_\alpha \cdot \hat{\boldsymbol{\epsilon}}|b\rangle e^{i(\omega t - \mathbf{k}\cdot\mathbf{R}_0)} + \text{c.c.}$ In what follows this will allow us to construct our gauge theory using this form of light matter coupling.

3.6 Artificial electromagnetism for a Λ atom

It was shown in the previous section how a set of charges interacting with a real gauge potential can be understood in terms of the electric dipole operator. Here, we will use this formalism to develop artificial gauge potentials for a 3 level Λ atom.

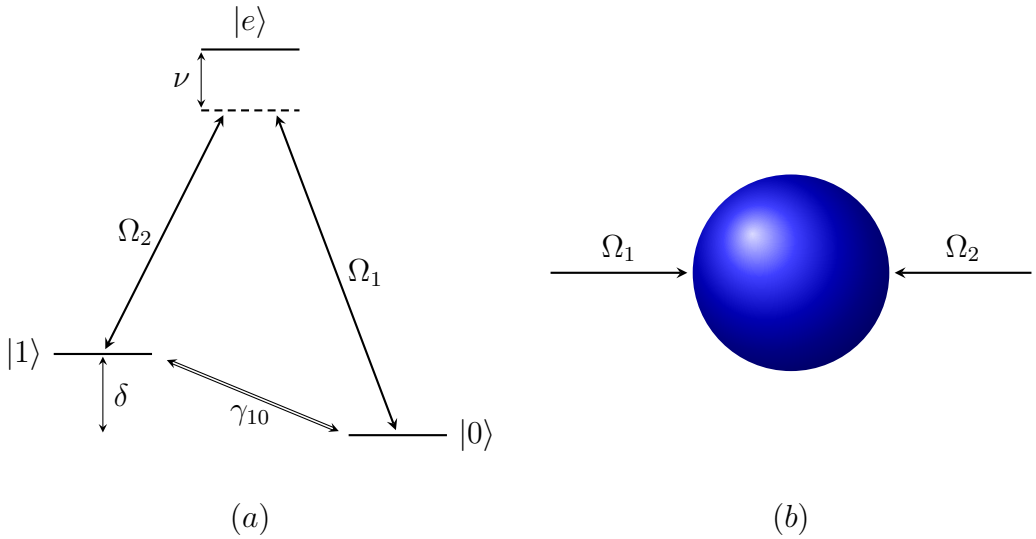

Figure 3.1: For (a), the states $|0\rangle$ and $|1\rangle$ are coupled to the excited state $|e\rangle$ with the lasers with Rabi frequencies denoted Ω_1 and Ω_2. The excited state $|e\rangle$ has a detuning ν, and decay of the population from $|0\rangle$ to $|1\rangle$ is accounted for by γ_{10}. Meanwhile, (b) shows a schematic of the BEC coupled to the two light fields $\Omega_{1,2}$.

Figure 3.1 (a) shows the level structure of the Λ atom. The state space is spanned by $\{|0\rangle, |1\rangle, |e\rangle\}$, and we take the state $|0\rangle$ to be at zero energy. The Λ atom will form a pedagogical tool for of our analysis of artificial electromagnetism, as we shall see such a system allows us to answer the following questions

- How does the adiabatic theorem allow us to construct a gauge theory for a charge neutral Bose-Einstein condensate?
- What are the consequences of using adiabaticity to describe the atom's motion?
- What is special about the limit of large two-photon detuning ν, such that $\nu \gg \Omega_{1,2}$ is satisfied?

To address the first question, let us write down the Hamiltonian that encapsulates the light-matter coupling. This can be written in the basis $\{|0\rangle, |1\rangle, |e\rangle\}$ as

$$\hat{\mathcal{H}}_\Lambda(t) = \hbar \begin{pmatrix} 0 & 0 & \Omega_1^* \cos(\omega_1 t) \\ 0 & \delta & \Omega_2^* \cos(\omega_2 t) \\ \Omega_1 \cos(\omega_1 t) & \Omega_2 \cos(\omega_2 t) & \omega \end{pmatrix}, \tag{3.6.1}$$

where the Rabi frequency that couples the state $|i\rangle$ to $|e\rangle$ is given by $\Omega_i = eE_0\langle e|\mathbf{r}\cdot\hat{\boldsymbol{\epsilon}}|i\rangle/\hbar$. In section 3.5 it was shown that a time dependent Hamiltonian can be transformed using a unitary operator $\hat{U}(t)$. This approach can be adopted here as well. The unitary operator $\hat{U}(t)$ is defined here as $\hat{U}(t) = |0\rangle\langle 0| + \exp(-i(\omega_1 - \omega_2)t)|1\rangle\langle 1| + \exp(-i\omega_1 t)|e\rangle\langle e|$. Now, in the interaction picture the Hamiltonian, equation (3.6.1) becomes

$$\mathcal{H}'_\Lambda = \frac{\hbar}{2} \begin{pmatrix} 0 & 0 & \Omega_1^* \\ 0 & 2(\nu_1 - \nu_2) & \Omega_2^* \\ \Omega_1 & \Omega_2 & 2\nu_1 \end{pmatrix}, \tag{3.6.2}$$

where $\nu_{1,2}$ are the detunings from resonance of the states $|0\rangle$ and $|1\rangle$ respectively. To write equation (3.6.1) above, the rotating wave approximation has been used so that terms oscillating at twice the optical frequency are dropped. If we further assume that we are in resonance so that $\nu_1 = \nu_2 = 0$, then $\hat{H}'_\Lambda$ can be diagonalised to give the dressed states $\{|D\rangle, |\pm\rangle\}$, with respective eigenvalues $\{0, \pm\Omega\}$. The states $|D\rangle$ and $|B\rangle$ are the dark and bright states which are defined as

$$|D\rangle = (\Omega_2|0\rangle - \Omega_1|1\rangle)/\Omega \qquad \text{and} \qquad |B\rangle = (\Omega_1^*|0\rangle + \Omega_2^*|1\rangle)/\Omega, \tag{3.6.3}$$

and the total Rabi frequency is $|\Omega| = \sqrt{|\Omega_1|^2 + |\Omega_2|^2}$. Hence, the doublet states are defined as $|\pm\rangle = (|B\rangle \pm |e\rangle)/\sqrt{2}$. As the dark state $|D\rangle$ is decoupled from the

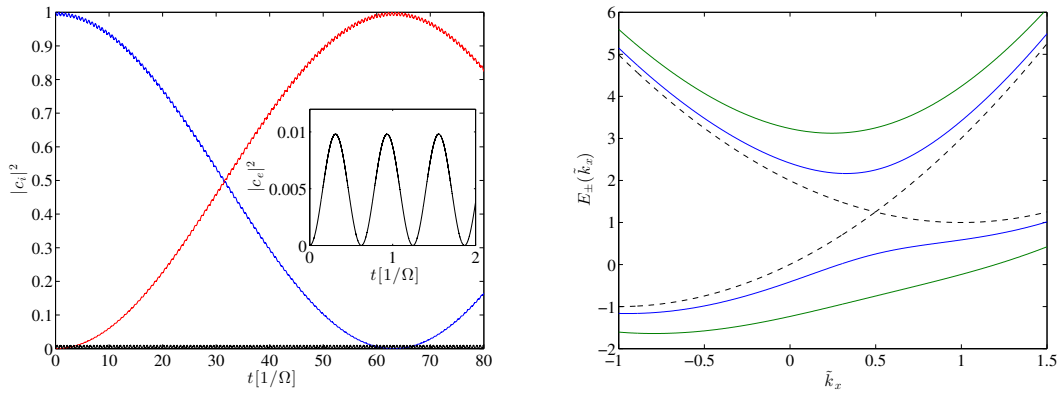

(a) (b)

Figure 3.2: In (a) the numerical solutions for the Λ system defined by equation (3.6.2) with $\Omega = \Omega_{1,2}$ are shown for $\nu/\Omega = 10$. The populations $|c_0(t)|^2$, $|c_1(t)|^2$ and $|c_e(t)|^2$ are given by the blue, red and black curves. The inset shown the population $|c_e(t)|^2$. In (b) we see the dispersion as calculated from equation (3.6.6). The units of momentum and energy are $\tilde{k}_x = k_x/k_r$ and $E_r = \hbar^2 k_r^2/2m$. The curves are shown for $\hbar\Omega_R/E_r = \{0, 2, 4\}$ in black (dashed), blue and green respectively. The detuning is $\hbar\delta/E_r = 2$.

excited state $|e\rangle$, it is immune from spontaneous emission. This particular atomic configuration, figure 3.1 is an example of Electromagnetically Induced Transparency (EIT), where two coherent optical pathways ($\Omega_{1,2}$ in our example) destructively interfere, which at resonance leads to an induced transparency [48, 73]. Let us now consider again the Born-Oppenheimer methodology introduced in section 3.4. The full state of the system is given by equation (3.4.1), where the sum is taken over the dressed basis $\{|D\rangle, |\pm\rangle\}$. Then let us assume that atomic motion occurs exclusively in the dark state $|D\rangle$, such that $|\psi\rangle = \psi_D(\mathbf{r}, t)|D\rangle$. The equation of motion for ψ_D is given by

$$i\hbar\frac{\partial\psi_D}{\partial t} = \left[\frac{1}{2m}(\hat{\mathbf{p}} - \mathbf{A})^2 + W + \langle\mathcal{H}'_\Lambda\rangle\right]\psi_D, \tag{3.6.4}$$

where the gauge potential is defined as $\mathbf{A} = i\hbar\langle D|\nabla D\rangle$, and the scalar geometric phase is $W = \hbar^2|\langle B|\nabla D\rangle|^2/2m$. The quantity $\langle\hat{\mathcal{H}}'_\Lambda\rangle = \langle D|\hat{\mathcal{H}}'_\Lambda|D\rangle$ is identically zero for atoms moving in the dark state. Equation (3.6.4) assumes that the atomic motion is adiabatic in the dressed state $|D\rangle$. However, there is an alternative way to analyse the three level system that relies instead on the assumption $\nu \gg \Omega_{1,2}$. To analyse this situation, we write the state as $|\psi(t)\rangle = \sum_{j=0,1,e} c_j(t)|j\rangle$, and because the detuning ν is large compared to the Rabi frequencies $\Omega_{1,2}$ transitions occur by two-photon Raman transitions. Here, one beam (Ω_1) excites the atom to a virtual excited state (dashed line in figure 3.1(a)), while the second beam (Ω_2) de-populates the atom into the state $|1\rangle$. This allows for transitions between the two ground states via the excited state, although the population of the state $|e\rangle$ remains negligible. In the limit that $\nu \gg \Omega_{1,2}$ one can assume that the occupation of the state $|e\rangle$ is

negligible. Figure 3.2 (a) shows the numerical solution to the set of equations for the amplitudes $\dot{c}_i$. In this limit, the inset of figure 3.2 (a) shows the population $|c_e(t)|^2$, which is of order 1%. Hence, equation (3.6.2) can be reduced in the limit $c_e \approx 0$ to the truncated Hamiltonian

$$\mathcal{H}_{R-\Lambda} = -\frac{\hbar}{4\nu}\begin{pmatrix} |\Omega_1|^2 & \Omega_1^*\Omega_2 \\ \Omega_1\Omega_2^* & |\Omega_2|^2 \end{pmatrix}. \tag{3.6.5}$$

The stimulated emission of photons causes atoms in different states to experience a net momentum. Now, if we include the atom's kinetic energy the Hamiltonian of the problem is $\hat{\mathbf{p}}^2/2m + \mathcal{H}_{\mathrm{R}-\lambda}$. As such, the one dimensional momentum space dressed basis can then be written $\{|0, k_x - k_r\rangle, |1, k_x + k_r\rangle\}$, and if we identify the Raman frequency $\Omega_R = -\Omega_1^*\Omega_2/2\nu$ and effective 'detunings' $\delta = -|\Omega_1|^2/2\nu = |\Omega_2|^2/2\nu$ then one obtains

$$\mathcal{H}_{R-\Lambda}(k_x) = \begin{pmatrix} \frac{\hbar^2}{2m}(k_x - k_r)^2 + \hbar\delta/2 & \hbar\Omega_R/2 \\ \hbar\Omega_R/2 & \frac{\hbar^2}{2m}(k_x + k_r)^2 - \hbar\delta/2 \end{pmatrix}. \tag{3.6.6}$$

Equation (3.6.6) is formally equivalent to the scheme discussed by Spielman [42], the spectrum of which is shown in figure 3.2 (b) for different values of Ω_R. The figure shows how increasing the strength of the Raman coupling between the two ground states causes a gap to appear in the dressed dispersion. When $\delta = 0$, $E_\pm(k_x)$ displays a double well structure, but at finite detuning this degeneracy is broken and the system possess a unique single particle ground sate located at the minimum of the $E_-(k_x)$ branch. This approach has been extended to generate uniform [2] as well as non-uniform [3] gauge potentials for a condensate of ^{87}Rb atoms in the $F = 1$ manifold. Further, this technique has been extended to the case of three ground states to realise the spin-orbit effect [4], and most recently for the spin Hall effect [7], where the condensate feels a spin dependent force that arrises from the pseudo-spin structure of the underlying single particle Hamiltonian.

3.7 The tripod configuration

In the previous section, two methods were described that showed how it is possible to engineer gauge potentials using light matter interactions for multi level atomic systems. Let us now consider an atomic system related to that of figure 3.2, where one has an additional ground state, a scheme known as the tripod configuration. Let us consider the situation where three lasers couple the states $|1\rangle, |2\rangle, |3\rangle$ to the excited state $|e\rangle$ with Rabi frequencies given by $\Omega_{1,2,3}$. This situation is depicted in figure 3.3. The approach here will be complimentary to that of section 3.6, where the light-atom interaction is diagonalised by first removing the parts of the Hamiltonian

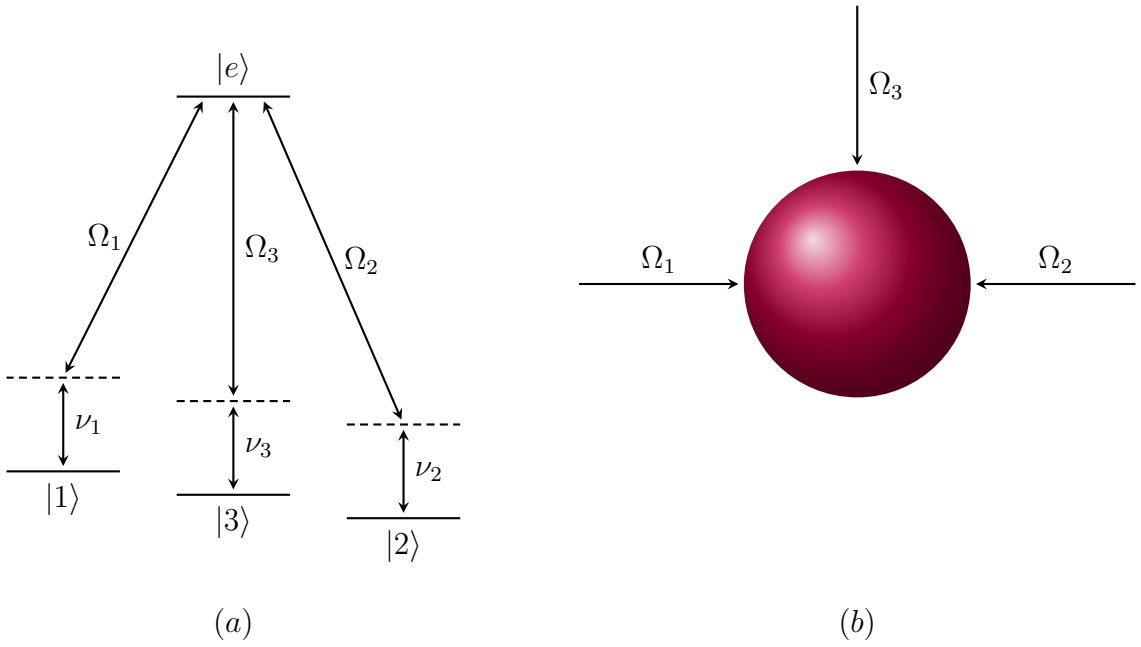

Figure 3.3: For (a), the states $|1\rangle, |3\rangle, |2\rangle$ are coupled to the excited state $|e\rangle$ with the lasers with Rabi frequency $\Omega_{1,3,2}$. The detuning from resonance for the state $|j\rangle$ is given by ν_j. Meanwhile, (b) shows a schematic of the BEC coupled to the counter propagating fields $\Omega_{1,2}$ and the third orthogonal laser field, Ω_3.

that describe the free evolution of the atomic degrees of freedom. The Hamiltonian for the tripod configuration is given by

$$\hat{H}_{\text{tripod}} = \sum_{j=e,1}^{N=3} \hbar\omega_j |j\rangle\langle j| - \sum_{j=1}^{N_l=3} \hat{\mathbf{d}}_j \cdot \mathbf{E}_j(\mathbf{r}, t), \tag{3.7.1}$$

where the dipole operator is given by $\hat{\mathbf{d}} = \mathbf{d}_{ej}|e\rangle\langle j| + \mathbf{d}^*_{ej}|j\rangle\langle e|$ and the electric field coupling level $|j\rangle$ and $|e\rangle$ is defined by $\mathbf{E}_j(\mathbf{r}, t) = \mathcal{E}(\mathbf{r})e^{i\bar{\omega}_j t}$+c.c. There are N atomic levels and N_l lasers. The energies of the atomic states are denoted $\hbar\omega_j$ while those of the photons driving transitions between $|j\rangle$ and $|e\rangle$ are given by $\hbar\bar{\omega}_j$. To remove the first term on the right hand side of equation (3.7.1), we perform the unitary transformation on the tripod configuration, defined by

$$\hat{U}(t) = \exp\left(\frac{i}{\hbar} t \sum_{j=e,1}^{N=3} \hbar\omega_j |j\rangle\langle j|\right) = \sum_{j=e,1}^{N=3} e^{i\omega_j t}|j\rangle\langle j|. \tag{3.7.2}$$

Equation 3.7.2 leads naturally to the interaction picture Hamiltonian

$$\hat{H}^I_{\text{tripod}} = \hat{U}(t)\hat{H}_{\text{tripod}}\hat{U}^\dagger(t) + i\hbar\dot{\hat{U}}(t)\hat{U}^\dagger(t). \tag{3.7.3}$$

After some algebra, one obtains the following form of the interaction picture Hamiltonian $\hat{H}^I_{\text{tripod}}$ from equations (3.7.2) and (3.7.3)

$$\hat{H}^I_{\text{tripod}} = -\hbar \sum_{j=1}^{N_l=3} \left\{ \Omega_j(\mathbf{r})|e\rangle\langle j|e^{-i\nu_j t} + \tilde{\Omega}_j(\mathbf{r})|e\rangle\langle j|e^{-i(\nu_j+2\bar{\omega}_j)t} + \text{h.c.} \right\}. \tag{3.7.4}$$

Equation 3.7.4 contains two types of terms: transitions occurring with Rabi frequency $\Omega_j(\mathbf{r}) = \mathbf{d}_{ej}\cdot\mathcal{E}(\mathbf{r})/\hbar$, and those defined by the frequency $\tilde{\Omega}_j(\mathbf{r}) = \mathbf{d}_{ej}\cdot\mathcal{E}^*(\mathbf{r})/\hbar$. The detuning from resonance is given by $\nu_j = \omega_e - \omega_j - \bar{\omega}_j$. Terms proportional to $\tilde{\Omega}(\mathbf{r})$ can be dropped as they occur at twice the transition frequency $\bar{\omega}_j$. This is known as the rotating wave approximation [74]. In the work considered throughout this thesis, the analysis of the multi-level system is simplified by working with transitions on resonance, $\nu_j = 0$.This allows us to write the light-matter coupling, equation 3.7.4 as

$$\hat{H}^I_{\text{tripod}} = -\hbar \sum_{j=1}^{N_l=3} \left\{ \Omega_j(\mathbf{r})|e\rangle\langle j| + \Omega_j^*(\mathbf{r})|j\rangle\langle e| \right\}. \tag{3.7.5}$$

The diagonalization of the interaction tripod Hamiltonian, equation 3.7.5 yields the four dressed states, defined in a similar way to the three level system by two manifolds of (unnormalized) bright and dark states, with

$$|D_1\rangle = \frac{\Omega_3}{\Omega_1}|1\rangle - |3\rangle, \tag{3.7.6}$$

$$|D_2\rangle = \frac{\Omega_2}{\Omega_1}|1\rangle + |2\rangle, \tag{3.7.7}$$

$$|B\rangle = \Omega_1^*|1\rangle + \Omega_2^*|2\rangle + \Omega_3^*|3\rangle. \tag{3.7.8}$$

The effect of adding a third level to form the tripod has yielded a second dark state, degenerate at zero energy with the first. The other two dressed states can then be defined in terms of the unnormalized doublet $|\pm\rangle = |B\rangle \pm |e\rangle$, with energies $\Omega^{\pm} = \pm\Omega$, where $\Omega = \sqrt{\sum_j |\Omega_j|^2}$ (positive). As they stand, the dressed states are not in a particularly useful form. To aid calculation, one can define new dark and bright states in terms of the old ones by parameterising the Rabi frequencies Ω_j in terms of the spherical 'coordinates' defined by

$$\Omega_1 = \Omega \sin\theta \cos\phi e^{iS_1}, \tag{3.7.9}$$

$$\Omega_2 = \Omega \sin\theta \sin\phi e^{iS_2}, \tag{3.7.10}$$

$$\Omega_3 = \Omega \cos\theta e^{iS_3}. \tag{3.7.11}$$

These equations interpreted geometrically describe a sphere of radius $|\Omega|$ with azimuthal angle ϕ and polar angle θ. These definitions allow us to simplify equations 3.7.6 to 3.7.8 by defining the new dressed states as [75]

$$|D_1^{\text{new}}\rangle = -\cos\phi e^{iS_{21}}|D_2\rangle, \tag{3.7.12}$$
$$|D_2^{\text{new}}\rangle = -\sin\theta|D_1\rangle + \cos\theta\sin\phi e^{iS_{32}}|D_2\rangle, \tag{3.7.13}$$
$$|B^{\text{new}}\rangle = e^{iS_3}|B\rangle, \tag{3.7.14}$$

where the phase angle is defined as $S_{ij} = S_i - S_j$. Thus, the dressed states become

$$|D_1^{\text{new}}\rangle = \sin\phi e^{iS_{31}}|1\rangle - \cos\phi e^{iS_{32}}|2\rangle, \tag{3.7.15}$$
$$|D_2^{\text{new}}\rangle = \cos\theta\cos\phi e^{iS_{31}}|1\rangle + \cos\theta\sin\phi e^{iS_{32}}|2\rangle - \sin\theta|3\rangle, \tag{3.7.16}$$
$$|B^{\text{new}}\rangle = \sin\theta\cos\phi e^{iS_{31}}|1\rangle + \sin\theta\sin\phi e^{iS_{32}}|2\rangle + \cos\theta|3\rangle. \tag{3.7.17}$$

This normalized basis has been used to study many effects owing to the robustness of the pair of dark states $|D_1\rangle$ and $|D_2\rangle$ [40]. Using the formalism developed in section 3.4, an equation of motion is obtained by projecting onto the dark states with equation (3.4.6). Taking the sum over the dark subspace, one obtains

$$i\hbar\frac{\partial}{\partial t}\mathbf{\Psi}(\mathbf{r}) = \left(\frac{1}{2m}(\hat{\mathbf{p}} - \mathbf{A})^2 + \mathbf{\Phi} + \langle\hat{H}^I_{\text{tripod}}\rangle\right)\mathbf{\Psi}(\mathbf{r}), \tag{3.7.18}$$

where one has $\mathbf{\Psi}(\mathbf{r}) = (\psi_{D_1}(\mathbf{r}), \psi_{D_2}(\mathbf{r}))^T$ and similarly to the Λ configuration discussed previously $\langle\hat{H}^I_{\text{tripod}}\rangle = \sum_{i=1}^{2}\langle D_i|\hat{H}^I_{\text{tripod}}|D_i\rangle = 0$. From equation (3.4.8) the scalar potential has matrix elements given by

$$\mathbf{\Phi}_{n,m} = \frac{1}{2m}\sum_{l=\pm}\mathbf{A}_{n,l}\cdot\mathbf{A}_{l,m}, \tag{3.7.19}$$

where $n, m \in \{D_1, D_2\}$. The Hamiltonian in equation (3.7.19) is now a 2×2 matrix whose solutions are given by the spinor $\mathbf{\Psi}(\mathbf{r})$. Finally, let us consider the gauge structure of the potentials $\mathbf{A}$ and $\mathbf{\Phi}$. A local, length preserving unitary transformation can be defined that transforms the vector $\mathbf{\Psi} \to \hat{U}(\mathbf{r})\mathbf{\Psi}$. Accordingly one finds the new vector and scalar potentials are given by

$$\mathbf{A} \to \hat{U}^\dagger(\mathbf{r})\mathbf{A}\hat{U}(\mathbf{r}) + i\hbar\hat{U}^\dagger(\mathbf{r})\nabla\hat{U}(\mathbf{r}) \qquad \text{and} \qquad \hat{U}^\dagger(\mathbf{r})\mathbf{\Phi}\hat{U}(\mathbf{r}). \tag{3.7.20}$$

Further, the gauge structure can also give rise to an effective magnetic field $\mathbf{B}$, whose components are related to the vector potential $\mathbf{A}$ through the relations [9]

$$B_i = \frac{1}{2}\epsilon_{ijk}F_{kl} \qquad \text{and} \qquad F_{kl} = \partial_k A_l = \partial_l A_k - \frac{i}{\hbar}[A_k, A_l], \tag{3.7.21}$$

because the components of $\mathbf{A}$ do not in general commute, the term proportional to $[A_k, A_l]$ in equation 3.7.21 is non zero. The generation of gauge potentials with multi-level atomic systems has been explored in a variety of contexts, including the study of non-Abelian effects, where the components of the gauge potential do not commute. This situation was developed further to show how these setups can be utilised to study non-Abelian magnetic monopoles [76] and also Dirac strings [77].

3.8 Discrete systems

In this final section we briefly review how one can simulate gauge theories using optical lattices. In analogy with their continuum cousins, several proposals have been given to generate gauge potential in lattice systems. The simplest method is to rotate the lattice, outside of the Hubbard regime [78, 79]. Another method is to use a bath of atoms in order to generate the gauge potential [80]. One can also 'shake' (oscillate) one of the mirrors used to create the standing wave for the optical lattice [59, 60], resulting in a modified hopping parameter. These two methods do not specifically rely on the internal states of the atoms. The method we will focus on to study artificial gauge theories in discrete systems will be laser assisted tunnelling [43,81], where a state dependent lattice is used to generate the magnetic flux required to simulate the gauge field.

Consider a quantum particle confined in the 2D square lattice with period a_x along x and a_y along the y direction. The appropriate lattice potential is then given by

$$V_{\text{lattice}}(x, y) = V_0 \Big\{ \sin^2(\pi x/a_x) + \sin^2(\pi y/a_y) \Big\}. \tag{3.8.1}$$

Working in the region where the tight-binding approximation is valid leads to the Hamiltonian in second quantised form given by

$$\hat{H} = \sum_{\substack{n,m \\ n',m'}} J^{\,n,m}_{\,n',m'} \hat{a}^\dagger_{n,m} \hat{a}_{n',m'}, \tag{3.8.2}$$

where the tunnelling matrix elements $J^{\,n,m}_{\,n',m'}$ in equation 3.8.2 are defined as

$$J^{\,n,m}_{\,n',m'} = \int d^2\mathbf{r}\; w^*_{n,m}(\mathbf{r}) \left(\frac{1}{2m} \hat{\mathbf{p}}^2 + V_{\text{lattice}}(x, y) \right) w_{n',m'}(\mathbf{r}). \tag{3.8.3}$$

Equation (3.8.3) contains the Wannier functions $w_{n,m}(\mathbf{r})$ which are the orthogonal set of functions that constitute the basis of the discrete system. Now in the tight

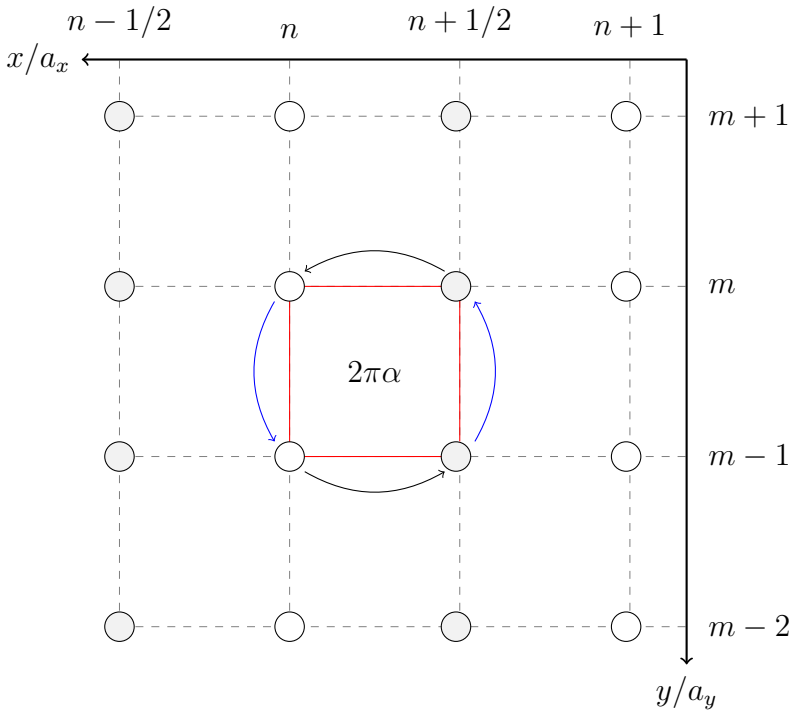

Figure 3.4: Schematic representation of the tunnelling events required to generate a magnetic flux. The white (grey) circles indicate atoms in the ground (excited) state $|g\rangle$ ($|e\rangle$). When the quantum particle transverses the cell (red outline) it acquires a phase $2\pi\alpha$. Transitions from $|g\rangle \to |g\rangle$ and $|e\rangle \to |e\rangle$ are due to standard quantum mechanical tunnelling, while transitions from $|g\rangle \to |e\rangle$ and $|e\rangle \to |g\rangle$ are caused by resonant laser-assisted tunnelling.

binding regime the Hamiltonian, equation (3.8.2) reduces to

$$\hat{H}_{TB} = -J \sum_{\langle n,m \rangle} \hat{a}^{\dagger}_{n,m} \hat{a}_{n',m'}, \tag{3.8.4}$$

where $\hat{a}_{n,m}$ is the annihilation operator for a particle in the state $w_{n,m}(\mathbf{r})$ and $\langle \cdots \rangle$ indicates the sum is taken over nearest neighbours only. Within the tight binding approximation, hopping to more distant sites can be neglected. Now, for a particle carrying a charge e, the Hamiltonian that we wish to simulate can be written as

$$\hat{H} = -J \sum_{n,m} e^{\pm i\phi_{n,m}} \hat{a}^{\dagger}_{n\pm1,m} \hat{a}_{n,m} - J \sum_{n,m} \hat{a}^{\dagger}_{n,m\pm1} \hat{a}_{n,m}, \tag{3.8.5}$$

where the phase $\phi_{n,m}$ is defined as

$$\phi_{n,m} = \frac{e}{\hbar} \int_{\mathbf{r}_{n,m}}^{\mathbf{r}_{n+1,m}} \mathbf{A} \cdot d\mathbf{l}. \tag{3.8.6}$$

The integral, equation (3.8.6) is taken along a straight line that connects sites on different internal states, $|g\rangle$ or $|e\rangle$. The phase factor $\exp(\pm i\phi_{n,m})$ can be interpreted as the Aharonov-Bohm phase that the quantum particle accumulates as it transverses the lattice (see figure 3.4). The total flux accumulated by a particle taken around an elementary cell is given by

$$\sum_{\square} \phi_{n,m} = \frac{eBa_x a_y}{\hbar} = 2\pi\alpha, \tag{3.8.7}$$

where the symbol $\square$ indicates the summation is taken over the cell indicated in red in figure 3.4, and is a gauge invariant quantity.

3.9 Summary

In this chapter the concept of gauge potentials for ultracold atoms was introduced. It was described how the adiabatic theorem can be used to construct geometric phases for a quantum particle that are mathematically equivalent to an electromagnetic gauge potential. From a more practical perspective, two experimentally relevant atomic schemes were discussed, a three level (Λ) and a four level (tripod) system. It was shown in both cases that the dressed states are comprised of a bright and a dark manifold. Equations of motion for both systems were obtained for these dark states, which are of scalar and matrix form for the three and four level system respectively. Finally, the generation of gauge potentials on a lattice was described, in terms of laser-assisted tunnelling. It was discussed how a state dependent lattice can be used to achieve a non-zero magnetic flux in these discrete systems.

Chapter 4

Localization and Disorder

4.1 Anderson Localization

One of the most important hallmarks associated with the coherence of waves is constructive and destructive interference. It is the case for atomic condensates that the coherent nature of the ground state allows one to investigate a broad spectrum of problems that would be intractable in other condensed matter systems. Of principle example are the charge carriers in solids where the Coulomb interactions between particles often mask the subtle effects caused by the wave nature of particle motion within the crystalline environment.

On the other hand, atomic condensates do not suffer this limitation, indeed we are in a situation where we can directly image the density of the quantum gas, and it is this attractive prospect which has led to impressive progress in the quantum simulation of single and many particle effects.

The theory of the transport of waves offers an intriguing route with which to explore another of the paradigms of condensed matter, disorder. Principally we are interested in understanding the effect of the coherent propagation of matter waves in a weak disorder. The effect of the destructive interference by the scattering of waves with a weak disorder leads to Anderson localization, which is characterised by the exponential decay of the wave function [82].

One-dimensional Anderson localization is caused by destructive interference in a weak, disordered potential (referred to as diagonal disorder) and leads to exponential

localization of the particles [83–86]. This behaviour may change in half-filled disordered metals [87], random spin-Peierls and spin-ladder systems [88], or as recently predicted in photonic systems with electromagnetically induced transparency [89]. Delocalized zero-energy states, known as mid-gap states can emerge in these systems showing a power-law behaviour for the correlations due to a Dyson singularity in the Density of States (DOS) [90]. Such anomalous localization originates from the chiral symmetry of the corresponding 1D Hamiltonian and can be realised in the system with off-diagonal disorder known as a random-mass Dirac model or the fluctuating gap model (FGM) [91–94]. The singularity in the DOS was discovered in 1953 by Freeman Dyson [95] who calculated the density of phonon modes in a chain of 1D harmonic oscillators with random masses and random couplings. It emerges at the band centre and strongly affects the localization properties, leading to a diverging localization length at $E = 0$. However, as was shown by Fleishman and Licciardello [96] the $E = 0$ state is not extended due to strong fluctuations. In fact, it can be shown that there exists a Dyson singularity for any distribution of off-diagonal disorder [97, 98]. Interestingly, the FGM can also be mapped onto a chain of identical atoms with a random XY model [99].

In cold atom systems disorder is typically induced by a random potential and is thus of diagonal type. Here we show that the combination of a random potential and SO coupling induced by the motion in space dependent laser fields can give rise to effective off-diagonal disorder. Light-induced SO coupling has been shown to lead to an effective Dirac dynamics in [8]. By investigating the density of states of the corresponding disorder model we derive conditions under which power-law localization can be observed and argue that they are indeed connected to the emergence of a Dyson singularity in the DOS. It is shown by simulating the time evolution of a gaussian wave packet that there is a crossover from exponential (Anderson) localization to an anomalous power-law behaviour as the SO coupling strength is increased. It is noted that a model similar to what follows was considered in [100], but only for the case of diagonal disorder, where the kinetic energy term is neglected. The kinetic term can only be neglected under special circumstances and drastically alters the behaviour of the system, leading to richer physics.

In the first part of this chapter it is shown how a pseudospin structure can be generated for an ensemble of non-interacting ultracold atoms, and in particular how a Dirac cone can be produced. The role of and effect of disorder in this system is then described for the spin-orbit coupled quantum gas.

4.2 Dark-state dynamics for the tripod coupling

Consider an ensemble of cold atoms exposed to three laser fields in a tripod-type linkage pattern [101] as depicted in figure 4.1. The atoms are characterised by a manifold of three ground states $\{|1\rangle, |2\rangle, |3\rangle\}$ coupled to a common excited state $|0\rangle$ via a corresponding control laser of wave-number κ. We assume two of the control lasers to be counter-propagating along the x-axis with Rabi frequencies

$$\Omega_1 = \Omega \sin\theta e^{-i\kappa x}/\sqrt{2}, \tag{4.2.1}$$

$$\Omega_2 = \Omega \sin\theta e^{i\kappa x}/\sqrt{2}, \tag{4.2.2}$$

$$\Omega_3 = \Omega \cos\theta e^{-i\kappa y}, \tag{4.2.3}$$

and $\Omega = \sqrt{\sum_{i=1}^{3} |\Omega_i|^2}$ denotes the total Rabi frequency. We can write the interaction picture Hamiltonian of the resulting tripod scheme as $\hat{H}_0 = -\hbar \sum_{i=1}^{3} (\Omega_i |0\rangle\langle i| + h.c.)$. This Hamiltonian has four dressed states which can be split into two manifolds, the dark and bright states (see section 3.7 for details). It is convenient to re-define the dressed states as linear combinations of $|D_1\rangle$ and $|D_2\rangle$. [1] The new dark states are hence given by

$$|D_1\rangle = \frac{1}{\sqrt{2}} e^{-i\kappa y}(e^{i\kappa x}|1\rangle - e^{-i\kappa x}|2\rangle), \tag{4.2.4}$$

$$|D_2\rangle = \frac{1}{\sqrt{2}} \cos\theta (e^{i\kappa x}|1\rangle + e^{-i\kappa x}|2\rangle) - \sin\theta |3\rangle, \tag{4.2.5}$$

which have zero energy and do not couple to the state $|0\rangle$. The bright states are formed from a doublet $|\pm\rangle = \frac{1}{\sqrt{2}}(|B\rangle \pm |0\rangle)$ with energy $\pm\hbar\Omega$, and the state $|B\rangle$ is given by

$$|B\rangle = \frac{1}{\sqrt{2}} \sin\theta e^{-i\kappa y} \left(e^{i\kappa x}|1\rangle + e^{-i\kappa x}|2\rangle \right) + \cos\theta |3\rangle. \tag{4.2.6}$$

The full dressed basis is then expressed as $\{|D_1\rangle, |D_2\rangle, |+\rangle, |-\rangle\}$. By expressing the general state of the system as $|\xi(\mathbf{r}, t)\rangle = \sum_{i=1}^{4} \psi_i(\mathbf{r}, t)|\chi_i(\mathbf{r})\rangle$, an equation of motion for the atoms in the dark-state manifold is obtained by projecting onto

[1] As described in section 3.7 (equations (3.7.12) to (3.7.14)), the states $|D_i\rangle$ and $|B\rangle$ are written in terms of the eigenstates as

$$|D_1^{\text{new}}\rangle = -\frac{1}{\sqrt{2}} e^{-i\kappa(x+y)}|D_2\rangle,$$

$$|D_2^{\text{new}}\rangle = -\sin\theta |D_1\rangle + \frac{1}{\sqrt{2}} \cos\theta e^{-i\kappa(x+y)}|D_2\rangle,$$

$$|B^{\text{new}}\rangle = e^{-i\kappa y}|B\rangle.$$

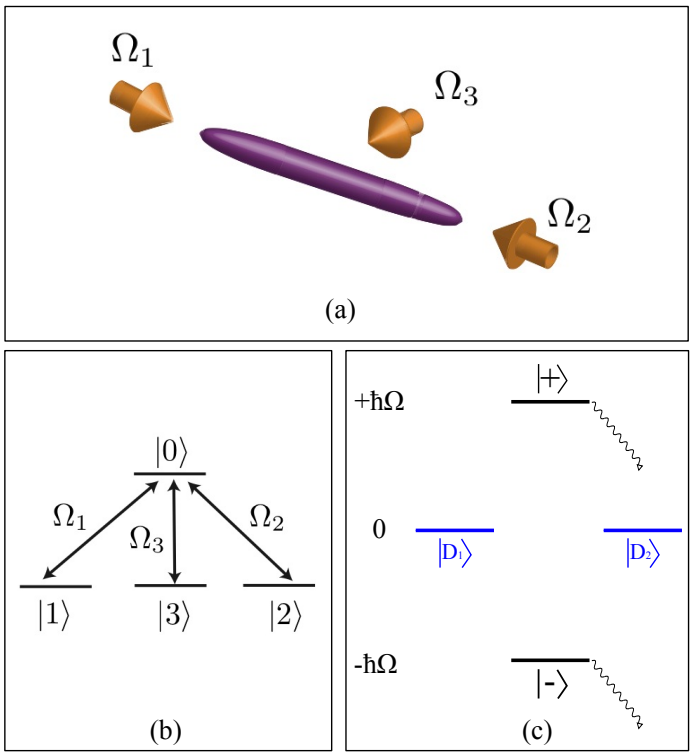

Figure 4.1: Top: Schematic representation of the experimental system (a). The condensate is placed into a tight cigar-shaped trap and driven with three lasers with Rabi frequencies Ω_1,Ω_2 and Ω_3. Below: Atomic (b) and dressed states (c). The two dark states $|D_1\rangle$ and $|D_2\rangle$ are decoupled from $|0\rangle$.

the two degenerate dark-states. The wave functions $\psi_{D_1}(\mathbf{r},t)$ and $\psi_{D_2}(\mathbf{r},t)$ are the associated probability amplitudes for the two dark-states. An effective equation for the centre-of-mass amplitudes $\psi_i(\mathbf{r},t)$ is then given by [50]

$$i\hbar\frac{\partial\mathbf{\Psi}}{\partial t} = \left(\frac{1}{2m}(\hat{\mathbf{p}}-\mathbf{A})^2 + \mathbf{V} + \mathbf{\Phi}\right)\mathbf{\Psi}, \tag{4.2.7}$$

where $\hat{\mathbf{p}}$ is the momentum operator, m the atomic mass, and $\mathbf{\Psi}(\mathbf{r}) = (\psi_{D_1}(\mathbf{r}), \psi_{D_2}(\mathbf{r},t))^{\mathrm{T}}$ is a two-component vector. The gauge potential $\mathbf{A}$, also known as the Mead-Berry connection [63, 64] arises from the coordinate-dependence of the dark-states and is given by $\mathbf{A}_{k,n} = i\hbar\langle D_k(\mathbf{r})|\nabla D_n(\mathbf{r})\rangle$. The external potential has matrix elements $\mathbf{V}_{k,n} = \langle D_k(\mathbf{r})|\hat{V}|D_n(\mathbf{r})\rangle$, where the potential in the atomic basis is assumed to be diagonal, i.e. $\hat{V} = \sum_{i=1}^{3} V_i(\mathbf{r})|i\rangle\langle i|$. The scalar potential, defined by equation (3.7.19) is given by

$$\mathbf{\Phi}_{k,n} = \frac{\hbar^2}{2m}\sum_{l=3}^{4}\mathbf{A}_{k,l}\cdot\mathbf{A}_{l,n}, \tag{4.2.8}$$

where the index $l = 3, 4$ sums over the bright-states orthogonal to the dark-subspace. Our aim is to study a 1D gas which is subject to a disorder potential, as such we apply an additional strong transverse trapping potential to freeze out the transverse

degrees of freedom. In this limit Eq. (4.2.7) reduces to a 1D equation with a 2 x 2 matrix structure. In particular one finds $\mathbf{A} = -\hbar\kappa\cos\theta\hat{\sigma}_x$, while the scalar geometric phase $\mathbf{\Phi}$ and potential $\mathbf{V}$ are given respectively by

$$\mathbf{\Phi} = \frac{\hbar^2\kappa^2}{2m}\begin{pmatrix} \sin^2\theta & 0 \\ 0 & \sin^2(2\theta)/4 \end{pmatrix}, \tag{4.2.9}$$

$$\mathbf{V} = \begin{pmatrix} V_1 & 0 \\ 0 & V_1\cos^2\theta + V_3\sin^2\theta \end{pmatrix}, \tag{4.2.10}$$

and $V_1 = V_2$. We are justified in reducing the centre of mass dynamics to 1D as long as the transversal trap frequency is much larger than any other energy scale in the system such as temperature, collisional interactions and kinetic energy. By choosing the potentials V_i as $V_1 = \hbar\Delta(x) - \hbar^2\kappa^2/2m$ and $V_3 = -\hbar\Delta(x)(1+\cos^2\theta)/(1-\cos^2\theta) - \hbar^2\kappa^2\cos^2\theta/2m$, where the disorder potential is $\Delta(x)$ we arrive at

$$i\hbar\frac{\partial\mathbf{\Psi}}{\partial t} = \left(\frac{\hat{\mathbf{p}}_x^2}{2m} + v_D\cos(\theta)\hat{\mathbf{p}}_x\cdot\hat{\sigma}_x + \hbar\Delta(x)\hat{\sigma}_z\right)\mathbf{\Psi}, \tag{4.2.11}$$

with $v_D = \hbar\kappa/m$. The potential V_3 cannot be realised experimentally in the limit $\cos\theta \to 1$, as in this limit $V_3 \to \infty$. However, by sensible choice of parameters, this limit can be approached sufficiently closely. Equation 4.2.11 describes a massive particle with spin-orbit coupling subject to the potential $\Delta(x)$. The corresponding single particle dispersion relation for a constant potential $\Delta(x) = \Delta_0$ is given by

$$E_\pm(\mathbf{k}) = \frac{\hbar^2\mathbf{k}^2}{2m} \pm \sqrt{\hbar^2\Delta_0^2 + v_D^2\cos^2(\theta)\hbar^2\mathbf{k}^2}, \tag{4.2.12}$$

where $\pm$ refers to the upper and lower branch of dispersion respectively. Equation 4.2.12 is shown in figure 4.2. In the limit of constant mass $\Delta(x) = \Delta_0$, equation 4.2.11 is translationally invariant and can therefore be diagonalised in a plane wave basis. The two eigenstates denoted $\Psi_k^\pm$ are given by

$$\Psi_k^\pm = \begin{pmatrix} \beta_0^\pm(k) \\ 1 \end{pmatrix} e^{ikx}, \tag{4.2.13}$$

and the dimensionless quantity $\beta_{\mathrm{n}}^\pm(k)$ is defined as

$$\beta_{\mathrm{n}}^\pm(k) = \frac{\hbar\Delta_{\mathrm{n}} \pm \sqrt{(\hbar\Delta_{\mathrm{n}})^2 + (v_D\cos\theta\hbar|\mathbf{k}|)^2}}{v_D\cos\theta\hbar|\mathbf{k}|}. \tag{4.2.14}$$

4.3 Pseudospin and the Dirac equation

In the previous section it was described how using appropriately designed light-matter interactions an effective single particle equation of motion emerges for a Bose-

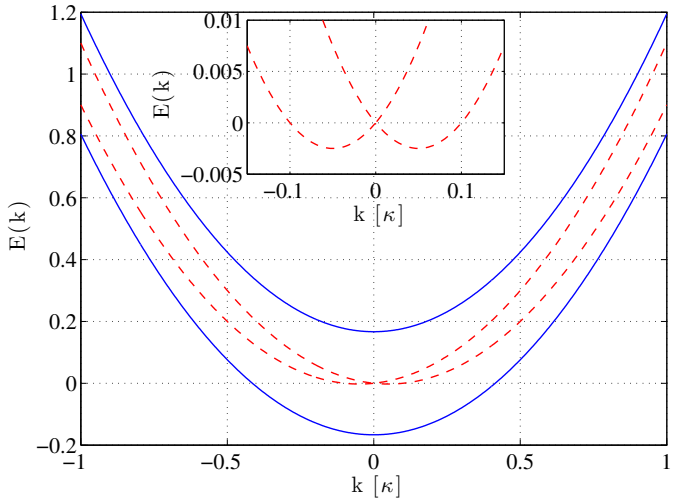

(a)

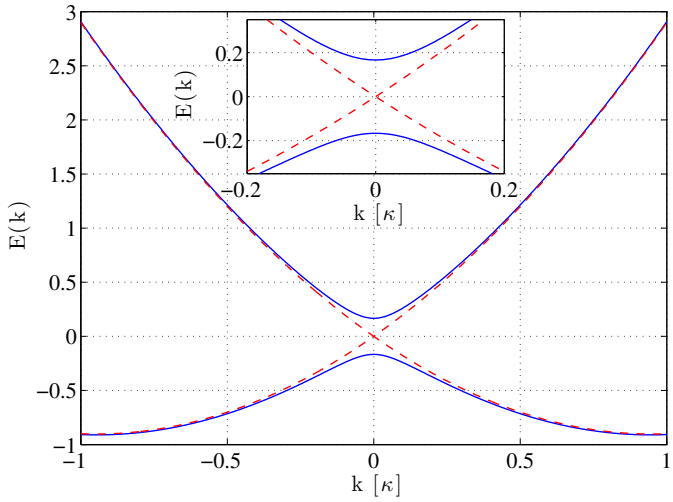

(b)

Figure 4.2: Plots showing the dispersion in the Schrödinger and Dirac limit. In (a) $\cos\theta = 0.05$, whilst for (b) $\cos\theta = 0.95$. The blue solid lines are for $\Delta_0 = mv_D^2/3\hbar$, whereas the red dashed curves $\Delta_0 = 0$.

Einstein condensate that features a pseudospin structure. Our goal is to simulate quasi-relativistic phenomena, in which case the Hamiltonian of equation (4.2.11) can be reduced to a Dirac like Hamiltonian for the dynamics of the atoms moving in the two dark states. The Dirac equation [16] describes spin one half particles, and incorporates special relativity in a consistent fashion. The implications of Dirac's famous equation are still being studied today, and is one of the jewels of theoretical physics. In covariant form it reads

$$i\hbar\partial_t\Psi(\mathbf{r}) = \left(c\sum_i \alpha_i\hat{\mathbf{p}}_i + mc^2\beta\right)\Psi(\mathbf{r}), \tag{4.3.1}$$

where c is the speed of light and the summation is taken over the coordinate space x,y,z. The spinor $\Psi(\mathbf{r})$ has 4 components, representing the two spin states in the positive and negative dispersion branch respectively. The quantities α_i and β are 4 x 4 matrices that obey the important clifford algebra:

$$\alpha_i\alpha_j + \alpha_j\alpha_i = 2\delta_{i,j}\mathbb{1}_{4\text{x}4}, \tag{4.3.2}$$

$$\alpha_i\beta + \beta\alpha_i = 0, \tag{4.3.3}$$

$$\alpha_i^2 = \beta^2 = \mathbb{1}_{4\text{x}4}. \tag{4.3.4}$$

To fulfil these conditions, we use the standard representation of α_i and β which are given by [102]:

$$\alpha_i = \sigma_x \otimes \sigma_i = \begin{pmatrix} 0 & \sigma_i \\ \sigma_i & 0 \end{pmatrix}, \tag{4.3.5}$$

$$\beta = \sigma_z \otimes \mathbb{1}_{2\text{ x }2} = \begin{pmatrix} \mathbb{1}_{2\text{ x }2} & 0 \\ 0 & -\mathbb{1}_{2\text{ x }2} \end{pmatrix}. \tag{4.3.6}$$

The effective equation of motion for the quantum gas, equation (4.2.11), differers from equation (4.3.1) due to the presence of the kinetic energy term, and also the disparate matrix size of the two Hamiltonians. However, in the limit $\langle\hat{\mathbf{p}}_x^2/2m\rangle \ll v_D\langle\hat{\mathbf{p}}_x\rangle\cos\theta$ equation (4.2.11) reduces to an effective 2 x 2 Dirac equation with a "speed of light" $c_* = v_D\cos\theta$ and a smooth space-dependent mass $\hbar\Delta(x)/c_*^2$. On the other hand, when $\langle\hat{\mathbf{p}}_x^2/2m\rangle \gg v_D\langle\hat{\mathbf{p}}_x\rangle\cos\theta$ the spin-orbit coupling becomes negligible and the problem reduces to two uncoupled massive Schrödinger particles moving in an external potential [8, 50].

Pseudospin structured Hamiltonians are by no means unique to atomic condensates, and have been studied in other condensed matter systems, the prime example being graphene [103], whose pseudospin structure arises from carrier transport in the two independent sublattices of the monolayer crystal. In this case the effective massless Dirac equation is

$$\hat{H}_D = -i\hbar v_F\boldsymbol{\sigma}_\perp\cdot\boldsymbol{\nabla}, \tag{4.3.7}$$

where v_F is the Fermi velocity and $\boldsymbol{\sigma}_\perp = \hat{e}_x\hat{\sigma}_x + \hat{e}_y\hat{\sigma}_y$ is the 2D pseudospin operator. The physics associated with the mathematical structure of Dirac-like equations offers an intriguing avenue in which to investigate relativistic effects in the ultracold low momentum regime. Already, effects such as Zitterbewegung [8] and negative reflection [52] have been described for spin-orbit coupled cold atom systems. Further, the experimental realisation of Zitterbewegung has also been reported for a system

of trapped ions [104], and recently for a Bose condensate [51].

4.4 Disorder model

It will be assumed in the following sections that the random potential is described by local, Gaussian white noise with

$$\overline{\Delta(x)\Delta(x')} = \Gamma v_D \delta(x - x'), \quad \overline{\Delta(x)} = 0, \tag{4.4.1}$$

where the overline denotes disorder average and all higher correlation functions factorize. For vanishing SO coupling one expects exponential localization of the particles according to the usual Anderson scenario [90,105–108]. On the other hand, any small SO coupling dominates in the region of small kinetic energy. Neglecting the kinetic energy term proportional to $\langle \hat{\mathbf{p}}_x^2 \rangle$ in equation (4.2.11), rather than the SO coupling, one obtains an effective Dirac equation for a particle with a spatially random mass. This model, also known as the fluctuating gap model [93, 94] is characterised by a Dyson singularity in the DOS [109], which is a consequence of the chiral symmetry of equation (4.2.11) without the kinetic energy term, and which leads to a power-law dependence of the correlation function. The absence of any exponential contribution to the correlation functions can most easily be seen by considering the divergent behaviour of the localization length $L_{\mathrm{loc}} = 1/\gamma(E)$ as a function of the energy E, which is inversely proportional to the Lyapunov exponent $\gamma(E)$. The latter can be related to the integrated DOS $N(E)$ by the associated Kramers-Kronig relation [110]

$$\gamma(E) = \frac{1}{\pi} \int dE' \frac{N(E')}{E' - E}, \tag{4.4.2}$$

where

$$N(E) \approx \frac{1}{\ln^2 |E|}. \tag{4.4.3}$$

The DOS $\rho(E) = \mathrm{d}N/\mathrm{d}E$ of the FGM exhibits a singular behaviour when approaching the band-centre, i.e. $E \to 0$, known as the Dyson singularity introduced above [90]. This implies that that the localization length $\zeta(E \approx 0)$ exhibits a logarithmic divergence as the energy E approach the band centre.

4.5 Experimental realization

Let us turn our attention to a possible experimental realization based on an ensemble of optically addressed ultracold ^{87}Rb atoms. First, we discuss how to single out the tripod linkage pattern as shown in figure 4.3. We choose the ground-states as $|1\rangle = |F = 2, m_F = -1\rangle$, $|2\rangle = |F = 2, m_F = +1\rangle$ and $|3\rangle = |F = 1, m_F = 0\rangle$ of the

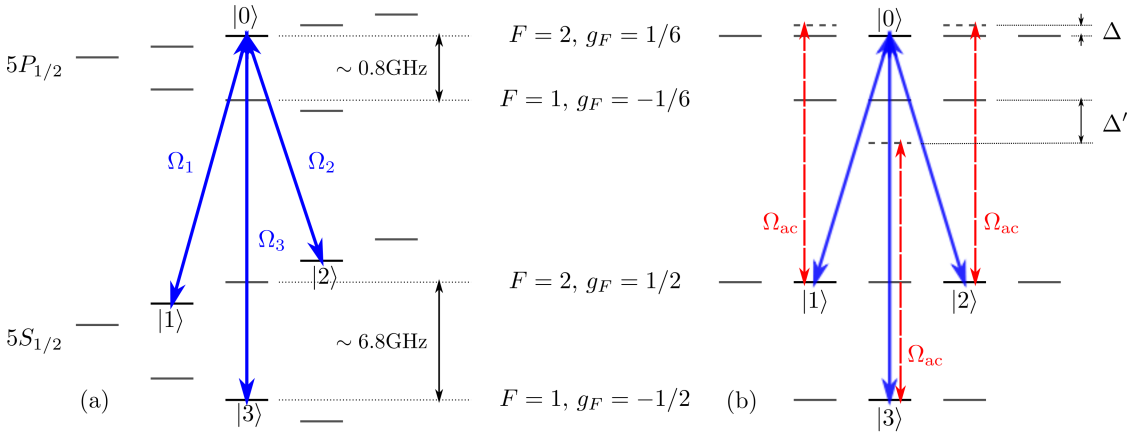

Figure 4.3: Experimental implementation in ^{87}Rb. A homogeneous magnetic field creates different Zeeman splittings in the hyperfine manifolds to isolate a single tripod-linkage pattern. (b) Off-diagonal disorder with $V_- = V_2$ is created by a single field Ω_{AC}. Opposite, large detunings Δ and Δ' lead to opposite signs of the ac-Stark shifts of states $|1\rangle$ and $|2\rangle$ with respect to that of state $|3\rangle$. Disorder is created by a spatially fluctuating amplitude of Ω_{AC}, realised, e.g. by a speckle pattern [111].

$5S_{1/2}$ ground-state manifold of ^{87}Rb. These states are coupled via $\sigma^{\pm}$ polarised ($\Omega_{1,2}$) or π-polarised light (Ω_3), respectively, to the excited state $|0\rangle = |F = 2, m_F = 0\rangle$ of the $5P_{1/2}$-manifold. To prevent the coupling fields from driving other transitions we apply an additional magnetic field to induce a Zeeman splitting of the different m_F-states which due to different Landé-g_F factors will be shifted out of resonance. It should be noted that a generalisation to a multiple-state configuration including all Zeeman-levels or a different choice of states are possible and have been experimentally realised [112, 113].

The disorder potential can be created using speckle potentials [105, 107] or incommensurate optical lattices [106], which induce spatially varying ac-Stark shifts. Denoting the amplitude of the speckle potential Ω_{AC}, for far off-resonant dressing of the atoms with Ω_{AC} the ground-states experience an ac Stark-shift proportional to $\Omega_{\mathrm{AC}}^2/\Delta$ (for states $|1\rangle$, $|2\rangle$) and $\Omega_{\mathrm{AC}}^2/\Delta'$ (for state $|3\rangle$), where Δ and Δ' denote the detunings of the speckle field from the respective resonance. Note that the signs of the two shifts are opposite for states $|1\rangle$, $|2\rangle$ and $|3\rangle$ if sgn(Δ)=-sgn(Δ') (see figure 4.3(b)). This can easily be achieved in ^{87}Rb as the hyper-fine energy splitting in the $5S_{1,2}$-manifold is substantially larger than in the $5P_{1/2}$-manifold. This results in an opposite sign of the potential for the dark-states necessary to generate the mass-disorder for the spinors. Any finite offset of the mass can be eliminated by an additional two-photon detuning of the coupling fields $\Omega_{1,2,3}$. Note that the fields generating the disorder do not contribute to the generation of the dark-states and hence do not induce any non-adiabatic dynamics in the dark-state subspace.

Finally, the angle θ, which governs the effective strength of the spin-orbit coupling, depends only on the ratio of the Rabi frequencies and as such it is insensitive to overall amplitude fluctuations as long as the fields are derived from the same source.

4.6 Wave packet dynamics

It was shown in the previous section how the generation of a pseudo spin structured Hamiltonian can be accomplished by the choice of appropriately designed laser fields, including the disorder potential that we wish to understand. It is not immediately obvious how one should choose the parameters of the problem to access the two momentum regimes, Schrödinger and Dirac. To answer this question we introduce the dimensionless units of length $\xi = \Gamma x/v_D$ and the dimensionless time $\tau = \Gamma t$, which transforms equation 4.2.11 into

$$i\frac{\partial}{\partial\tau}\mathbf{\Psi} = -\frac{\hbar\Gamma}{2mv_D^2}\frac{\partial^2}{\partial\xi^2}\mathbf{\Psi} - i\cos\theta\hat{\sigma}_x\frac{\partial}{\partial\xi}\mathbf{\Psi} + \tilde{\Delta}(\xi)\hat{\sigma}_z\mathbf{\Psi}, \tag{4.6.1}$$

where $\tilde{\Delta}(\xi) = \Delta(\xi)/\Gamma$. To understand the dynamics associated with equation 4.6.1, numerical simulations of the wave packet dynamics of an initially localized gaussian state of the form $\mathbf{\Psi}(x, t = 0) = (2\sqrt{2\pi}\mathrm{erf}(L/\sqrt{2}L_0))^{-1/2}\exp(-x^2/4L_0^2)(1, i)^T$ were performed where the only adjustable parameter is $\cos\theta$, which encapsulates the spin-orbit coupling strength. The numerical simulations were performed using FORTRAN. An outline of the calculations can be found in Appendix A.

Figure 4.4 shows the results of the numerical integration of equation 4.2.11. By propagating the gaussian wave packet in a random disorder potential and averaging the final density $\mathbf{\Psi}^\dagger(\xi, t_F)\mathbf{\Psi}(\xi, t_F)$, the localization properties of the spin-orbit coupled quantum gas can be understood. Figures 4.4 (a) and (b) show the Schrödinger limit where $\cos\theta = \{0.01, 0.05\}$ respectively. The red straight line is an exponential fit given by $\exp(-|x|/L_{\mathrm{loc}})$, and the localization length was found to be given by $L_{\mathrm{loc}} \approx 12v_D/\Gamma$. The crossover region is shown in figures 4.4 (c) with $\cos\theta = 0.5$. Here, neither Anderson nor anomalous localization can be clearly discerned. The Dirac limit with $\cos\theta = 1.0$ is shown in figure 4.4 (d), where the red straight line is the fit $|\xi|^{-3/2}$. The inset shows the same data in semi-log, where it can be seen that there is no linear region, and hence no Anderson localization in the Dirac regime.

4.7 Scattering theory for a model disorder potential

In order to motivate a clearer understanding of the role of the pseudo spin structured Hamiltonian given by equation (4.2.11), we analyse the propagation of a single plane wave (see equations (4.2.13) and (4.2.14)) through the disorder potential, which is

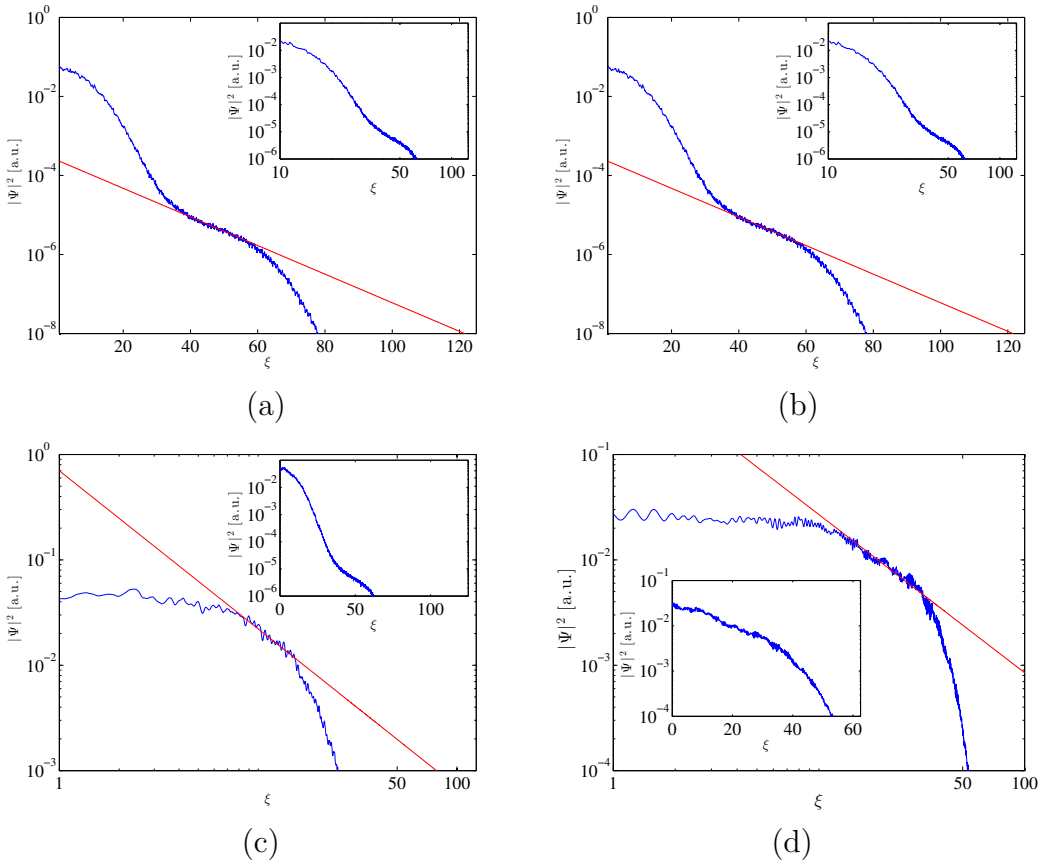

Figure 4.4: Density profiles of an initially localized wave packet of size $L_0\Gamma/v_D = 7.5$ after a time evolution $t_F\Gamma = 80$ according to equation (4.6.1) with $\hbar\Gamma/mv_D^2 = 0.1$, after averaging over 100 independent disorder realisations. The system size was taken to be $2L\Gamma/v_D = 240$ and $n_{\text{kinks}} = 6.25\Gamma/v_D$, i.e. $\Delta_0^2/\Gamma^2 = 6.25$. Figure (a) and (b) show the Schrödinger limit with $\cos\theta = (0.01, 0.05)$ respectively. The red (straight) line corresponds to an exponential fit showing the expected Anderson localization. The inset shows the same density in log-log. Figure (c) shows the density in the crossover regime with $\cos\theta = 0.5$ in log-log representation (semi-log in the inset) and a power-law fit (red straight line) with exponent 3/2. Finally, (d) shows the Dirac limit with $\cos\theta = 1$ in log-log; the power-law behaviour is clearly visible for large distances $\xi \gg 1$.

modelled as a series of potential barriers of independent heights. The methodology which we will follow here has been used to study the one-dimensional transport properties of Dirac Hamiltonians [100], where it was shown that delocalized states can emerge under special conditions. The model we present differs from that discussed in [100] as the disorder studied here is in the mass term of the Dirac equation, further our Hamiltonian includes a kinetic energy term.

To calculate the transport properties of the one-dimensional system, (see figure 4.5 (a)) consider the scattering of waves from a single potential barrier. The amplitudes for the incoming/outgoing waves on the left are given by $\psi_{\text{L}}^{\text{in}}$ and $\psi_{\text{L}}^{\text{out}}$, whilst the amplitudes for the respective waves on the right of the barrier are given by $\psi_{\text{R}}^{\text{in}}$ and

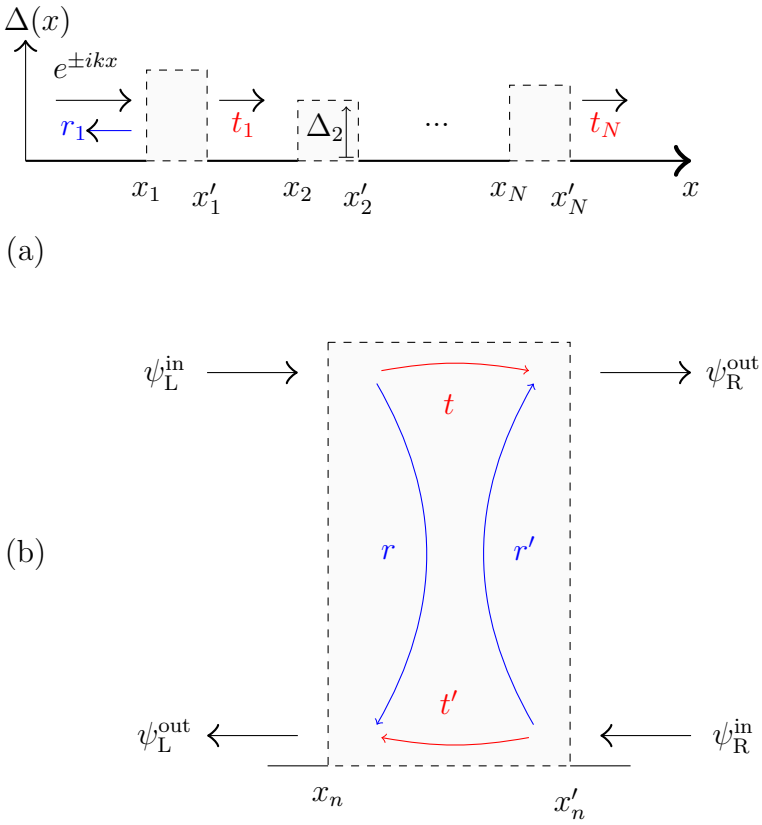

Figure 4.5: The random mass $\Delta(x)$ that appears in equation 4.2.11 is modelled as a series of barriers of height Δ_{n} in (a). For each barrier, there are four scattering processes: reflection, r', r, transmission t', t for waves travelling to the left/right respectively, as shown in (b).

$\psi_{\mathrm{R}}^{\mathrm{out}}$. The state vector for waves on the left and right can be written

$$\psi_\lambda(x) = \psi_\lambda^{\mathrm{in}} \begin{pmatrix} 1 \\ 1 \end{pmatrix} e^{+ikx} + \psi_\lambda^{\mathrm{out}} \begin{pmatrix} -1 \\ 1 \end{pmatrix} e^{-ikx}, \tag{4.7.1}$$

where $\lambda = \mathrm{L,R}$. On the other hand, the corresponding state for waves inside the barrier is given by

$$\psi_{\mathrm{C}}(x) = \psi_{\mathrm{C}}^{\mathrm{in}} \begin{pmatrix} \beta_{\mathrm{n}}^{+}(k) \\ 1 \end{pmatrix} e^{+ik_{\mathrm{n}}x} + \psi_{\mathrm{C}}^{\mathrm{out}} \begin{pmatrix} \beta_{\mathrm{n}}^{-}(k) \\ 1 \end{pmatrix} e^{-ik_{\mathrm{n}}x}, \tag{4.7.2}$$

where the wave vector inside the n^{th} barrier is denoted k_{n} and $\beta_{\mathrm{n}}^{\pm}(k)$ is defined per equation 4.2.14. The amplitudes that appear in equations 4.7.1 and 4.7.2 are related to one another via the relationships $\psi_{\mathrm{L}}^{\mathrm{out}} = r\psi_{\mathrm{L}}^{\mathrm{in}} + t'\psi_{\mathrm{R}}^{\mathrm{in}}$ and $\psi_{\mathrm{R}}^{\mathrm{out}} = t\psi_{\mathrm{L}}^{\mathrm{in}} + r'\psi_{\mathrm{R}}^{\mathrm{in}}$, where r', r and t', t are the reflection and transmission coefficients for waves travelling to the left/right respectively. Writing these two relationships in matrix form yields the

scattering or S-matrix [114]:

$$\begin{pmatrix} \psi_{\mathrm{L}}^{\mathrm{out}} \\ \psi_{\mathrm{R}}^{\mathrm{out}} \end{pmatrix} = \mathrm{S} \begin{pmatrix} \psi_{\mathrm{L}}^{\mathrm{in}} \\ \psi_{\mathrm{R}}^{\mathrm{in}} \end{pmatrix}, \qquad \text{with} \qquad \mathrm{S} = \begin{pmatrix} r & t' \\ t & r' \end{pmatrix}. \tag{4.7.3}$$

The scattering matrix S defined in equation 4.7.3 is for our single channel problem a 2×2 matrix whose entries can be related to the probability of reflection and transmission by $R = |r|^2$ and $T = |t|^2$ respectively. Probability flux conservation requires that $\mathrm{S}^\dagger\mathrm{S} = \mathbb{1}$. For a multi-channel scattering problem the quantities t and r are matrix valued, then calculation of the transmission T requires summing over all channels of the problem.[2] Rather than computing S for our system, it is more convenient to work with the transfer matrix, M. The transfer matrix instead considers waves that are reflected or transmitted from one side in terms of waves reflected and transmitted from the other side of the potential barrier, in which case we can formulate the scattering problem as

$$\begin{pmatrix} \psi_{\mathrm{R}}^{\mathrm{out}} \\ \psi_{\mathrm{R}}^{\mathrm{in}} \end{pmatrix} = \mathrm{M} \begin{pmatrix} \psi_{\mathrm{L}}^{\mathrm{out}} \\ \psi_{\mathrm{L}}^{\mathrm{in}} \end{pmatrix}, \qquad \text{with} \qquad \mathrm{M} = \begin{pmatrix} \frac{1}{t^*} & -\frac{r^*}{t^*} \\ -\frac{r}{t} & \frac{1}{t} \end{pmatrix}. \tag{4.7.4}$$

Calculation of wave transport across the N scattering potentials is reduced to finding the product of the N transfer matrices that constitute the disorder potential. The calculation of M for the n^{th} potential barrier with the underlying Hamiltonian equation 4.2.11 is performed using the boundary conditions of the problem: $\psi_{\mathrm{L}}(x_n) = \psi_{\mathrm{C}}(x_n)$, $\psi_{\mathrm{C}}(x'_n) = \psi_{\mathrm{R}}(x'_n)$, $\psi'_{\mathrm{L}}(x_n) = \psi'_{\mathrm{C}}(x_n)$ and $\psi'_{\mathrm{C}}(x'_n) = \psi'_{\mathrm{R}}(x'_n)$. Denoting the transfer matrix $\mathrm{M_n}$, and using equations 4.7.1 and 4.7.2 one finds the matrix elements are given by

$$(\mathrm{M_n})_{11} = \left(\cos(k_{\mathrm{n}}\delta) + i\frac{k_{\mathrm{n}}^2 + k^2}{2k_{\mathrm{n}}k} \sin(k_{\mathrm{n}}\delta) \right) e^{-ik\delta}, \tag{4.7.5}$$

$$(\mathrm{M_n})_{12} = i\frac{k_{\mathrm{n}}^2 - k^2}{2k_{\mathrm{n}}k} \sin(k_{\mathrm{n}}\delta) e^{-ik\alpha}. \tag{4.7.6}$$

The other two matrix elements are given by $(\mathrm{M_n})_{22} = (\mathrm{M_n})^*_{11}$ and $(\mathrm{M_n})_{21} = (M_{\mathrm{n}})^*_{12}$ and we define $\delta = x'_{\mathrm{n}} - x_{\mathrm{n}}$ and $\alpha = x'_{\mathrm{n}} + x_{\mathrm{n}}$. To investigate the transport properties of the one-dimensional system we also require the displacement operator that maps the free propagation of the vector $(\psi_{\mathrm{L}}^{\mathrm{out}}, \psi_{\mathrm{L}}^{\mathrm{in}})^T$ over a distance $\xi = x_{\mathrm{n}+1} - x_{\mathrm{n}'}$, which is given by $\mathrm{D} = \mathrm{diag}\{e^{-ik\xi}, e^{+ik\xi}\}$. The full transfer matrix $\mathcal{M}$ then consists of an

[2] For n incoming modes and n' outgoing modes r and t are n x n and n' x n matrices respectively, and the total transmission is calculated from $T = \mathrm{tr}(tt^\dagger)$.

altering product of the matrices $\mathrm{M_n}$ and D:

$$\mathcal{M} = \mathrm{M}_N \mathrm{D} \mathrm{M}_{N-1} \mathrm{D} \cdots \mathrm{M}_2 \mathrm{D} \mathrm{M}_1. \tag{4.7.7}$$

In general, the calculation of equation 4.7.7 can be performed using the unimodular property of transfer matrices or alternately numerical simulations. The transmission probability for the full chain is then calculated as $\mathcal{T} = 1/|\mathcal{M}_{11}|^2$, and the Lyapunov exponent, equation 4.4.2 (or inverse localization length, L_{loc}) is related at zero temperature to $\mathcal{T}$ by

$$\gamma = \frac{1}{L_{\mathrm{loc}}} = -\lim_{L_0 \to +\infty} \frac{\langle \ln \mathcal{T} \rangle}{L_0}, \tag{4.7.8}$$

where for a system comprised of N_{b} barriers $L_0 = N_{\mathrm{b}}(\delta + \xi)$ defines the total length of the one-dimensional system, and $\langle \cdots \rangle$ denotes averaging over independent realisations of the disorder potential.

In figure 4.6 (a) and (b) we see the results of the numerical computation of equations 4.7.7 and 4.7.8. The localization length L_{loc} is plotted as a function of spin-orbit coupling strength $\cos\theta$ in figure 4.6 (a). It can be seen that as the coupling becomes stronger, the localization length increases. The inset to figure 4.6 (a) shows the Lyapunov exponent γ. As can be seen at large spin-orbit coupling, $\gamma \to 0$, and the particle is delocalized. Further, one can also investigate the energy dependence of the localization length within the one-dimensional model. Figure 4.6 (b) shows L_{loc} plotted as a function of the dimensionless variable E/mv_D^2 for different values of $\cos\theta$. One can see that L_{loc} is a monotonically increasing function in each case, and the increasing coupling strength $\cos\theta$ = (0.05,0.5,095) causes a larger localization length for a given value of E/mv_D^2.

Each data point in figure 4.6 (a) and (b) was obtained by averaging over 1000 independent realisations of the disorder with 1000 individual transfer matrices. The disorder was generated uniformly on [-2,2] such that the mean mass was typically $\langle \Delta(x) \rangle \approx 10^{-3} mv_D^2/\hbar$.

To gain a qualitative understanding of the inherent physics, we can consider the nature of the tunnelling dynamics in the spin-orbit coupled Hamiltonian, equation 4.2.11. If one considers a single quantum particle scattering from an impurity potential, then for a non-relativistic particle one expects an evanescent mode to propagate inside the barrier. However, this assumes that the underlying particle dynamics is governed by a Schrödinger like equation with diagonal disorder. The tunnelling

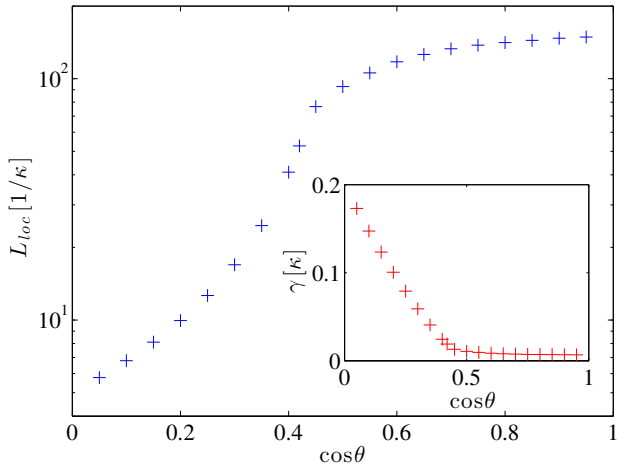

(a)

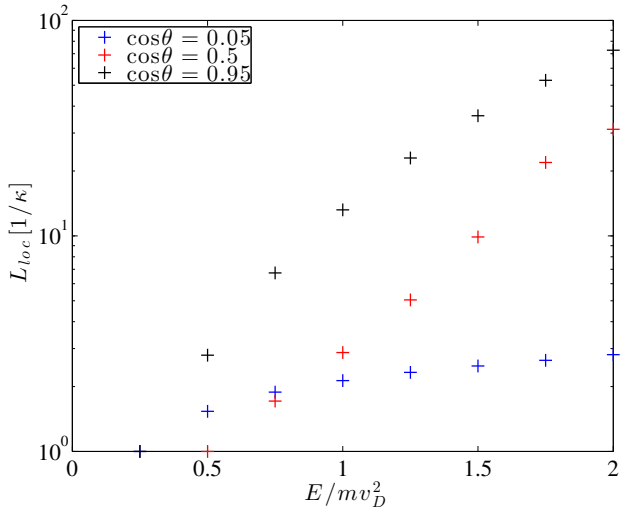

(b)

Figure 4.6: The localization length L_{loc} is shown in (a), as calculated from equation 4.7.7. The units of length are $1/\kappa$, the energy was chosen to be $E = 2mv_D^2$. The length scales were chosen such that $\delta = \xi = 0.4\kappa^{-1}$. In (b) the localization length is plotted as a function of energy for fixed spin-orbit strength with $\cos\theta$=(0.05,0.5,0.95) respectively.

behaviour of relativistic particles on the other hand leads to the counterintuitive situation whereby the reflection amplitude is exactly zero, independent of the height of the potential barrier, a phenomenon known as Klein tunnelling [115]. It is this behaviour which leads to the increase in the localization length via delocalization.

4.8 Power law correlation derivation

It was shown previously in section 4.6 how a power law scaling is obtained from the density of a wave packet after long-time propagation with disorder in the Dirac limit. This unusual effect is connected to the solution of equation (4.2.11) at zero energy by the so called fluctuating gap model (FGM) [91, 92]. To understand this effect,

we perform the transformation $\mathbf{\Psi} = \exp(-imc_*x\hat{\sigma}_x/\hbar)\mathbf{\Phi}$ with equation (4.2.11), yielding the transformed Hamiltonian

$$\mathcal{H} = -\frac{\hbar^2}{2m}\frac{\partial^2}{\partial x^2} - \frac{mc_*^2}{2} + \hbar\Delta(x)[\cos(2\eta)\hat{\sigma}_z + \sin(2\eta)\hat{\sigma}_y], \tag{4.8.1}$$

which obeys the Schrödinger equation $i\hbar\dot{\mathbf{\Phi}} = \mathcal{H}\mathbf{\Phi}$, where $\eta = mc_*x/\hbar$. Next we introduce the ansatz $\mathbf{\Phi} = \chi_+\exp(i\eta) + \chi_-\exp(-i\eta)$ into equation (4.8.1) above, which gives

$$\begin{aligned} i\hbar\Big(\dot{\chi}_+e^{i\eta} + \dot{\chi}_-e^{-i\eta}\Big) =& \hbar\Delta(x)[\cos(2\eta)e^{i\eta}\hat{\sigma}_z\chi_+ + \cos(2\eta)e^{-i\eta}\hat{\sigma}_z\chi_- \\ &+ \sin(2\eta)e^{i\eta}\hat{\sigma}_y\chi_+ + \sin(2\eta)e^{-i\eta}\hat{\sigma}_y\chi_-] - \frac{\hbar^2}{2m}\Big(\chi_+''e^{i\eta} \\ &+\chi_-''e^{-i\eta}\Big) + i\hbar c_*\Big(\chi_-'e^{-i\eta} - \chi_+'e^{i\eta}\Big). \end{aligned} \tag{4.8.2}$$

We can simplify equation (4.8.2) by dropping terms proportional to $\partial_x^2\chi_\pm$ and fast oscillating exponentials using the assumption $\hbar\Gamma/mv_D^2 \ll \cos^2\theta$. Collecting terms using the four component spinor $\boldsymbol{\chi} = (\chi_+, \chi_-)^T$ one obtains

$$i\hbar\dot{\boldsymbol{\chi}} = -i\hbar c_*\hat{\tau}_z \otimes \mathbb{1}\frac{\partial\boldsymbol{\chi}}{\partial x} + \frac{\hbar\Delta(x)}{2}\Big(\hat{\tau}_x \otimes \hat{\sigma}_z + \hat{\tau}_y \otimes \hat{\sigma}_y\Big)\boldsymbol{\chi}, \tag{4.8.3}$$

and $\hat{\sigma}_i$, $\hat{\tau}_i$, $i \in \{x, y, z\}$ act on the momentum or internal degree of freedom, respectively[3]. Equation (4.8.3) is a generalisation of the model considered in [91, 92]. The zero-energy (mid-gap) state can be found by looking for solutions with $E = 0$. In the $E = 0$ limit equation (4.8.3) can be simplified to

$$\frac{d\boldsymbol{\chi}}{dx} = \frac{\Delta(x)}{2c_*}\big[\hat{\tau}_y \otimes \hat{\sigma}_z - \hat{\tau}_x \otimes \hat{\sigma}_y\big]\boldsymbol{\chi}. \tag{4.8.4}$$

The (unnormalized) solution is given by

$$\boldsymbol{\chi}(x) = \exp\left\{\frac{\hat{\alpha}}{2c_*}\int_{-\infty}^{x} dx'\Delta(x')\right\}\boldsymbol{\chi}_0, \tag{4.8.5}$$

the matrix $\hat{\alpha} = \hat{\tau}_y \otimes \hat{\sigma}_z - \hat{\tau}_x \otimes \hat{\sigma}_y$ and has eigenvalues (-2,0,0,2). By choosing $\boldsymbol{\chi}_0$ to be an eigenvector with eigenvalue ± 2 we obtain power-law intensity correlations with scaling $C(x) \approx (\Gamma|x|/v_D)^{-3/2}$, in agreement with the numerical simulations presented in section 4.6.

[3]Here one has the definitions $\hat{\tau}_x = \begin{pmatrix} 0 & 1 \\ 1 & 0 \end{pmatrix}$, $\hat{\tau}_y = \begin{pmatrix} 0 & -i \\ i & 0 \end{pmatrix}$ and $\hat{\tau}_z = \begin{pmatrix} 1 & 0 \\ 0 & -1 \end{pmatrix}$.

4.9 Density of states for tripod-coupled atoms with disorder

Let us now turn our attention to the role of the density of states of the spin-orbit coupled system with off-diagonal disorder, equation (4.6.1), to investigate what determines the crossover from Anderson-like to anomalous localization. For a free Schrödinger particle the density of states has a singularity at $\omega = 0$. Figure 4.1 shows how the presence of the spin-orbit coupling shifts the band edge of the spectrum away from zero to $\omega_{\text{edge}} = -mc_*^2/2 = -mv_D^2 \cos^2\theta/2$. In the Dirac limit one has $mv_D^2 \to \infty$, and the band edge moves to infinity. In the pure Schrödinger case weak disorder leads to a smoothing of the band edge peak [116], making the density of states finite, which is a required condition for the observation of the exponentially localized state [117]. To investigate the density of states for our spin-orbit coupled system in the presence of disorder we numerically simulate equation (4.6.1). As will be the case in any experiment we assume for this a discretized model and furthermore a finite disorder-correlation length[4]. A smaller correlation length is accompanied by slower numerical convergence of the density of states, see [93] for details. Localized and extended states are separated by a mobility edge in momentum space associated with using a finite disorder correlation length, but was chosen large enough not to affect the results. Figure 4.7 shows the density of states for different values of the dimensionless quantity $\hbar\Delta_0/mc_*^2$, where Δ_0 characterises the root mean square value of the Gaussian disorder amplitude in the discretized model. One can relate it to the continuum quantity via $\Gamma = \Delta_0^2/(v_D^2 n_{\text{kinks}})$, with n_{kinks} being the impurity density.

For $mc_*^2 \to \infty$, i.e. in the Dirac limit one recognises a Dyson-like singularity at $\omega = 0$. The emergence of a Dyson singularity can in general be taken as an indicator for anomalous, that is, non-exponential localization properties [90]. In the fluctuating gap model the Dyson singularity has been shown to lead to power-law correlations [91]. As $mc_*^2 \sim mv_D^2 \cos^2\theta$ decreases the band edge approaches the singularity and consequently the singularity is smoothed out. It is noted that a true singularity is present only in the exact Dirac limit, but as can be seen from figure 4.7 a pronounced peak survives as long as the spin-orbit coupling, i.e. mc_*^2 is sufficiently large. In this limit one finds a localization scenario where power-law correlations dominate for very long time scales. In order to quantify this we define, following [93], the width $\Delta\omega_{\text{D}}$ of the Dyson singularity as the minimum of the den-

[4]The numerical calculation used an exponentially correlated disorder with $\overline{\Delta_i \Delta_j} = \Delta_0^2 \Delta x / L_{\text{corr}} \exp\{-|i-j|\Delta x/2L_{\text{corr}}\}$ with correlation length $L_{\text{corr}} = 2\Delta x$, where Δx is the discretization length.

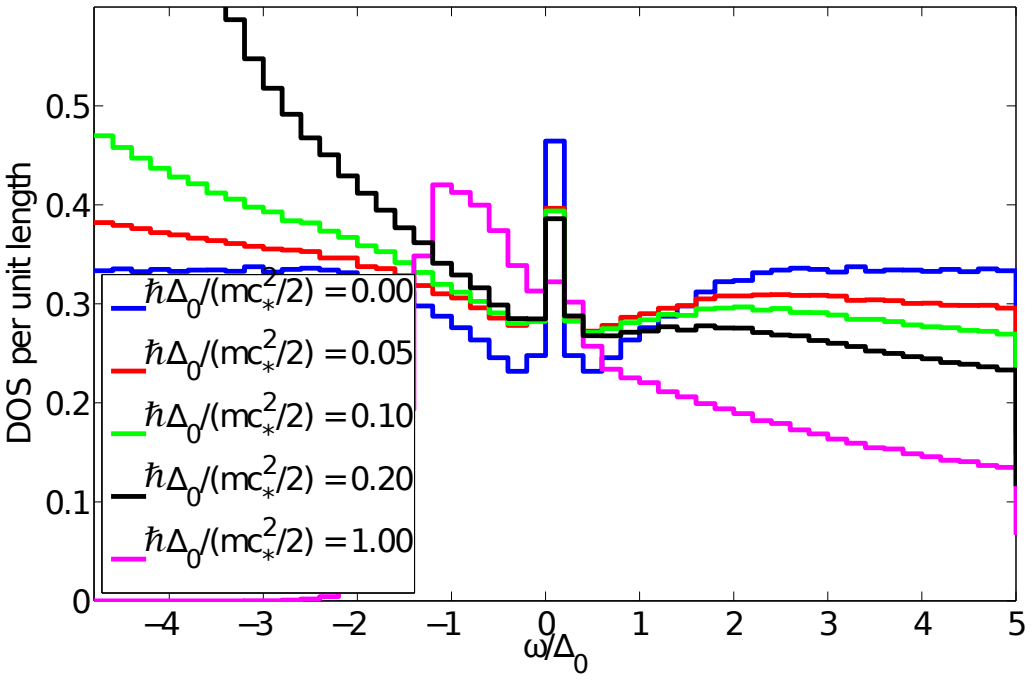

Figure 4.7: Density of states per unit length for a spin-orbit coupled massive Schrödinger particle in a random potential with a finite disorder correlation length for various values of the band edge mc_*^2. As the band edge moves closer to $\omega = 0$, the washing out of the Dyson singularity of the free Dirac case (blue line) becomes more prominent, until the almost purely disordered Schrödinger case (magenta line) is reached. Data provided by Dr Johannes Otterbach [111].

sity of states, giving $\Delta\omega_{\mathrm{D}} = \alpha\Gamma$, where $\alpha = 0.6257\ldots$. Hence, to obtain dynamics associated with the Dyson singularity the condition

$$mv_D^2 \cos^2\theta \gg \hbar\Gamma \tag{4.9.1}$$

should be satisfied in order to ensure that the band edge is sufficiently far away from the singularity.

The emergence of the Dyson singularity affects the dynamics of the system around $\omega = 0$. Experimentally this is reflected in a drastically different behaviour of the density of profile after a long-time expansion of an initially localized wave packet. From equation (4.9.1) we expect that for $\cos^2\theta \gg \hbar\Gamma/mv_D^2$ the effective Dirac dynamics along with the creation of anomalous power-law correlations dominates the system, whereas in the opposite limit we expect Anderson like localization. The power-law behaviour of correlations will also be reflected in the density distribution of an expanding wave packet, which is an important experimentally measurable quantity. To see this, we note that in the power-law case there is no intrinsic length scale.

As such we expect that an initially well localized wave packet will show the same behaviour as a wave packet with an initial delta-distribution $\boldsymbol{\Psi}(x, t = 0) = \delta(x)\boldsymbol{\chi}$, where $\boldsymbol{\chi}$ is a vector of unit length. The time-evolution of this wave packet is given by

$$\boldsymbol{\Psi}(x,t) = \sum_n [\boldsymbol{\phi}_n^*(0) \cdot \boldsymbol{\chi}]\boldsymbol{\phi}_n(x)e^{-i\omega_n t}, \tag{4.9.2}$$

where $\boldsymbol{\phi}_n(x)$ is the stationary state of a particular disorder realization belonging to the state of energy ω_n. The long-time evolution is then given by

$$\overline{|\Psi(x, t \to \infty)|^2} = \sum_n \overline{|\boldsymbol{\phi}_n(x)|^2 |\boldsymbol{\phi}_n(0)|^2}. \tag{4.9.3}$$

The right hand side of equation 4.9.3 corresponds to the localization criterion defined in [90], and it is sufficient to investigate the long-time behaviour of the density in order to determine localization properties. In the Schrödinger limit all correlations of the type $C_n(x) = \overline{|\boldsymbol{\phi}_n(x)|^2 |\boldsymbol{\phi}_n(0)|^2}$ decay exponentially [90], i.e. $C_n(x) \sim e^{-|x|/L_{\text{loc}}}$, where the localization length L_{loc} is at most of the order of the system size. On the other hand, within the FGM the typical localization length of correlation functions scales as $L_{\text{loc}} \sim |\ln \epsilon|^2$ [92], where ϵ is defined as the distance from the centre of the band. Clearly for small energies this length will be much larger than the size of the system, consequently the correlation functions will be of a similar form to the zero-energy correlation function decaying with a power-law scaling as $C_n(x) \sim (\Gamma|x|/v_D)^{-3/2}$ at large distances [92]. Accordingly, one expects quite different scaling behaviour in the two different limits of large and small spin-orbit coupling.

4.10 Summary

In this chapter the 1D dynamics of a spin-orbit coupled massive Schrödinger particle subject to a δ-correlated disorder potential was investigated. It was shown that for weak spin-orbit coupling the system is equivalent to two independent Schrödinger particles with diagonal disorder. In the opposite limit the system is described by the random-mass Dirac model with off-diagonal disorder. The model can be implemented with current state of the art techniques by using atomic dark-states or Raman transitions [42] in cold atom systems. It was found that by calculating the system's density of states and direct numerical simulation of the time evolution of an expanding wave packet there is a crossover from an exponential (Anderson) localized regime to a power-law regime governed by a Dyson singularity when varying the strength of the spin-orbit coupling relative to the disorder strength. Further, the dependence of the localization length on the spin-orbit coupling strength was investigated using a transfer matrix technique. It was observed that for fixed energy the localization length tends to increase as one approaches the Dirac limit.

The crossover can be observed by expansion of an initially localized wave packet with an appropriately chosen width of the momentum distribution in a random potential. Future investigations should include interaction effects, which will allow the study of models such as the relativistic Thirring model [118] for fermions as well as for bosons with a random mass. Interactions may well accelerate the crossover to non-exponential behaviour as they tend to delocalize particles. It is also interesting to investigate whether the model can be recast in terms of a critical theory similar to those studied in phase transitions [119], to study the nature of the crossover.

Chapter 5

Simulating an Interacting Gauge Theory

5.1 Introduction

Our understanding of the fundamental interactions between elementary particles is founded on gauge fields. The role of the gauge field is to mediate the interaction between particles. The simplest example we know of is electromagnetism where charged particles interact through exchanging virtual photons. The Coulomb potential between charged particles is encompassed by this gauge theory which can be recast in the familiar form of Maxwell's equations in the classical limit. Gauge theories are not restricted to electromagnetism only. The interactions in nuclei are governed by more complicated objects as far as gauge fields are concerned. There one has to use higher dimensions which typically requires a non-Abelian theory, such as the Yang-Mills field for the gluons [15]. For all this to hold, the gauge fields must be dynamical. In other words we must be allowed to construct a Lagrangian which also describes the propagation of the gauge field in vacuum. Solving the full quantum dynamics of such systems is a formidable task [120]. The solution could be to design a special purpose quantum simulator [1].

Recently, the first few theoretical proposals in this direction have appeared [54, 121–123], where it was shown that it is in principle possible to simulate a dynamical gauge theory using cold atoms trapped in optical lattices. These schemes require different atomic species that play the role of quantum matter, represented by (for example) the fermionic field $\hat{\Psi}(\mathbf{r})$ and also bosonic gauge fields $\hat{a}$. Smaller steps towards the ambitious goal of simulating aspects of the standard model using possibly less demanding experimental techniques may provide some important insights (see

for instance [54, 124, 125]). A more modest problem that generated intense interest in the late 1990s was the quest for finding a pure gauge theory with solutions given by the one-dimensional analog of the well-known two-dimensional anyons [126]. The first attempt in this direction [127] failed to describe one-dimensional anyon solutions [128], but the associated semiclassical, non-linear model of the interacting gauge theory supported chiral solitons, as shown by Aglietti, Griguolo, Jackiw, Pi and Seminara (AGJPS) [129]. The generation of chiral solitons is clearly also an interesting goal to pursue in its own right due to the unconventional coherent transport mechanisms in the superfluid regime.

It will be demonstrated how under proper conditions conveniently engineered laser fields similar to those employed in Refs. [2–4] can induce an effective density-dependent vector potential in a weakly-interacting ultracold Bose gas, which constitutes the semiclassical limit of an interacting gauge theory for bosons. When the system is tightly confined such that it forms a quasi-one-dimensional gas, it is described, in a one-to-one fashion, by the AGJPS gauge theory [129]. Further, density-dependent gauge fields are shown to lead to remarkable consequences, including density-dependent persistent currents in ring geometries, drifts in the free expansion dynamics, and chiral solitons in a Bose-Einstein condensate (BEC).

5.2 Electromagnetism and gauge potentials

In order to motivate and clarify some of the properties one expects from a gauge theory, including the correspondence between the symmetries and the emergent currents, it is instructive to consider the role of the gauge field in a familiar example, namely electromagnetism. In the classical theory of Maxwell, the vector and scalar potentials given respectively by $\mathbf{A}(\mathbf{r},t)$ and $\Phi(\mathbf{r},t)$ determine the electric and magnetic field strengths $\mathbf{E}(\mathbf{r},t)$ and $\mathbf{B}(\mathbf{r},t)$. A phenomenological description of the physics of the unified theory is given by the Lagrangian density $\mathcal{L}_{\mathrm{EM}}$, which in the presence of a charge and current density can be written as [130]

$$\mathcal{L}_{\mathrm{EM}} = \frac{\epsilon_0}{2}|\mathbf{E}(\mathbf{r},t)|^2 - \frac{1}{2\mu_0}|\mathbf{B}(\mathbf{r},t)|^2 - \rho(\mathbf{r},t)\Phi(\mathbf{r},t) + \mathbf{J}(\mathbf{r},t)\cdot\mathbf{A}(\mathbf{r},t), \qquad (5.2.1)$$

where $\rho(\mathbf{r},t)$ defines the charge density and $\mathbf{J}(\mathbf{r},t)$ is the current density. To construct the classical equations of motion for the fields $\mathbf{E}(\mathbf{r},t)$ and $\mathbf{B}(\mathbf{r},t)$ we identify the dynamical variables of the theory, namely $\mathbf{A}(\mathbf{r},t)$ and $\Phi(\mathbf{r},t)$, which leads to the

Euler-Lagrange equations

$$\frac{d}{dt}\frac{\delta \mathcal{L}_{\mathrm{EM}}}{\delta \dot{\Phi}} = \frac{\delta \mathcal{L}_{\mathrm{EM}}}{\delta \Phi} + \nabla \cdot \frac{\delta \mathcal{L}_{\mathrm{EM}}}{\delta \nabla \Phi}, \tag{5.2.2}$$

$$\frac{d}{dt}\frac{\delta \mathcal{L}_{\mathrm{EM}}}{\delta \dot{A}_i} = \frac{\delta \mathcal{L}_{\mathrm{EM}}}{\delta A_i}. \tag{5.2.3}$$

The relationship between the electric and magnetic fields and the potentials is given by $\mathbf{E}(\mathbf{r},t) = -\nabla\Phi(\mathbf{r},t) - \partial_t \mathbf{A}(\mathbf{r},t)$ and $\mathbf{B}(\mathbf{r},t) = \nabla \times \mathbf{A}(\mathbf{r},t)$ respectively. These relationships along with equations (5.2.2) and (5.2.3) allow us to derive Maxwell's equations in the presence of a charge density. In particular one obtains Gauss' law from (5.2.2) and the Maxwell-Ampère law from (5.2.3). Maxwell's equations are then given by

$$\nabla \cdot \mathbf{E}(\mathbf{r},t) = \rho(\mathbf{r},t)/\epsilon_0, \qquad \nabla \times \mathbf{B}(\mathbf{r},t) = \mu_0 \mathbf{J}(\mathbf{r},t) + \mu_0\epsilon_0 \frac{\partial \mathbf{E}(\mathbf{r},t)}{\partial t}, \tag{5.2.4}$$

$$\nabla \times \mathbf{E}(\mathbf{r},t) = -\frac{\partial \mathbf{B}(\mathbf{r},t)}{\partial t}, \qquad \nabla \cdot \mathbf{B}(\mathbf{r},t) = 0. \tag{5.2.5}$$

The potentials $\mathbf{A}(\mathbf{r},t)$ and $\Phi(\mathbf{r},t)$ do not possess a unique definition, a property known as gauge freedom, which can be seen by making the transformations

$$\mathbf{A}(\mathbf{r},t) \to \mathbf{A}(\mathbf{r},t) + \nabla\Lambda(\mathbf{r},t), \tag{5.2.6}$$

$$\Phi(\mathbf{r},t) \to \Phi(\mathbf{r},t) - \frac{\partial \Lambda(\mathbf{r},t)}{\partial t}, \tag{5.2.7}$$

where $\Lambda(\mathbf{r},t)$ is an arbitrary scalar function. These definitions leave the fields $\mathbf{E}(\mathbf{r},t)$ and $\mathbf{B}(\mathbf{r},t)$ unchanged by virtue of the definitions given previously. The Maxwell relations given by equation (5.2.4) allow us to write the conservation law $\partial_t \rho(\mathbf{r},t) + \nabla \cdot \mathbf{j}(\mathbf{r},t) = 0$ which expresses the conservation of the electric charge [72],

$$Q = \int d^3\mathbf{r}\ \rho(\mathbf{r},t). \tag{5.2.8}$$

Let us consider the form of minimal coupling that represents the interaction of a charged quantum particle with a magnetic field. The Hamiltonian is written as

$$\hat{\mathcal{H}}_e = \frac{1}{2m}\big(-i\hbar\nabla - e\mathbf{A}(\mathbf{r},t)\big)^2 + e\Phi(\mathbf{r},t), \tag{5.2.9}$$

where e is the electron charge. The gauge field appearing in equation (5.2.9) is a dynamical variable of the theory, and as such it obeys an equation of motion. To construct the wave equation for the potential $\mathbf{A}(\mathbf{r},t)$ the Maxwell-Ampère law and

the definition of the potential $\mathbf{E}(\mathbf{r},t)$ can be combined to give

$$\nabla^2\mathbf{A}(\mathbf{r},t) - \epsilon_0\mu_0\frac{\partial^2\mathbf{A}(\mathbf{r},t)}{\partial t} = 0, \tag{5.2.10}$$

which is written in the limit that $\rho(\mathbf{r},t)$=0. We can write the classical solutions to equation (5.2.10) in terms of the Fourier decomposition of the vector potential $\mathbf{A}(\mathbf{r},t)$, yielding

$$\mathbf{A}(\mathbf{r},t) = \sum_\lambda \int \frac{d\mathbf{k}}{\sqrt{\epsilon_0}}\left(\frac{A_\lambda(\mathbf{k})\boldsymbol{\epsilon}_\lambda(\mathbf{k})e^{i\mathbf{k}\cdot\mathbf{r}-i\omega_\mathbf{k}t}}{\sqrt{(2\pi)^3}2\omega_\mathbf{k}} + \text{c.c.}\right), \tag{5.2.11}$$

where $A_\lambda(\mathbf{k})$ specifies the amplitude of the particular mode with associated wave vector $\mathbf{k}$ and polarisation λ. Finally, the vector $\boldsymbol{\epsilon}_\lambda$ specifies the direction of polarisation of the mode. By performing a full quantum treatment of the theory, the Fourier components $A_\lambda(\mathbf{k})$ appearing in equation (5.2.11) are upgraded to Bosonic creation and annihilation operators.

5.3 An interacting gauge theory

To truly simulate a gauge theory one has to be able to construct gauge fields that are themselves dynamical objects, as was shown in the previous section for classical Electromagnetism. This leads not only to the equations of motion for the Electric and Magnetic fields, but also to an equation of motion for the gauge field itself, whose solutions in vacuum are just plane waves. On the other hand, if we consider an ensemble of (charge neutral) atoms, there is no natural coupling to a gauge potential.

There are however a number of ways to artificially induce artificial magnetic fields in ultracold atomic gases ranging from stirring the cloud by a laser spoon or using asymmetric external traps [131] to laser assisted tunneling in optical lattices which induce the required phases for the tunneling amplitudes between the different lattice sites [43,45]. For ultracold atoms optically induced gauge potentials can also be created based on dark state dynamics [46, 132, 133] or Raman transitions [2–4]. These gauge potentials all have in common that they are static and given by the external rotation frequency or laser parameters; there is no dependence on the density of the atomic cloud in the gauge potential using these techniques.

In order to simulate a gauge theory where there is an effective back action between the condensate and the gauge potential, one needs to be in a situation where the gauge field itself is made to depend on the density of the quantum gas. If we consider a gas of optically addressed two-level atoms forming a BEC with internal

state space given by $\{|1\rangle, |2\rangle\}$, then the microscopic N-body Hamiltonian will be given by

$$\hat{H} = \sum_{q=1}^{N} \left(\frac{\hat{\mathbf{p}}_q^2}{2m} + \hat{H}_q^{lm} + \hat{V}_q \right) \otimes \hat{1}_q + \sum_{q<l=1}^{N} \hat{\mathcal{V}}_{q,l} \otimes \hat{1}_{q,l}, \tag{5.3.1}$$

where

$$\hat{H}_q^{lm} = \frac{\hbar\Omega}{2} \begin{pmatrix} 0 & e^{-i\phi_q} \\ e^{i\phi_q} & 0 \end{pmatrix} \tag{5.3.2}$$

is the Hamiltonian for the light-matter interaction and $\hat{V}_q$ is a single-particle external potential which will in the following be assumed to be zero for simplicity. The $\hat{1}_{q,\ldots}$ is the identity operator acting on the subspace excluding particles $q, \ldots$, whereas $\hat{\mathcal{V}}_{q,l} = \mathrm{diag}[g_{11}, g_{12}, g_{12}, g_{22}]\delta(\mathbf{r}_q - \mathbf{r}_l)$ is a 4×4 diagonal matrix describing the two-body interaction with coupling strengths $g_{ij} = 4\pi\hbar^2 a_{ij}/m$, with a_{ij} the s-wave scattering length between the components i and j. In equation (5.3.2), Ω is the two-photon Rabi frequency characterising the light-matter coupling, $\phi_q \equiv \phi(\mathbf{r}_q)$ is the laser phase at particle k's position, and the laser detuning from the atomic resonance is chosen to be zero for simplicity. However, the meanfield terms stemming from $\hat{\mathcal{V}}_{q,l}$ will introduce an effective detuning. The corresponding Hamiltonian which takes into account collisional meanfield effects is then given by

$$\hat{H}_{GP} = \frac{\hat{\mathbf{p}}^2}{2m} \otimes \hat{1} + \hat{\mathcal{V}} + \hat{U} + \hat{V}, \tag{5.3.3}$$

where $\hat{\mathcal{V}} = (1/2)\mathrm{diag}[g_{11}\rho_1 + g_{12}\rho_2, g_{22}\rho_2 + g_{12}\rho_1]$, with $\rho_i = |\Psi_i|^2$ $(i = 1, 2)$ the density of population in the atomic state i, such that $\langle \hat{H} \rangle_{\Psi_{GP}} = \langle \Psi | \hat{H}_{GP} | \Psi \rangle$, where

$$|\Psi_{GP}\rangle = \bigotimes_{k=1}^{N} |\Psi_k\rangle, \tag{5.3.4}$$

is the Hartree wave function for atoms in the state $|\Psi\rangle$. Bose-Einstein condensates have particle densities that are typically of the order 10^{13}–10^{15} cm^{-3}, as such it appropriate to model the scattering to leading order by two-body zero range interactions. To construct an interacting gauge theory, we make use of the dilute property of the gas to construct a perturbation theory using the atomic dressed states of the light-matter coupling Hamiltonian, which can be written as

$$|\chi_{\pm}^{(0)}\rangle = \frac{1}{\sqrt{2}}(|1\rangle \pm e^{i\phi}|2\rangle). \tag{5.3.5}$$

We wish to diagonalize $\hat{U} + \mathcal{V}$ by treating the particle interactions as weak compared to the light-matter coupling, so that the chemical potential satisfies $\mu(\mathbf{r}) \ll \hbar\Omega$.

Consequently, the perturbed dressed states can be written as

$$|\chi_\pm\rangle = |\chi_\pm^{(0)}\rangle \pm \frac{g_{11}-g_{22}}{8\hbar\Omega}\rho_\pm|\chi_\mp^{(0)}\rangle, \tag{5.3.6}$$

and the perturbed spatially varying eigenvalues $g\rho_\pm \pm \hbar\Omega/2$ now contain a contribution from the local chemical potential of the gas, and the effective scattering parameter becomes $g = (g_{11}+g_{22}+2g_{12})/4$. We transform the interaction term $\mathcal{V}$ in equation (5.3.1) into the $\pm$ basis by the unitary transformation $\hat{U}^\dagger\hat{\mathcal{V}}\hat{U}$, where the transformation between the atomic and dressed basis is given by

$$\Psi_{l\in\{1,2\}} = \sum_{i=\{+,-\}} \langle l|\chi_i^{(0)}\rangle\Psi_i. \tag{5.3.7}$$

The two-body interaction matrix $\mathcal{V}_\pm$ then reads

$$\hat{\mathcal{V}}_\pm = \begin{pmatrix} g & \frac{1}{4}(g_{11}-g_{22}) \\ \frac{1}{4}(g_{11}-g_{22}) & g \end{pmatrix}\rho_\pm. \tag{5.3.8}$$

To build an interacting gauge theory, a state vector comprised of the two basis functions $|\xi\rangle = \sum_{i=+,-}\Psi_i|\chi_i\rangle$ can be defined. By projecting onto one of the these states we assume the adiabatic theorem is valid, which requires that the un-projected state have negligible population. Thus, the effective Hamiltonian equation (5.3.1) becomes

$$\hat{H}_\pm = \frac{1}{2m}(\hat{\mathbf{p}}-\mathbf{A}_\pm)^2 + V_\pm(\mathbf{r}) + E_0 + \frac{g}{2}\rho_\pm, \tag{5.3.9}$$

with $E_0 = W \pm \hbar\Omega/2$. The density-dependent geometric phase $\mathbf{A}_\pm = i\hbar\langle\chi_\pm|\nabla\chi_\pm\rangle$ arises from the spatial dependence of the perturbed dressed states. The scalar geometric phase is defined as $W = \frac{\hbar^2}{2m}|\langle\chi_-|\chi_+\rangle|^2$. Using the definition of $|\chi_\pm\rangle$ the vector geometric phase is then given to leading order by

$$\mathbf{A}_\pm = \mathbf{A}^{(0)} \pm \mathbf{a}_1\rho_\pm(\mathbf{r}). \tag{5.3.10}$$

There is a single as well as a many-body contribution to $\mathbf{A}_\pm$, where the single particle vector potential is defined as $\mathbf{A}^{(0)} = -\frac{\hbar}{2}\nabla\phi$ and $\mathbf{a}_1 = \nabla\phi(g_{11}-g_{22})/8\Omega$ determines the strength of the density-dependent vector potential. To study the dynamics of the condensate, we can derive a Gross-Pitaevskii like equation of motion by minimising the energy functional $\mathcal{E} = \langle\Psi|(i\hbar\partial_t - \hat{H}_\pm)|\Psi\rangle$. Without loss of generality we minimise with respect to Ψ_+^* [1] by calculating $\delta\mathcal{E}/\delta\Psi^* = 0$, and drop the $\pm$ subscripts on $\rho_\pm$,

[1] To calculate this one can use the rule $\frac{\delta F[\phi(\mathbf{r})]}{\delta\phi} = \frac{\partial f}{\partial\phi} - \frac{d}{dt}\frac{\partial f}{\partial\dot{\phi}} - \nabla\cdot\frac{\partial f}{\partial\nabla\phi}$,where the functional $F[\phi(\mathbf{r})]$ is defined $F[\phi(\mathbf{r})] = \int d^3\mathbf{r} f(\mathbf{r};\phi,\dot{\phi},\nabla\phi)$.

$\Psi_\pm$ and $\mathbf{A}_\pm$, thus the mean-field equation of motion reads

$$i\hbar\frac{\partial\Psi}{\partial t} = \left[\frac{(\hat{\mathbf{p}}-\mathbf{A})^2}{2m} + \mathbf{a}_1\cdot\mathbf{j} + V(\mathbf{r}) + E_0 + g\rho\right]\Psi, \tag{5.3.11}$$

and to be consistent with perturbation theory W is given to leading order by $W = |\mathbf{A}^{(0)}|^2/2m$. Interestingly, we now have two distinct types of nonlinearity appearing in equation (5.3.11), the standard $|\Psi(\mathbf{r})|^2$ term from two-body inter-particle scattering as well as a current $\mathbf{j}$ that appears at the mean-field level, given by

$$\mathbf{j} = \frac{\hbar}{2mi}\left[\Psi\left(\nabla + \frac{i}{\hbar}\mathbf{A}\right)\Psi^* - \Psi^*\left(\nabla - \frac{i}{\hbar}\mathbf{A}\right)\Psi\right]. \tag{5.3.12}$$

It is interesting to compare equation (5.3.11) with Maxwell's equations, (5.2.4) and (5.2.5). In particular we note that both the Maxwell Ampère law and the mean field equation of motion for $\Psi(\mathbf{r})$ depend on a current density, although it must be remembered that each is quite different. As with the single particle case, the continuity equation that connects the probability density to the probability current is given by

$$\partial_t\rho + \nabla\cdot\mathbf{j} = 0, \tag{5.3.13}$$

although it is stressed that the current $\mathbf{j}$ appearing in equation (5.3.11) is a purely collective effect. Experimental realisation would rely on several conditions being fulfilled. One would require atoms with long lived excited states; for example the transition ${}^1S_0 \leftrightarrow {}^1P_1$ in Sr might be suitable [134]. Further, it is clearly important that the adiabatic condition be fulfilled, so transitions to other atomic states must be suppressed. One avenue to attain this could be to generalise the discussion here to dark states [40], which do not suffer from spontaneous emission. Finally, a relatively large difference of the scattering lengths $a_{11} - a_{22}$ is required in order to observe affects associated with the interacting gauge theory described in this section. This point is discussed in more detail in section 5.5.

5.4 Microscopic mean-field derivation

One can also obtain the above results by considering a microscopic formulation of the problem. In the dilute limit where two-body scattering gives the dominant contribution to the many-body system, one can write down equation (5.3.1) for $N = 2$,

$$\hat{H} = \sum_{i\neq j}\frac{1}{2m}\hat{\mathbf{p}}_i^2\otimes\hat{1}^{(j)} + \hat{H}_{\text{lm}}^{(12)} + \hat{V}_{\text{2-body}}. \tag{5.4.1}$$

The operator $\hat{H}_{\text{lm}}^{(12)}$ describes the light-matter coupling in the two-body Hilbert space $\mathcal{H}^{(12)} = \mathcal{H}^{(1)} \otimes \mathcal{H}^{(2)}$, which can be written

$$\hat{H}_{\text{lm}}^{(12)} = \hat{H}^{(1)} \otimes \hat{1}^{(2)} + \hat{1}^{(1)} \otimes \hat{H}^{(2)}. \tag{5.4.2}$$

And the two-body interaction $\hat{V}_{\text{2-body}}$ in equation (5.4.1) is given by

$$\hat{V}_{\text{2-body}} = \sum_{\sigma_1,\sigma_2} g_{\sigma_1,\sigma_2}(\mathbf{r}_1 - \mathbf{r}_2)|\sigma_1\sigma_2\rangle\langle\sigma_1\sigma_2|. \tag{5.4.3}$$

In the two-particle Hilbert space $\mathcal{H}^{(12)}$, the spin like variables $\sigma_i \in \{\uparrow,\downarrow\}$ appearing in equation (5.4.3) are given by $|\uparrow\rangle = (1,0)^{\text{T}}$ and $|\downarrow\rangle = (0,1)^{\text{T}}$. Hence, the single particle eigenstates of $\hat{H}_{\text{lm}}^{(j)} = \hbar\Omega(e^{-i\phi_j}|\uparrow\rangle^{(j)}\langle\downarrow|^{(j)} + \text{h.c.})/2$ appear (analogously with equation (5.3.5)) as $|\chi_{\pm}^{(0)}\rangle^{(j)} = (|\uparrow\rangle^{(j)} \pm e^{i\phi_j}|\downarrow\rangle^{(j)})/\sqrt{2}$ for particle j. These definitions allow us to construct a two particle gauge theory using the perturbed dressed states of the light-matter interaction. The Schrödinger equation for the full problem is given by $E_n|\chi_n\rangle = \hat{H}|\chi_n\rangle$, where $\hat{H} = \hat{H}_{\text{lm}}^{(12)} + \hat{V}_{\text{2-body}}$. In the space $\mathcal{H}^{(12)}$ the unperturbed eigenstates of $\hat{H}_{\text{lm}}^{(12)}$ are denoted by

$$\text{triplet} \begin{cases} |\chi_{++}^{(0)}\rangle &= |\chi_{+}^{(0)}\rangle^{(1)} \otimes |\chi_{+}^{(0)}\rangle^{(2)}, \\ |\chi_{--}^{(0)}\rangle &= |\chi_{-}^{(0)}\rangle^{(1)} \otimes |\chi_{-}^{(0)}\rangle^{(2)}, \\ |\chi_{\text{b}}^{(0)}\rangle &= \frac{1}{\sqrt{2}}\Big(|\chi_{+}^{(0)}\rangle^{(1)} \otimes |\chi_{-}^{(0)}\rangle^{(2)} + |\chi_{-}^{(0)}\rangle^{(1)} \otimes |\chi_{+}^{(0)}\rangle^{(2)}\Big), \end{cases} \tag{5.4.4}$$

$$\text{singlet} \left\{ |\chi_{\text{f}}^{(0)}\rangle = \frac{1}{\sqrt{2}}\Big(|\chi_{+}^{(0)}\rangle^{(1)} \otimes |\chi_{-}^{(0)}\rangle^{(2)} - |\chi_{-}^{(0)}\rangle^{(1)} \otimes |\chi_{+}^{(0)}\rangle^{(2)}\Big). \right. \tag{5.4.5}$$

The perturbed dressed states can be subdivided into two categories; states that are symmetric and form a triplet with total spin 1, and a second anti-symmetric spin zero singlet state given by equations (5.4.4) and (5.4.5) respectively. One can further show that equations (5.4.4) to (5.4.5) have eigenvalues given by $\{+\hbar\Omega, -\hbar\Omega, 0, 0\}$, hence the perturbed dressed states are defined to first order by

$$|\chi_n\rangle = |\chi_n^{(0)}\rangle + \sum_{k\neq n} \frac{\langle\chi_k^{(0)}|\hat{V}_{\text{2-body}}|\chi_n^{(0)}\rangle}{E_n^{(0)} - E_k^{(0)}}|\chi_k^{(0)}\rangle, \tag{5.4.6}$$

where $k, n \in \{++, --, \text{b}, \text{f}\}$. Construction of the gauge theory is then accomplished in the manner already described in section 3.4 which leads to the re-definition of the matrix elements of the gauge potential $\mathbf{A}_{l,k}^{j} = i\hbar\langle\chi_l|\hat{\nabla}_j\chi_k\rangle$. There is a choice of four possible states that one can project onto. Now the full state vector is given by equation (3.4.1), so if we project onto one of the triplet states, then the wave function $\psi(\mathbf{r})$ must also be symmetric, so overall the state has the correct bosonic

symmetry. Alternately we could project onto the singlet state, in which case the wave function $\psi(\mathbf{r})$ must instead also be anti-symmetric. Here, we project onto the $++$ triplet state. Proceeding, one finds the useful relation

$$\mathbf{A}^{(j)} = \mathbf{A}^{j}_{(0)} - 2\hbar \mathrm{Im}\Big(\langle \chi^{(1)}_{l} | \hat{\nabla}_j \chi^{(0)}_{l} \rangle \Big) + \mathcal{O}(V^2_{\text{2-body}}), \tag{5.4.7}$$

which combined with equations (5.4.4),(5.4.5) and (5.4.6) allows us to calculate the gauge potentials for the two particle theory, thus one finds

$$\mathbf{A}^{j}_{++} = \mathbf{A}^{j}_{(0)} - \frac{\hat{\nabla}_j \phi_j}{4\Omega}(V_{\uparrow\uparrow} - V_{\downarrow\downarrow}), \tag{5.4.8}$$

$$\mathbf{A}^{j}_{--} = \mathbf{A}^{j}_{(0)} + \frac{\hat{\nabla}_j \phi_j}{4\Omega}(V_{\uparrow\uparrow} - V_{\downarrow\downarrow}), \tag{5.4.9}$$

$$\mathbf{A}^{j}_{\mathrm{b}} = \mathbf{A}^{j}_{(0)}, \tag{5.4.10}$$

where the interaction ($\hat{V}_{\text{2-body}}$) matrix elements are given in the spin space by $g_{\sigma_1,\sigma_2} = 4\pi\hbar^2 a_{\sigma_1,\sigma_2}/m$. The single particle gauge potential for particle j is defined as $\mathbf{A}^{j}_{(0)} = i\hbar\langle \chi^{(0)}_{n} | \hat{\nabla}_j \chi^{(0)}_{n} \rangle$. The above ruminations have revealed that at the microscopic level the two particle theory is described by canonical momenta that feature delta functions [127, 129]. The corresponding mathematical treatment of such a system is inherently problematic, as the square of the delta function is not a distribution. To proceed, one can first remove the single particle contribution by defining $\psi_l = \exp(i \int \mathbf{A}^{j}_{(0)} \cdot dx_j/\hbar)\psi_l$. Then, we project onto the '$++$' triplet state, which gives

$$i\hbar\dot{\psi}_{++} = \Bigg[\sum_{j=1}^{2} \frac{1}{2m} \Big\{ \hat{\mathbf{p}}_j + \mathbf{a}^{j}_{1} \delta(x_1 - x_2) \Big\}^2 + g\delta(x_1 - x_2) \Bigg] \psi_{++}. \tag{5.4.11}$$

Analogously with the mean-field derivation presented in section 5.3, the scattering parameter is defined as $g = (g_{\uparrow\uparrow} + g_{\downarrow\downarrow} + 2g_{\downarrow\uparrow})/4$ and the strength of the gauge field for particle j is $\mathbf{a}^{j}_{1} = \hat{\nabla}_j \phi_j (g_{\uparrow\uparrow} - g_{\downarrow\downarrow})/4\Omega$. Insight can be gained into equation (5.4.11) by switching to relative and centre of mass coordinates, by defining $r = x_1 - x_2$ and $x = (x_1 + x_2)/2$, and defining [129]

$$\psi_{++}(t; x_1, x_2) = e^{-iE_{++}t/\hbar} e^{iPx/\hbar} u_{++}(r), \tag{5.4.12}$$

where the centre of mass momentum is P. If we then insert equation 5.4.12 into 5.4.11 we obtain the expression

$$E_{++}u_{++}(r) = \Bigg(\frac{1}{m} \Big\{ -\hbar^2 \frac{\partial^2}{\partial r^2} + \Big[\frac{P}{2} + \mathbf{a}^{j}_{1} \delta(r) \Big]^2 \Big\} + g\delta(r) \Bigg) u_{++}(r). \tag{5.4.13}$$

Equation 5.4.13 demonstrates the absence of Galilean invariance at the microscopic level, due to the presence of the momentum P. We will see later the consequences this has for the allowed states of motion of the condensate. To obtain the corresponding mean-field Hamiltonian, equation (5.4.11) can be generalised to N particles to give

$$\hat{H}_{\mathrm{N}} = \sum_{j=1}^{N} \frac{1}{2m}(\hat{\mathbf{p}}_j + \mathbf{A}_j)^2 + g\sum_{j\neq k}^{N} \delta(x_j - x_k), \tag{5.4.14}$$

and one has

$$\mathbf{A}_j = \sum_{j\neq k}^{N} a_1^j \delta(x_j - x_k). \tag{5.4.15}$$

To obtain the corresponding mean-field result, we make the replacement $\vec{\mathbf{A}} \rightarrow \langle\vec{\mathbf{A}}\rangle_{GP} + \delta_j$, where δ_j is the fluctuation, and the average is taken with respect to the Hartree wave function, equation 5.3.4. One can then show that $\langle\vec{\mathbf{A}}\rangle_{GP} = \mathbf{a}_1\rho(x)$, and if we neglect the fluctuations, one obtains an effective Hamiltonian from the definition $\langle\hat{H}\rangle_{\Psi_{GP}} = \langle\Psi|\hat{H}_{GP}|\Psi\rangle$,

$$\hat{H}_{GP} = \frac{1}{2m}(\hat{\mathbf{p}} + \mathbf{a}_1\rho)^2 + \frac{g}{2}\rho. \tag{5.4.16}$$

Equation (5.4.16) is in full agreement with equation (5.3.9). In particular one sees that the mean-field contribution to the gauge potential strength $\mathbf{a}_1^j \rightarrow \mathbf{a}_1$ is correctly accounted for, and taking the Hartree average has restored the extra factor of two in the definition of $\mathbf{a}_1$.

5.5 One-dimensional physics

The density-dependent vector potential gives rise to a number of interesting and counterintuitive scenarios. To illustrate this we will in the following sections assume that the cloud of atoms is tightly confined such that any motion in the transversal direction is frozen out, a situation which is realisable experimentally with a strongly anisotropic trapping potential [135,136]. In such a situation the dynamics of the gas is well described by an effectively one dimensional mean field description. By choosing the phase to be $\phi = kx$ for the incident laser, together with the transformation $\Psi(x) = e^{-ikx/2}\psi(x)$ equation (5.3.11) is transformed into

$$i\hbar\frac{\partial\psi}{\partial t} = \left[\frac{1}{2m}(\hat{p} - a_1\rho)^2 + a_1 j(x) + \tilde{W} + g\rho\right]\psi, \tag{5.5.1}$$

where $\tilde{W} = \hbar^2k^2/8m$, and $a_1 = k(g_{11} - g_{22})/8\Omega S_t$ characterises the strength of the current nonlinearity. The effective transversal area of the 1D cloud is given by S_t. This model is mathematically equivalent to the AGJPS model [129], with the

additional nonlinear interaction term $g\rho$. The current $a_1 j(x)$ can be made influential provided that the mean field shift is relatively large. The combination of the three parameters Ω, ρ and $g_{11} - g_{22}$ in a_1 allows one to tune experimentally the strength of the gauge field. For example, with an atomic density of 6.0×10^{14} cm^{-3}, a difference of scattering lengths $a_{11} - a_{22} = 5nm$ using for instance optical Feshbach resonances [137–140], and a two-photon Rabi frequency of 185 kHz, one obtains the ratio $(g_{11} - g_{22})\rho/\hbar\Omega = 0.01$ which can affect the dynamics. It should be noted that for standard BEC setups such as ^{87}Rb, this parameter would in fact be vanishingly small due to the small difference between the scattering lengths. However, by carefully tuning the parameters this can be circumvented, as illustrated.

5.6 Variational theory

To facilitate a feeling for the physics associated with the density dependent gauge potential, a variational methodology can be adopted. The Lagrangian density can be written as [141]

$$\mathcal{L} = \hbar \mathrm{Im}(\psi^* \dot{\psi}) + \frac{\hbar^2}{2m}|(\partial_x - i\frac{a_1}{\hbar}\rho(x))\psi|^2 + \frac{g}{2}|\Psi|^4, \tag{5.6.1}$$

where the field ψ in equation (5.6.1) depends on both space and time, i.e. $\psi \equiv \psi(x,t)$. A local gauge transformation can be defined that effectively decouples the momentum from the density in equation (5.6.1), by defining

$$\Psi(x,t) = \exp\left(\frac{ia_1}{\hbar}\int_{-\infty}^{x} dx' \rho(x',t)\right)\Phi(x,t). \tag{5.6.2}$$

Inserting equation (5.6.2) into equation (5.6.1) above, a new Lagrangian density is obtained

$$\mathcal{L}' = \hbar \mathrm{Im}(\Phi^* \dot{\Phi}) + \frac{\hbar^2}{2m}|\partial_x \Phi|^2 + a_1|\Phi|^2 \int_{-\infty}^{x} dx' \dot{\rho}(x',t) + \frac{g}{2}|\Phi|^4. \tag{5.6.3}$$

Where $\rho(x,t) = |\Phi(x,t)|^2$. The Lagrangian density, equation (5.6.3) now comprises a local as well as a non-local term proportional to a_1. To obtain the correct equation of motion for $\Phi(x,t)$, the action associated with this Lagrangian density must be minimised by taking the functional derivative of S, where the action S is defined as

$$S = \int_{t_1}^{t_2} dt \int dx\ \mathcal{L}'[x; \Phi, \dot{\Phi}, \partial_x \Phi]. \tag{5.6.4}$$

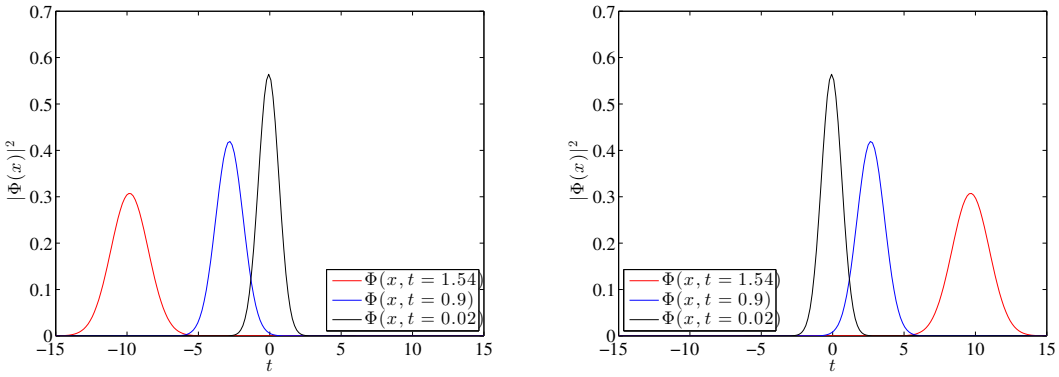

(a) (b)

Figure 5.1: Plots of $|\Phi(x,t)|^2$ showing the drift of the condensate, equation (5.6.5), with the centre of mass coordinate $x_0(t)$, per equation (5.6.9). The units of time are given by τ and the current strength can be defined as $a_1 = \lambda\sigma_0\sqrt{\pi}mk/\sqrt{2}N\tau$, then the dimensionless parameter $\lambda = -30$ in (a) and $\lambda = +30$ for (b) above.

To study the free expansion of the condensate, one can begin with a variational ansatz using the solution of a freely expanding gaussian wave packet where a drift velocity $\dot{x}_0$ of the centre of mass is also included [142],

$$\Phi(x,t) = \left(\frac{N^2}{\pi\sigma_x(t)^2}\right)^{1/4} \exp\left(-\frac{(x-x_0(t))^2}{2\sigma_x(t)^2}\right) e^{i\mathcal{S}}. \tag{5.6.5}$$

The spatially varying phase factor is given by $\mathcal{S} = m\dot{x}_0(x - x_0(t))/\hbar$, and $\sigma_x(t) = \sigma_0\sqrt{1+(t/\tau)^2}$ with $\tau = 2m/k^2\hbar$ is the time dependent width of the Gaussian and N is the number of particles. To study the motion of the centre of mass of the condensate, we can calculate the Lagrangian density by inserting equation (5.6.5) into equation (5.6.3), yielding

$$\begin{aligned}\mathcal{L}' =& \left(\frac{N^2}{\pi\sigma_x^2}\right)^{1/2} \exp\left(-\frac{(x-x_0)^2}{\sigma_x^2}\right)\left[m\ddot{x}_0(x-x_0) - m\dot{x}_0^2\right. \\ &\left. + \frac{\hbar^2}{2m}\frac{(x-x_0)^2}{\sigma_x^4} + \frac{1}{2}m\dot{x}_0^2\right] - \frac{a_1N^2}{\sigma_x^2}\exp\left(-\frac{(x-x_0)^2}{\sigma_x^2}\right) \\ &\times\left\{\frac{\dot{\sigma}_x}{\sqrt{2\pi}}\mathrm{erfc}\left(\frac{x_o - x}{\sigma_x}\right) + \frac{\dot{x}_0}{\pi}\exp\left(-\frac{(x-x_0)^2}{\sigma_x^2}\right)\right. \\ &\left. + \frac{\dot{\sigma}_x}{2\pi\sigma_x}\left[2(x_0-x)\exp\left(-\frac{(x-x_0)^2}{\sigma_x^2}\right) + \sqrt{\pi}\sigma_x\mathrm{erfc}\left(\frac{x_0-x}{\sigma_x}\right)\right]\right\} \\ &+ \frac{gN^2}{2\pi\sigma_x^2}\exp\left(-\frac{2(x-x_0)^2}{\sigma_x^2}\right),\end{aligned} \tag{5.6.6}$$

where $\mathrm{erfc}(x)$ is the complementary error function. Now, the Lagrangian of the problem is defined in the standard way as the integral over space of the Lagrangian

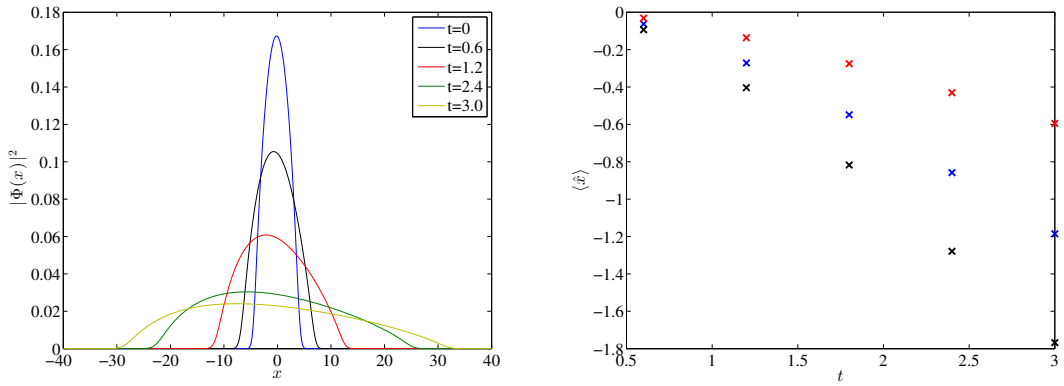

Figure 5.2: Snapshots of the free expansion of a harmonically trapped BEC with $(gN/S_t)(2m/\hbar^2 k) = 30$ and trap frequency $\omega_t = \hbar k^2/2m$. The expansion is asymmetric where a change of sign in a_1 changes the direction of the drift. The coupling strength for the gauge field was $(g_{11} - g_{22})kN/(S_t\hbar\Omega) = 5$ for the data shown in (a). In (b), the drift is shown as a plot of $\langle\hat{x}\rangle$ against t. The data shown in red, blue and black corresponds to the dimensionless quantities $(g_{11} - g_{22})kN/S_t\hbar\Omega = \{2.5, 5, 7.5\}$ respectively. Length is in units of $1/k$ and time in units of $2m/\hbar k^2$ [143].

density, equation (5.6.3). This gives

$$L(\dot{x}_0) = \int_{-\infty}^{\infty} dx\mathcal{L}'[x;\dot{x}_0] = -\frac{m\dot{x}_0^2 N}{2} + \frac{\hbar^2 N}{4m\sigma_x^2} + a_1\frac{\dot{x}_0 N^2\dot{\sigma}_x}{\sigma_x\sqrt{2\pi}} + \frac{gN^2}{\sqrt{8\pi}\sigma_x}. \tag{5.6.7}$$

In order to solve the variational problem, the equation of motion for $\dot{x}_0$ has to be obtained from the corresponding action principle, equation (5.6.4). Accordingly one obtains an equation of motion for the position $x_0(t)$ of the wave packet,

$$m\ddot{x}_0 = \frac{\sqrt{2}a_1 N\dot{\sigma}_x(t)}{\sqrt{\pi}\sigma_x(t)^2}. \tag{5.6.8}$$

Equation (5.6.8) can be solved with the initial conditions $x_0(t=0) = 0$ and $\dot{x}_0(t = 0) = 0$, and the definitions of $\sigma_x(t)$ and τ given previously; which gives the solution

$$x_0(t) = \left(\frac{\sqrt{2}a_1 N\tau}{\sigma_0\sqrt{\pi}m}\right)\left[\frac{t}{\tau} - \text{arcsinh}(t/\tau)\right]. \tag{5.6.9}$$

This solution gives us a way to understand the effect of the interacting gauge potential on the condensate as it expands. The increasing width as a function of time drives the drift of the centre of mass coordinate x_0. Figure 5.1 (a) and (b) show the variational condensate density profile, equation (5.6.5) plotted as a function of time. One can clearly see the drift, caused by the current coupling in equation (5.5.1) and (5.6.3).

A numerical solution is presented in figure 5.2, which shows that the free expansion is no longer symmetric. The asymmetry can be explained by the fact that when the cloud starts to expand it builds up a phase which is linear in position: $\mathcal{S}(x) = \beta(t)x$. This means that after some time the effective scattering length will be different for $x > 0$ and $x < 0$, which will result in asymmetric dynamics. In addition the current term induces a drift which is proportional to a_1 times the density of the BEC. In (a) we observe the time evolution of the density $|\Phi(x)|^2$ of the BEC, which clearly shows the non-symmetric expansion dynamics. Figure 5.2 shows the drift, which is calculated as the average $\langle \hat{x} \rangle$ for different current strengths. The ground state was calculated using imaginary time to find the lowest eigenvalue of equation (5.5.1).

5.7 The quantum ring

As a second example of the physics of the interacting gauge theory, consider a one-dimensional ringlike geometry in the $x - y$ plane and an additional laser beam propagating in the z direction which carries an orbital angular momentum with $\phi = l\theta$, where l is an integer. This configuration gives rise to a gauge potential in the azimuthal θ direction; hence, the situation is similar to the linear 1D case, but now with the periodic boundary conditions $\psi(\theta + n2\pi) = \psi(\theta)$. The equation of motion for ψ can be written

$$i\hbar\frac{\partial\psi}{\partial t} = \left[\frac{1}{2m}(\hat{p}_\theta - a_1\rho)^2 + a_1 j(\theta) + g\rho\right]\psi, \tag{5.7.1}$$

where the radial momentum operator appearing in equation (5.7.1) is defined $\hat{p}_\theta = -(i\hbar/R)\partial/\partial\theta$, and the current $j(\theta)$ is

$$j(\theta) = \frac{\hbar}{2mi}\left[\psi\left(\frac{\partial_\theta}{R} + a_1\frac{i}{\hbar}\rho\right)\psi^* - \psi^*\left(\frac{\partial_\theta}{R} - a_1\frac{i}{\hbar}\rho\right)\psi\right]. \tag{5.7.2}$$

The time-independent Gross-Pitaevskii equation on the ring of radius R is obtained from equation (5.7.1) by setting $\psi(\theta, t) = \psi(\theta)e^{-iEt/\hbar}$. By assuming a homogenous density ρ, the solutions are given by plane waves $\psi(\theta) = \sqrt{\frac{N}{2\pi R}}e^{iq\theta}$. The normalization condition for the ring becomes

$$R\int_0^{2\pi} d\theta|\psi(\theta)|^2 = N, \tag{5.7.3}$$

The dispersion relation E_q is found to be

$$E_q = \frac{1}{2m}\left(\frac{\hbar q}{R} - a_1\rho\right)^2 + a_1 j_q + g\rho, \tag{5.7.4}$$

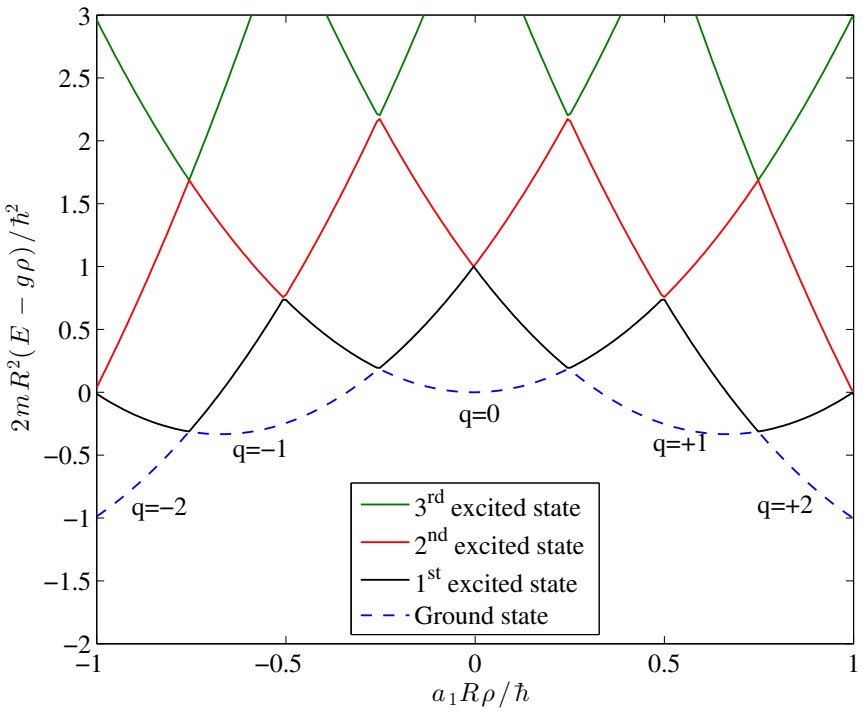

Figure 5.3: Dispersion relation, equation (5.7.4) for the quantum ring as a function of the dimensionless gauge field strength, $a_1 R\rho/\hbar$. The blue dotted lines indicate the ground state regions, while the black (solid) lines indicates the first excited state. At a critical density given by equation (5.7.6) the ground state changes from one angular momentum state to the next.

while the discrete current is given by $j_q = \hbar\rho/m(a_1\rho/\hbar - q/R)$. The dispersion relation, equation (5.7.4) is shown in figure 5.3. The energy difference between two differing angular momentum states can readily be calculated,

$$E_{q+1} - E_q = \frac{1}{2m}\left[\frac{2\hbar}{R}\left(\frac{\hbar q}{R} - a_1\rho\right) + \frac{\hbar^2}{R^2}\right] - \frac{a_1\hbar\rho}{mR}, \tag{5.7.5}$$

where q is an integer number which labels the quantized rotation of the cloud. It can be seen from equation (5.7.4) and equation (5.7.5) that the ground state configuration becomes a function of the number of particles. The strength of the gauge potential is given for the ring configuration by $a_1 = l(g_{11} - g_{22})/8R\Omega$. Interestingly, this implies that at a certain critical density,

$$\rho_c(q) = \frac{4\hbar\Omega}{l(g_{11} - g_{22})}(q + \frac{1}{2}), \tag{5.7.6}$$

the ground state changes from one rotational state to another with $q \to q+1$. This is in contrast to the standard situation for a ring BEC under rotation, where the onset of a current is given by the rotation frequency.

5.8 Chiral solitons

The semiclassical gauge theory described previously can also be shown to support soliton solutions. A soliton is a local, propagating disturbance that maintains its form. The two ingredients one needs to observe solitons are non-linearity and dispersion, and it is the balancing of these two effects that gives rise to solitons. Solitons have been observed and studied in many physical systems, including shallow water waves which are described by the Korteweg-de Vries equation [35], and optical pulses in fibres, which can be understood in terms of a nonlinear Schrödinger equation for the electric field of the light. As we shall see in the next section, there is an intimate connection between the existence of the chiral soliton and its Bogoliubov dispersion relation. From a theoretical perspective, the full analytical solution to the nonlinear problem can be obtained using the formalism of the inverse scattering transformation [144].

To obtain the fundamental soliton of the model (5.5.1), we solve the Gross-Pitaevskii equation by first performing the gauge transformation given by

$$\psi(x,t) = \exp\left(\frac{ia_1}{\hbar}\int_{-\infty}^{x} dx'\rho(x',t) - i\tilde{W}t/\hbar\right)\Phi(x,t). \tag{5.8.1}$$

Subsequently one then finds that equation (5.5.1) simplifies to

$$i\hbar\frac{\partial\Phi}{\partial t} = \left[-\frac{\hbar^2}{2m}\frac{\partial^2}{\partial x^2} - 2a_1 j(x) + g|\Phi|^2\right]\Phi, \tag{5.8.2}$$

where the gauge-transformed current becomes

$$j(x) = \frac{\hbar}{2mi}\left[\Phi^*(x)\partial_x\Phi(x) - \Phi(x)\partial_x\Phi^*(x)\right], \tag{5.8.3}$$

and the corresponding continuity equation is given by $\partial_t|\Phi|^2 + \partial_x j(x) = 0$. To solve equation (5.8.2), we use the ansatz [141]

$$\Phi(x,t) = \xi(x-ut)e^{i\theta(x,t)}, \tag{5.8.4}$$

where $\xi(x-ut)$ is a real valued function. The phase $\theta(x,t)$ will do two things: first, it will cancel the unwanted term proportional to $\partial_x\xi$, and further it will allow us to write down a cubic Schrödinger equation for the function ξ, whose solutions can be readily obtained. Inserting equation (5.8.4) into the continuity equation yields the following relationship

$$\frac{\partial\theta}{\partial x} = \frac{um}{\hbar}. \tag{5.8.5}$$

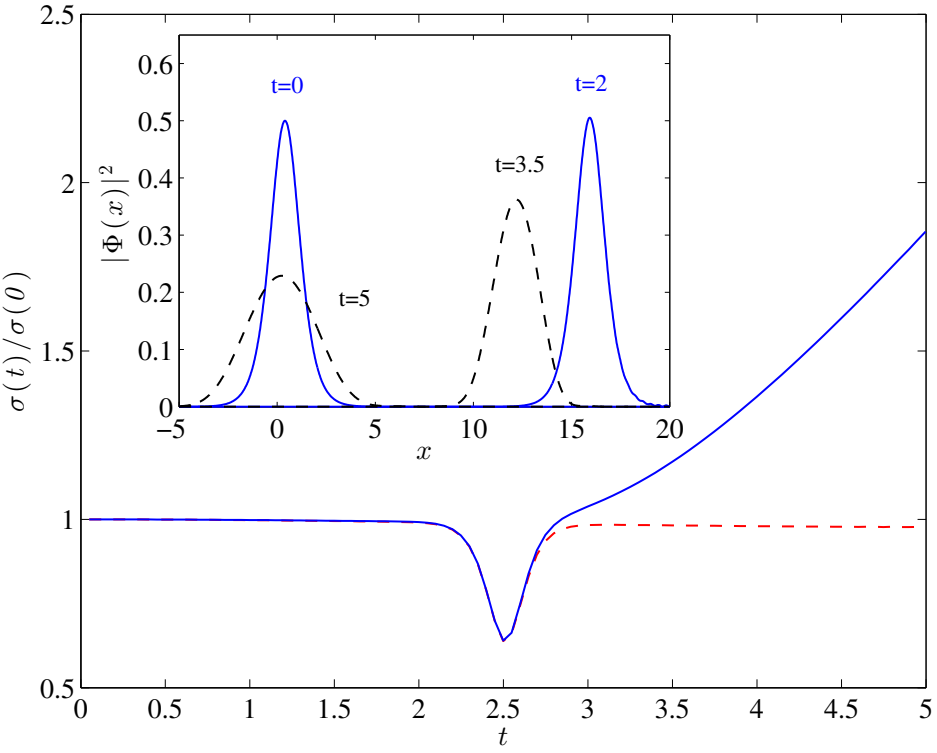

Figure 5.4: The normalized width $\sigma(t)/\sigma(0)$ of the bright soliton. The blue solid line shows $\sigma(t)/\sigma(0)$ with current strength $(g_{11} - g_{22})kN/(S_t\hbar\Omega) = 0.125$ and $(gn/S_t) \times (2m/\hbar^2 k) = -0.5$, while the red dashed line indicates the width of an initially identical soliton without the current nonlinearity ($a_1 = 0$). After reflection the soliton starts expanding due to the change in nonlinear strength. The inset shows snapshots of the density of the soliton prior to (solid blue) and after reflection (dashed black) at times $t = 0, 2.0, 3.5$ and 5.0. All lengths are in units of $1/k$ and time in units of $2m/\hbar k^2$ [143].

Now as long as equation (5.8.5) is satisfied, we have complete freedom to choose the form of the phase appearing in the ansatz, equation (5.8.4). A convenient choice then is to define

$$\theta(x,t) = \frac{umx - (\frac{1}{2}mu^2 + \mu)t}{\hbar}, \tag{5.8.6}$$

where μ is the chemical potential and u the speed of the soliton. The current consequently transforms into $j(x) = u\xi^2$. Using equation (5.8.6) and inserting the full ansatz (5.8.4) into equation (5.8.2), one finds that the resulting differential equation for $\xi(x - ut)$ is

$$\mu\xi = -\frac{\hbar^2}{2m}\partial_x^2\xi + (g - 2a_1u)\xi^3. \tag{5.8.7}$$

To solve equation (5.8.7), we first multiply both sides with $\partial_x\xi$ and integrate over x, and further define the scattering parameter $\tilde{g} = g - 2a_1u$, from which one obtains

the expression

$$\frac{\hbar^2}{2m}\int_{-\infty}^{x} dx\partial_x\left(\frac{1}{2}\partial_x\xi\right)^2 = \int_{-\infty}^{x} dx\partial_x\left[\tilde{g}\left(\frac{1}{4}\xi^4\right) - \mu\left(\frac{1}{2}\xi^2\right)\right]. \tag{5.8.8}$$

The type of soliton we obtain from equation (5.8.8) depends on the sign of $\tilde{g}$. For $\tilde{g} > 0$, one finds a dark soliton, which represents a local travelling disturbance in an otherwise uniform density. Hence, the boundary conditions for this solution are given by $\xi(x \to \pm\infty) = \sqrt{\rho_0}$, and the solution is found to be

$$\frac{\Phi(x,t)}{\sqrt{\rho_0}} = -\frac{\exp[i(mu(x-ut) - (\frac{1}{2}+\mu)t)/\hbar]}{\coth[(x-ut)/(\sqrt{2}l_0)]}, \tag{5.8.9}$$

where the healing length is defined as $l_0 = \hbar/\sqrt{2m\tilde{g}\rho_0}$ and the chemical potential is $\mu = \tilde{g}\rho_0$. For $\tilde{g} < 0$ the solution of equation (5.8.8) is instead the bright soliton, with the boundary conditions $\xi(x \to \pm\infty) = 0$. The soliton has a profile given by

$$\frac{\Phi(x,t)}{\sqrt{\rho_0}} = \frac{\exp[i(mu(x-ut) - (\frac{1}{2}-\mu)t)/\hbar]}{\cosh[(x-ut)/(\sqrt{2}l_0)]}, \tag{5.8.10}$$

with $\mu = |\tilde{g}|\rho_0/2$. The two solutions, equations (5.8.9) and (5.8.10) are chiral, which means that the solitons can only propagate in a specific direction for a chosen velocity. The concept of a chiral soliton can be illustrated by considering the reflection of a BEC from a hard wall. Figure 5.4 shows how a bright soliton initially moving in the positive x direction is destroyed after reflection. A standard bright soliton would retain its width $\sigma(t) = \sqrt{\langle\hat{x}^2\rangle - \langle\hat{x}\rangle^2}$ after reflection; whereas the chiral soliton is found to start to expand after reflection. The change in the nonlinear strength due to the change in momentum after the reflection results in a state which is not the soliton any more; hence the solution is no longer confined.

Finally, if $g = 2a_1u$ we are in a situation where the current nonlinearity cancels the mean field interactions between particles, with no soliton solutions present. Depending on the precise physical setup this particular situation may or may not be possible to reach due to a breakdown of the adiabatic assumption or a violation of the perturbative assumption.

5.9 Bogoliubov theory

It was shown in the previous section that the one-dimensional interacting gauge theory supports chiral solitons. The reason for this is the lack of Galilean invariance inherent to the model, equation (5.3.11). The collective modes of the condensate

give fundamental insight into the behaviour of the ultracold gas, and have attracted intense study for trapped gases [145], as well as more recently for schemes involving light induced gauge potentials [146]. Many of the dynamical properties of the condensate can be understood from considering the collective excitations of the ultracold gas. In particular, the excitation spectrum gives us important insight into the superfluid behaviour of the gas, and is also fundamental to the low temperature thermodynamic response of the cloud. There are several approaches to understanding the collective behaviour of the cloud, such as classical hydrodynamics which can also be used to analyse the surface structure of the condensate.

To calculate the collective excitations of the one-dimensional model, equation (5.8.2), the Gross-Pitaevskii equation can be linearized by considering the small amplitude oscillations of the wave function Φ around the ground state Φ_0. Hence using the substitution $\Phi = \Phi_0 + \delta\Phi$, where $\delta\Phi$ is the fluctuation, equation (5.8.2) transforms to

$$\begin{aligned} i\hbar\frac{\partial\delta\Phi}{\partial t} = &-\frac{\hbar^2}{2m}\partial_x^2\delta\Phi - \frac{a_1\hbar}{mi}\Big[|\Phi_0|^2\partial_x\delta\Phi + \Phi_0\partial_x\Phi_0\delta\Phi^* - \Phi_0^2\partial_x\delta\Phi^* \\ &- \Phi_0\partial_x\Phi_0^*\delta\Phi\Big] - 2a_1 j_0(x)\delta\Phi + g(2|\Phi_0|^2\delta\Phi + \Phi_0^2\delta\Phi^*)\Big], \end{aligned} \tag{5.9.1}$$

and the ground state current $j_0(x)$ is defined by equation (5.8.3). Now, to solve equation (5.9.1), we look for solutions which are periodic in time, the full ansatz for the problem being

$$\Phi(x,t) = \underbrace{\sqrt{n(x)}e^{-i\mu t/\hbar}}_{\Phi_0(x,t)} + \underbrace{e^{-i\mu t/\hbar}[u(x)e^{-i\omega t} - v^*(x)e^{i\omega t}]}_{\delta\Phi(x,t)}. \tag{5.9.2}$$

The functions $u(x)$ and $v(x)$ represent the collective modes of the condensate, with frequency ω. By inserting the definitions of Φ_0 and $\delta\Phi$ from equation (5.9.2) into equation (5.9.1) and collecting terms in $\exp(\pm i\omega t)$, one obtains the Bogoliubov-de Gennes differential equations

$$\hat{\mathcal{M}}\eta = \hbar\omega\hat{\sigma}_z\eta, \tag{5.9.3}$$

where the 2×2 matrix $\hat{\mathcal{M}}$ is given by

$$\hat{\mathcal{M}} = \begin{pmatrix} \mathcal{L}_0 - \mu - \frac{a_1\hbar}{mi}(n\partial_x - \frac{1}{2}\partial_x n) + 2gn & -\frac{a_1\hbar}{mi}(-\frac{1}{2}\partial_x n + n\partial_x) - gn \\ -\frac{a_1\hbar}{mi}(\frac{1}{2}\partial_x n - n\partial_x) - gn & \mathcal{L}_0 - \mu - \frac{a_1\hbar}{mi}(-n\partial_x + \frac{1}{2}\partial_x n) + 2gn \end{pmatrix},$$

and the vector $\eta = (u(x), v(x))^T$. The Bogoliubov equations exhibit translational invariance, hence one can solve the set of equations, (5.9.3) with a plane wave

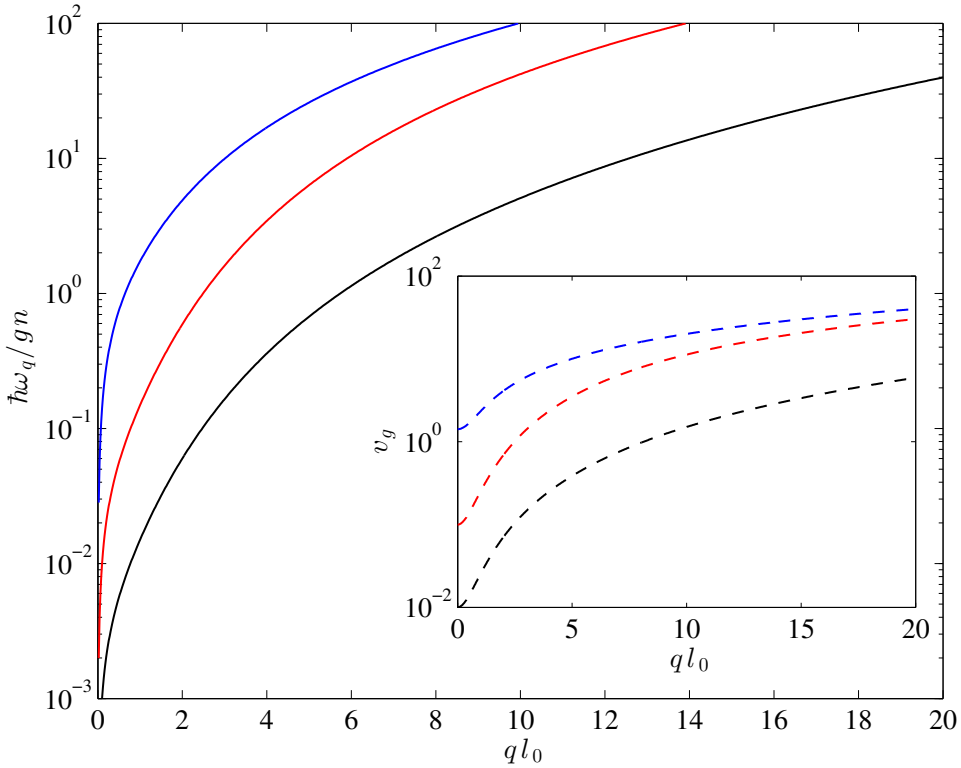

Figure 5.5: The dispersion relation, equation (5.9.5) is plotted as a function of the dimensionless variable ql_0, where l_0 is the healing length of the BEC. The inset shows the group velocity, $v_g = \partial\omega_q/\partial q$. Each of the coloured curves represents a different gauge field strength, $a_1\sqrt{2n/mg} = \{0, 10, 100\}$, for the blue, red and black sets of curves respectively.

solution of the form

$$\eta = \frac{1}{\sqrt{L}} \begin{pmatrix} u_q \\ v_q \end{pmatrix} e^{iqx}, \tag{5.9.4}$$

where L is the length of the one-dimensional system, and the coefficients u_q and v_q are to be determined. The spectrum can be obtained using equations (5.9.3) and (5.9.4), and is found to be

$$\hbar\omega_q = -\frac{a_1\hbar nq}{m} \pm \sqrt{\left(\frac{a_1\hbar nq}{m}\right)^2 + \epsilon_q^0(\epsilon_q^0 + 2gn)}, \tag{5.9.5}$$

with $\epsilon_q^0 = \hbar^2q^2/2m$. Figure 5.5 shows the Bogoliubov spectrum along with the group velocity. In the limit that $a_1 \to 0$ equation (5.9.5) reduces to the famous Bogoliubov spectrum for the interacting Bose gas. Now, for a soliton to exist, one needs a balance between effects of non-linearity and dispersion. As such, consider a localized disturbance within the density with amplitude Δn and size L_0. Within the disturbance the speed of sound will differ from the bulk of the condensate by an amount $\sim c_s(\Delta n/n)$, where c_s is the speed of sound, which can be obtained from

the small q regime of equation (5.9.5), and is found to be

$$c_s = -\frac{a_1 n}{m} + \sqrt{\frac{gn}{m}}. \tag{5.9.6}$$

As the wave vector of an excitation is of order $q \sim 1/L_0$, then dispersion will tend to increase the velocity by an amount $\sim c_s l_0^2/L_0^2$. Now for the two effects of dispersion and non-linearity to balance each other, it must hold that [35]

$$\frac{\Delta n}{n} + \frac{l_0^2}{L_0^2} = 0. \tag{5.9.7}$$

Alternately, the difference between the velocity of the disturbance, u and the sound speed, equation (5.9.6) must be equal to the amount the velocity is shifted, so that

$$|u - c_s| \sim c_s \frac{l_0^2}{L_0^2}. \tag{5.9.8}$$

As was shown in the previous section, the velocity of the soliton depends on the overall nonlinear strength, hence equations (5.9.7) and (5.9.8) are valid only for a fixed sign of u.

5.10 Summary

In this chapter it was shown how an interacting gauge theory for a BEC can be generated. The resulting gauge potential is not fully dynamical, in the sense that it is always zero if no matter field is present. The emerging gauge field does however depend on the density of the BEC, and therefore constitutes an interacting field with a back-action between the BEC dynamics and the gauge field. The mean-field equation of motion includes a current non-linearity and in the quasi-one-dimensional regime the model is identical to the Aglietti-Griguolo-Jackiw-Pi-Seminara gauge theory [129].

The coupling of the BEC to its current gives rise to a number of exotic types of dynamics. It was shown how the presence of topological states corresponding to persistent currents in a ring geometry depend on the number of particles. Also soliton solutions can be identified which are chiral in nature. Finally, the excitation spectrum of the condensate was also calculated with the Bogoliubov formalism. Analogies can be drawn between the atomic system considered here and models of field theories describing the fundamental forces between elementary particles. From a quantum simulation point of view, one possible extension would be the generalisation of the mechanisms discussed in this chapter to a pseudo-spin situation which

can also support non-Abelian gauge potentials [9, 57].

Chapter 6

Josephson Effects

6.1 Introduction

The question of how to study and understand the many-body problem lies at the heart of any realistic attempt to construct a theory of interacting particles in many sub-disciplines of physics. It is simply the case that by studying systems of particles with many different, interacting degrees of freedom one is left in a situation that is analytically and numerically intractable. One methodology to tackle this is to partition the particles according the types of motion that occur within the system. The most prominent example is given in atomic systems where the motion of the nucleus and the electrons are divided into slow and fast degrees of freedom respectively, the Born-Oppenheimer approximation.

The inherent coherence of the many-body system comprised of bosonic or fermionic matter provides an avenue with which to explore the low temperature properties of many different atomic systems. By addressing these atomic ensembles with shaped laser light, one can perform quantum simulation of a variety of otherwise inaccessible effects, as has already been discussed in the preceding chapters.

Some of the most striking effects of coherent matter in the ultracold temperature regime have been elucidated with bosonic atomic condensates. Early work focussed on understanding interference with matter waves [147, 148], Bragg scattering [149] and applications to matter wave optics such as the realization of nonlinear effects like solitons [150]. One of the most surprising yet paradigmatic effects in quantum mechanics is the quantum tunnelling of particles.

For macroscopic systems this is encompassed by the Josephson effect: the tunnelling current that is produced by placing an insulating barrier between two particle reservoirs. The inherent nonlinearities that are present in the study of interacting ultracold bosonic gases make these systems particularly interesting, and has lead to the prediction and realization of effects such as self-trapping [151–153]. Further, the effects of asymmetric potential wells [154] and extensions beyond the two-mode approximation have also been studied [155]. A detailed overview of these effects is given by Gati et al. [156]. Extensions of the Josephson effect to systems incorporating non-abelian gauge fields have recently been described [8, 157]. Here, it is shown how the interacting gauge theory presented previousely can be placed onto a two-site lattice, and study the population dynamics of the resulting lattice gauge theory.

A common feature of both the continuum [10, 40] and lattice gauge theories [158] for ultracold atoms is that they are static; in the sense that the gauge potentials are determined by the external laser coupling, and are not affected by the motion of the atoms. In the previous chapter, it was shown how an interacting gauge potential can be generated in the continuum for an ensemble of ultracold atoms, such that there is an effective back action between the gauge potential and the dressed states of the light-matter interaction, resulting in a gauge potential that depends on the density of the quantum gas. In this chapter it is demonstrated how this continuum interacting gauge theory can be applied to a two-site lattice, from which the coherent transport between the two sites is analysed via the nonlinear Josephson relations which are derived and solved numerically.

6.2 One-dimensional model

Previously, it was shown how at the mean-field level the one-dimensional Gross-Pitaevskii-like equation, (5.8.2) features a current non-linearity. It is this model that will be analysed, using a tight binding methodology. The Gross-Pitaevskii equation is given by

$$i\hbar\frac{\partial\Phi}{\partial t} = \bigg[-\frac{\hbar^2}{2m}\frac{\partial^2}{\partial x^2} - 2a_1 j(x) + g|\Phi|^2\bigg]\Phi, \tag{6.2.1}$$

and the current, $j(x)$ is given by

$$j(x) = \frac{\hbar}{2mi}\bigg[\Phi^*(x)\partial_x\Phi(x) - \Phi(x)\partial_x\Phi^*(x)\bigg]. \tag{6.2.2}$$

Where as before the factor a_1 governs the strength of the gauge potential, and $g = (g_{11} + g_{22} + 2g_{12})/4$ is the effective scattering parameter. To proceed, we upgrade the wave functions $\Phi(x)$ and $\Phi^*(x)$ to annihilation and creation operators respectively. Hence, the one-dimensional mean-field Hamiltonian in equation (6.2.1) appears in second-quantized form as

$$\hat{H} = \int dx\ \hat{\Phi}^\dagger(x)\bigg(-\frac{\hbar^2}{2m}\partial_x^2 + V(x)\bigg)\hat{\Phi}(x) + g\int dx\ \hat{\Phi}^\dagger(x)\hat{\Phi}^\dagger(x)\hat{\Phi}(x)\hat{\Phi}(x) - 2a_1\int dx\ \hat{\Phi}^\dagger(x)\hat{J}(x)\hat{\Phi}(x), \tag{6.2.3}$$

where the normal ordered current operator $\hat{J}(x)$ that appears in equation (6.2.3) above is given in second quantized form by

$$\hat{J}(x) = \frac{\hbar}{2mi}\bigg[\hat{\Phi}^\dagger(x)\partial_x\hat{\Phi}(x) - \partial_x\hat{\Phi}^\dagger(x)\hat{\Phi}^\dagger(x)\bigg]. \tag{6.2.4}$$

To proceed, we require a model potential $V(x)$. Typically one is interested in situations where the tight binding approximation can be made, such that the height of the lattice is greater than the chemical potential at each individual well. Experimentally, an extended one-dimensional lattice can be realised by counter-propagating laser beams and the fact that the energy of an individual atom is shifted by an amount $\Delta E = -\mathrm{Re}\{\alpha(\omega)\}\langle\mathcal{E}(\mathbf{r},t)^2\rangle_t$, where $\langle\mathcal{E}(\mathbf{r},t)^2\rangle_t$ is the time averaged electric field; and the polarizability associated with the two level system is given by [35]

$$\alpha(\omega) = \frac{|\langle 2|\mathbf{d}\cdot\hat{\boldsymbol{\epsilon}}|1\rangle|^2}{E_2 - i\hbar\nu_2/2 - E_1 - \hbar\omega}, \tag{6.2.5}$$

where the factor $\nu_2/2$ accounts for the finite lifetime of the excited state $|2\rangle$ and $\hat{\boldsymbol{\epsilon}}$ is a unit vector in the direction of the electric field.[1] The expression (6.2.5) can be derived using time-dependent perturbation theory for the electric field $\mathcal{E}(\mathbf{r},t)$. However, as we are interested in a two-site system, schemes involving electrostatic interactions [159] or atom chips [160] are more relevent. The appropriate model potential is then [161]

$$V(x) = b\bigg(x^2 - x_{\min}^2\bigg)^2. \tag{6.2.6}$$

The double-well potential defined by (6.2.6) above has its minima situated at $x = \pm x_{\min}$, and close to these points $V(x)$ is harmonic, an approximation that will be

[1] The factor of $\frac{1}{2}$ appearing in the denominator of $\alpha(\omega)$ is due to the probability of being in the excited state being the modulus squared. In turn the energy of the ground state acquires an imaginary component, due to the induced transitions to the excited state.

used to perform the tight binding calculation. Hence, the normalized local ground states of the left and the right well are given by

$$\eta_{l,r}(x) = \left(\frac{2}{\pi\sigma^2}\right)^{1/4} \exp\left(-\frac{(x \pm x_{\min})^2}{\sigma^2}\right) \tag{6.2.7}$$

respectively, and the width of the ground state in equation (6.2.7) is given by σ.

6.3 Mean-field tight binding calculation

Having written down the Hamiltonian for the many-body system in second-quantized form, equation (6.2.3) and defined the double-well potential (6.2.6), these ingredients can be brought together to derive a mean-field tight binding Hamiltonian. To do this the two-mode approximation can be used, which entails expanding the field operator $\hat{\Phi}(x)$ as

$$\hat{\Phi}(x) = \eta_l(x)\hat{c}_l + \eta_r(x)\hat{c}_r, \tag{6.3.1}$$

where the operator $\hat{c}_l$ and $\hat{c}_r$ destroy particles in the left and right wells respectively. It is assumed that there is a large separation between the ground state and the first excited state of each individual well so that the dynamics are well described by assuming the particles occupy one of the two ground states. By inserting equation (6.3.1) into equation (6.2.3) one obtains

$$\hat{H} = \sum_{ij} J_{ij}\hat{c}_i^\dagger\hat{c}_j + \sum_{ijkl} U_{ijkl}\hat{c}_i^\dagger\hat{c}_j^\dagger\hat{c}_k\hat{c}_l + \sum_{ijkl} \lambda_{ijkl}\hat{c}_i^\dagger\hat{c}_j^\dagger\hat{c}_k\hat{c}_l, \tag{6.3.2}$$

where the sums are taken over both the left and right wells. The parameters J_{ij}, U_{ijkl} and λ_{ijkl} are overlap integrals, and give a way to identify the most important terms in equation (6.3.2). The three overlap integrals are given by

$$J_{ij} = \int_{-\infty}^{\infty} dx \eta_i^*(x)\left(-\frac{\hbar^2}{2m}\partial_x^2 + V(x)\right)\eta_j(x), \tag{6.3.3}$$

$$U_{ijkl} = \frac{g}{2}\int_{-\infty}^{\infty} dx \eta_i^*(x)\eta_j^*(x)\eta_k(x)\eta_l(x), \tag{6.3.4}$$

$$\lambda_{ijkl} = -\frac{a_1\hbar}{m}\int_{-\infty}^{\infty} dx \eta_i^*(x)\mathrm{Im}\{\eta_j^*(x)\overset{\leftrightarrow}{\partial}_x\eta_k(x)\}\eta_l(x), \tag{6.3.5}$$

where one has for shorthand $A\overset{\leftrightarrow}{\partial}_x B = A\partial_x B - (\partial_x A)B$. Using the definition of the two ground states, equation (6.2.7) and the potential, equation (6.2.6) these integrals can be evaluated. Now as $J_{lr} = J_{rl} = J$, one finds that the leading contribution to

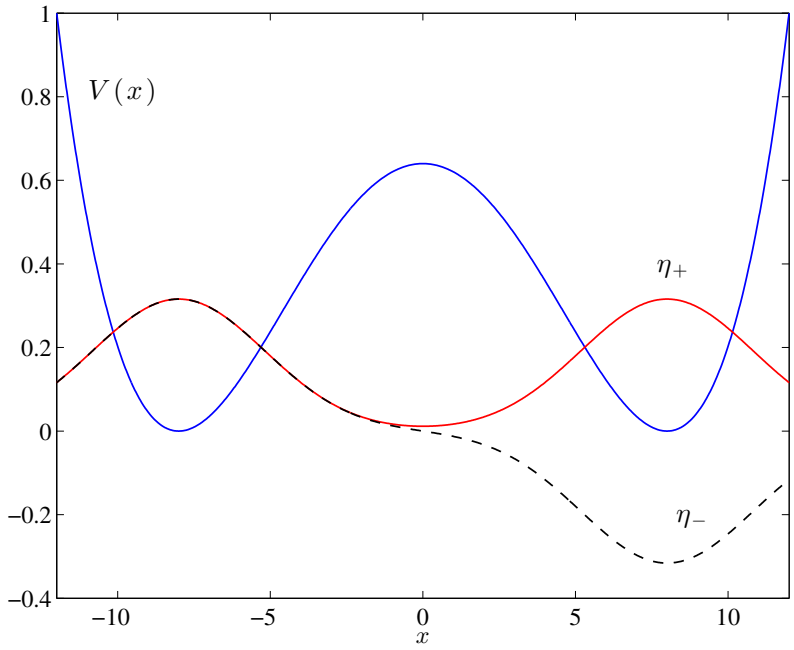

Figure 6.1: Plot of the double well potential, equation (6.2.6) (solid blue) along with the two single-particle symmetric and antisymmetric states given by η_+ (solid red) and η_- (black dashed) respectively.

J is given by

$$J \simeq 2\frac{\hbar^2}{m\sigma^2}\left(\frac{x_{\min}}{\sigma}\right)^2 \exp(-2x_{\min}^2/\sigma^2), \tag{6.3.6}$$

and as we assume that the particles tunnel between ground states, the on-site energies J_{ll} and J_{rr} do not contribute. One can perform similar calculations to obtain expressions for λ_{ijkl}. There are two contributions to this term, given by

$$\Gamma_1 = \frac{4a_1\hbar x_{\min}}{m\sqrt{\pi}\sigma^3}\exp(-3x_{\min}^2/\sigma^2), \quad \text{and} \quad \Gamma_2 = \frac{4a_1\hbar x_{\min}}{m\sqrt{\pi}\sigma^3}\exp(-4x_{\min}^2/\sigma^2). \tag{6.3.7}$$

Finally, the leading contribution to U is given by $U = g/\sqrt{\pi}\sigma$. These definitions, equations (6.3.6) and (6.3.7) allow us to write down the two-site lattice Hamiltonian

$$\begin{aligned}\hat{H} =& -J(\hat{c}_l^\dagger\hat{c}_r + \hat{c}_r^\dagger\hat{c}_l) + U(\hat{n}_l(\hat{n}_l-1) + \hat{n}_r(\hat{n}_r-1)) \\ &+ \Gamma_1(\hat{c}_l^\dagger\hat{j}\hat{c}_l + \hat{c}_r^\dagger\hat{j}\hat{c}_r) + \Gamma_2(\hat{c}_l^\dagger\hat{j}\hat{c}_r + \hat{c}_r^\dagger\hat{j}\hat{c}_l),\end{aligned} \tag{6.3.8}$$

where $\hat{n}_i = \hat{c}_i^\dagger\hat{c}_i$ is the number operator for site i and the discrete current operator for the two site lattice is $\hat{j} = -i(\hat{c}_r^\dagger\hat{c}_l - \hat{c}_l^\dagger\hat{c}_r)$. It is instructive to consider the model of equation (6.3.8) in the absence of interactions, $U = \Gamma_i = 0$. In this case one can diagonalize the resulting single particle hamiltonian by transforming the operators using the definitions $\hat{c}_+ = (\hat{c}_l + \hat{c}_r)/\sqrt{2}$ and $\hat{c}_- = (\hat{c}_l - \hat{c}_r)/\sqrt{2}$. Accordingly one finds

the transformed Hamiltonian becomes $\hat{H} = -J(\hat{c}_+^\dagger \hat{c}_+ - \hat{c}_-^\dagger \hat{c}_-)$. The operators $\hat{c}_+^\dagger$ and $\hat{c}_-^\dagger$ create particles in the symmetric state $\eta_+ = (\eta_l + \eta_r)/\sqrt{2}$ and the anti-symmetric state $\eta_- = (\eta_l - \eta_r)/\sqrt{2}$ respectively. Figure 6.1 shows the potential $V(x)$ plotted along with these two functions η_+ and η_-.

Equation (6.3.8) allows us to understand the effect of population dynamics between the two sites. It comprises the usual on-site interactions that appear in the Bose-Hubbard model given by the terms proportional to U, as well as the unconventional terms proportional to Γ_i (equation (6.3.7)) which originate from the current operator in the continuum model, equation (6.2.4). To study the population dynamics between the two wells we work with the operators $\hat{c}_i$ in the Heisenberg picture. The equations of motion for $\hat{c}_i$ are then given by

$$i\hbar \frac{d\hat{c}_i}{dt} = [\hat{c}_i, \hat{H}], \tag{6.3.9}$$

which yields

$$\begin{aligned} i\hbar \frac{d\hat{c}_l}{dt} =& - J\hat{c}_r + 2U\hat{n}_l\hat{c}_l + \Gamma_1(\hat{j}\hat{c}_l + i(\hat{n}_l + \hat{n}_r)\hat{c}_r) \\ &+ \Gamma_2(\hat{j}\hat{c}_r + i\hat{c}_l^\dagger \hat{c}_r \hat{c}_r + i\hat{n}_r\hat{c}_l), \end{aligned} \tag{6.3.10}$$

$$\begin{aligned} i\hbar \frac{d\hat{c}_r}{dt} =& - J\hat{c}_l + 2U\hat{n}_r\hat{c}_r + \Gamma_1(\hat{j}\hat{c}_r - i(\hat{n}_l + \hat{n}_r)\hat{c}_l) \\ &+ \Gamma_2(\hat{j}\hat{c}_l - i\hat{c}_r^\dagger \hat{c}_l \hat{c}_l - i\hat{n}_l\hat{c}_r). \end{aligned} \tag{6.3.11}$$

To gain an understanding of equations (6.3.10) and (6.3.11), it is assumed that the number of particles in both wells is so large that the operators $\hat{c}_l$ and $\hat{c}_r$ may be treated as classical quantities, and as such replaced by their expectation values c_l and c_r. Figure 6.2 shows the numerical solutions to these equations in different parameter regimes. In Figure 6.2 (a) and (c) the parameters $2U/J = 10$ and $\Gamma_1/J = 1$ were used, whilst for (b) and (d) $2U/J = 1$ and $\Gamma_1/J = 5$. For figures 6.2 (a) and (b) the initial phase difference was $\theta_l - \theta_r = \Delta\theta = 0$, but for figures (c) and (d) $\Delta\theta = \pi/2$ was used. Interestingly, one observes population oscillations when $\Delta\theta = 0$, which is not the case for the usual bosonic Josephson effect, where a non-zero phase difference is required for population dynamics.

Now, it was assumed that $x_{\min}/\sigma \gg 1$, so that $\Gamma_2 \ll \Gamma_1$, hence the terms proportional to Γ_2 in equation (6.3.10) and (6.3.11) can be dropped. Figure 1 shows the Rabi like oscillations that are synonymous with two level systems. In figure 6.2 (b) the larger current strength has caused the speed of the population oscillations to increase. On the other hand, 6.2 (c) shows how strong on-site interactions changes

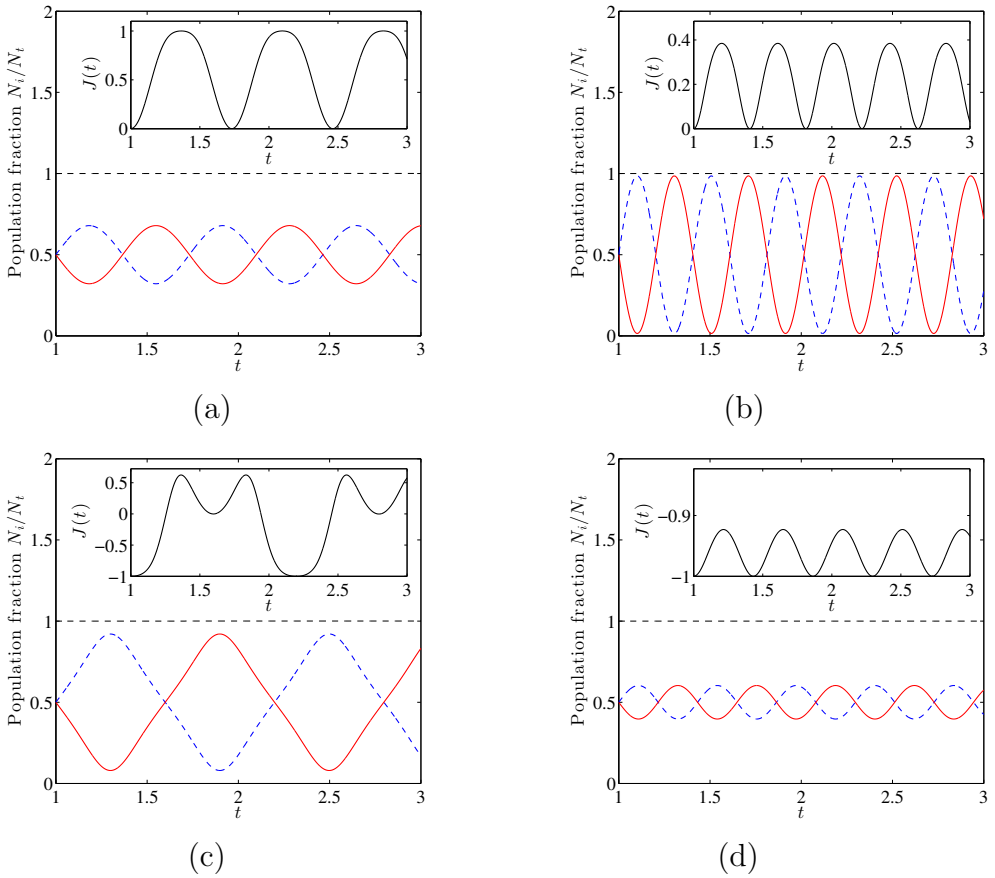

Figure 6.2: Numerical solutions to equations (6.3.10) and (6.3.11). The population $|c_l|^2$, $|c_r|^2$ and $\sum_i |c_i|^2$ are given by the blue dashed line, solid red line and dashed black lines respectively. The inset in each figure shows the current $J(t)$. The units of time are $\hbar/J$ [162].

the dynamics, the current showing an unusual 'dip' (see inset of 6.2 (c)). Finally, figure 6.2 (d) shows how the dynamics are reduced when there is an initial phase difference of $\pi/2$ between the sites and the current strength is stronger than the Hubbard term.

6.4 Phase-space analysis

Figure 6.2 shows how the discrete current non-linearity present in equation (6.3.8) affects the population oscillations between the two wells. To investigate the properties of this unusual nonlinear system further, we can re-cast the variables of the problem in terms of the population difference and the phase difference. This methodology has previously been utilised to show how a charge neutral interacting BEC in a symmetric double well potential can be understood in terms of a nonrigid pendulum [151, 163], and gives an intuitive way to study the phase-space properties of the many-body system [164]. As with the population dynamics shown in figure 6.2, the starting point for this analysis is the assumption that the number of parti-

cles is so large that the operators appearing in equation (6.3.8) can be replaced by their respective eigenvalues, which in turn can be replaced by the polar variables $c_i = \sqrt{N_i}e^{i\theta_i}$, where $i = l, r$. By further defining the population and phase differences by $z(t) = (N_l - N_r)/N_t$ and $\varphi(t) = \theta_r - \theta_l$, a classical Hamiltonian is obtained from equation (6.3.8)

$$H_{\text{classical}} = \frac{H}{JN_t} = \frac{\Lambda z^2}{2} - \sqrt{1-z^2}\cos(\varphi) - \gamma_1\sqrt{1-z^2}\sin(\varphi) \tag{6.4.1}$$

$$- \gamma_2(1-z^2)\sin(2\varphi) + \Delta E, \tag{6.4.2}$$

where the dimensionless parameters read $\Lambda = UN_t/J$, $\gamma_i = \Gamma_i N_t/J$ and $\Delta E = UN_t/2J$. The variables z and φ are canonically conjugate, the relevant momenta being

$$p_z = \frac{\partial L}{\partial \dot{z}} = -\varphi \qquad \text{and} \qquad p_\varphi = \frac{\partial L}{\partial \dot{\varphi}} = z, \tag{6.4.3}$$

where the corresponding Hamiltonian function is [165]

$$H = z\dot{\varphi} - \varphi\dot{z} - L(z, \dot{z}, \varphi, \dot{\varphi}). \tag{6.4.4}$$

Using equations (6.4.3) and (6.4.4), one finds the set of Hamilton's equations are given by

$$\frac{\partial H}{\partial z} = \dot{\varphi} \qquad \text{and} \qquad -\frac{\partial H}{\partial \varphi} = \dot{z}. \tag{6.4.5}$$

Now, using the Hamiltonian defined by equation (6.4.1) along with the relations (6.4.5), the coupled equations of motion are found to be

$$\dot{z} = -\sqrt{1-z^2}\sin(\varphi) + \gamma_1\sqrt{1-z^2}\cos(\varphi) + 2\gamma_2(1-z^2)\cos(2\varphi), \tag{6.4.6}$$

$$\dot{\varphi} = \frac{z}{\sqrt{1-z^2}}\cos(\varphi) + \Lambda z + \gamma_1\frac{z}{\sqrt{1-z^2}}\sin(\varphi) + 2\gamma_2 z\sin(2\varphi). \tag{6.4.7}$$

The classical Hamiltonian given by equation (6.4.1) and the nonlinear Josephson equations (6.4.6) and (6.4.7) give us a way to understand the dynamics and phase-space properties of the two-site model. In particular, we note that equation (6.4.1) can be understood in terms of a classical nonrigid pendulum. This model, equation (6.4.1) differs from that presented in [151] by the additional term proportional to γ_2. Now, in the tight-binding limit where $\Gamma_2 \ll \Gamma_1$, the term proportional to γ_2 in equation (6.4.1) can be dropped, hence we can map the classical Hamiltonian onto the nonrigid pendulum model as presented in [151, 163]. The result is that the phase angle φ has an extra initial offset term due to the current non-linearity of the

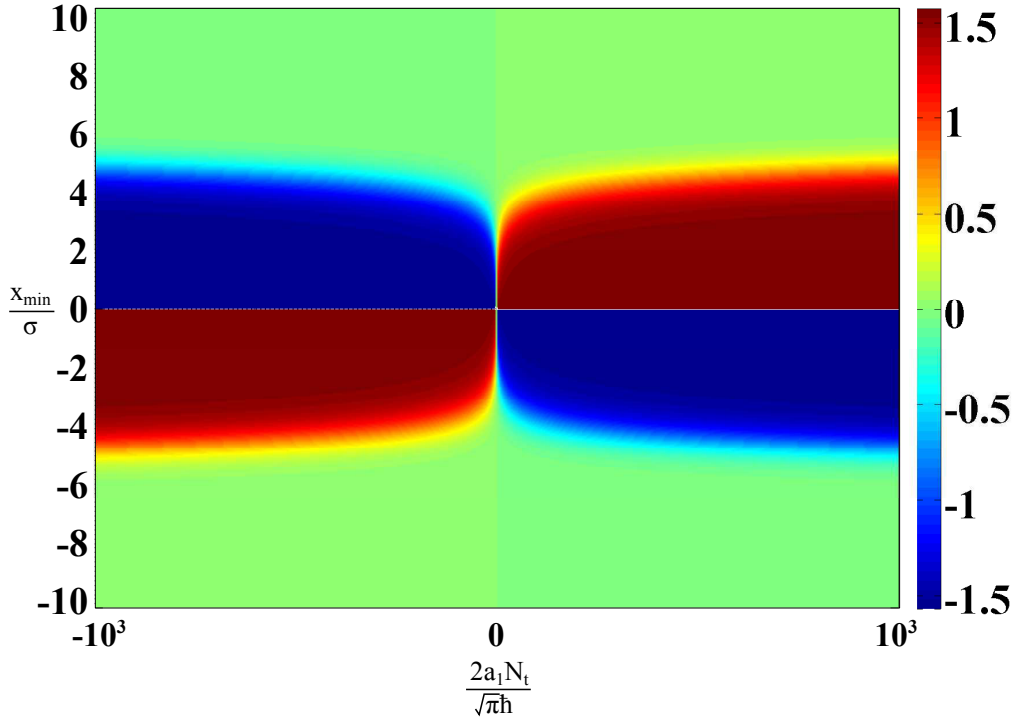

Figure 6.3: Surface plot of equation (6.4.9), as a function of the dimensionless gauge potential strength $2a_1N_t/\sqrt{\pi}\hbar$ and tight-binding parameter $x_{\min}/\sigma$. The colour indicates the angle, from $\varphi_0 = -\pi/2$ (dark blue) to $\varphi_0 = \pi/2$ (dark red).

underlying continuum model. In this limit equation 6.4.1 can be simplified to

$$H = \frac{\Lambda z^2}{2} - R\sqrt{1-z^2}\cos(\varphi - \varphi_0), \tag{6.4.8}$$

where $R = \sqrt{1+\gamma_1^2}$ and the angle $\varphi_0 = \arctan(\gamma_1)$, and we set $\Delta E = 0$ without loss of generality. Using the expressions for Γ_i already obtained, one can write down an explicit form for the angle φ_0 in terms of the variable $x_{\min}/\sigma$,

$$\varphi_0 = \arctan\left[\frac{2a_1N_t}{\sqrt{\pi}\hbar}\left(\frac{\sigma}{x_{\min}}\right)\exp(-x_{\min}^2/\sigma^2)\right]. \tag{6.4.9}$$

Figure 6.3 shows equation (6.4.9) plotted as a surface for various values of the dimensionless quantity $2a_1N_t/\sqrt{\pi}\hbar$ and $x_{\min}/\sigma$. One can see that the angle φ_0 changes both in sign and magnitude as a function of the parameters $x_{\min}/\sigma$ and $2a_1N_t/\sqrt{\pi}\hbar$. Indeed, it is seen that for any fixed gauge potential strength, for large $x_{\min}/\sigma$, $\varphi_0 \to 0$. Close to the origin $(0,0)$, the angle φ_0 changes sign. So, in order to make the angle φ_0 influential, one needs to have $a_1N_t/\hbar \gg 1$, a situation readily achievable, as it was assumed previously that $N_t \gg 1$ to obtain the underlying model, equation (6.4.1).

Figure 6.4 shows the phase-space trajectories of the variables z, φ. In figure 6.4(a)

we are interested in the phase-space with on-site interactions, $\Lambda = 2$, whereas figure 6.4(b) shows the phase-space plotted without on-site interactions, $\Lambda = 0$. This is justifiable as we could for example use Feshbach resonances in order to achieve $g = 0$, a point which was also made by the authors of [163]. The plots for $\Lambda = 2$ show how increasing the strength of the current causes the curves obtained from the numerical solutions to equations (6.4.6) and (6.4.7) to increase in size. For example, figure 6.4(b) shows how increasing the strength of the current without on-site interactions gives a displacement of the curves by an amount φ_0. To further quantify this, one can calculate the critical value Λ_c that determines the point at which the nonrigid pendulum is given an initial kick that pushes it over the vertical $\varphi = \pi$ point. The critical value that determines when this occurs is defined from equation (6.4.8) by the point at which [163]

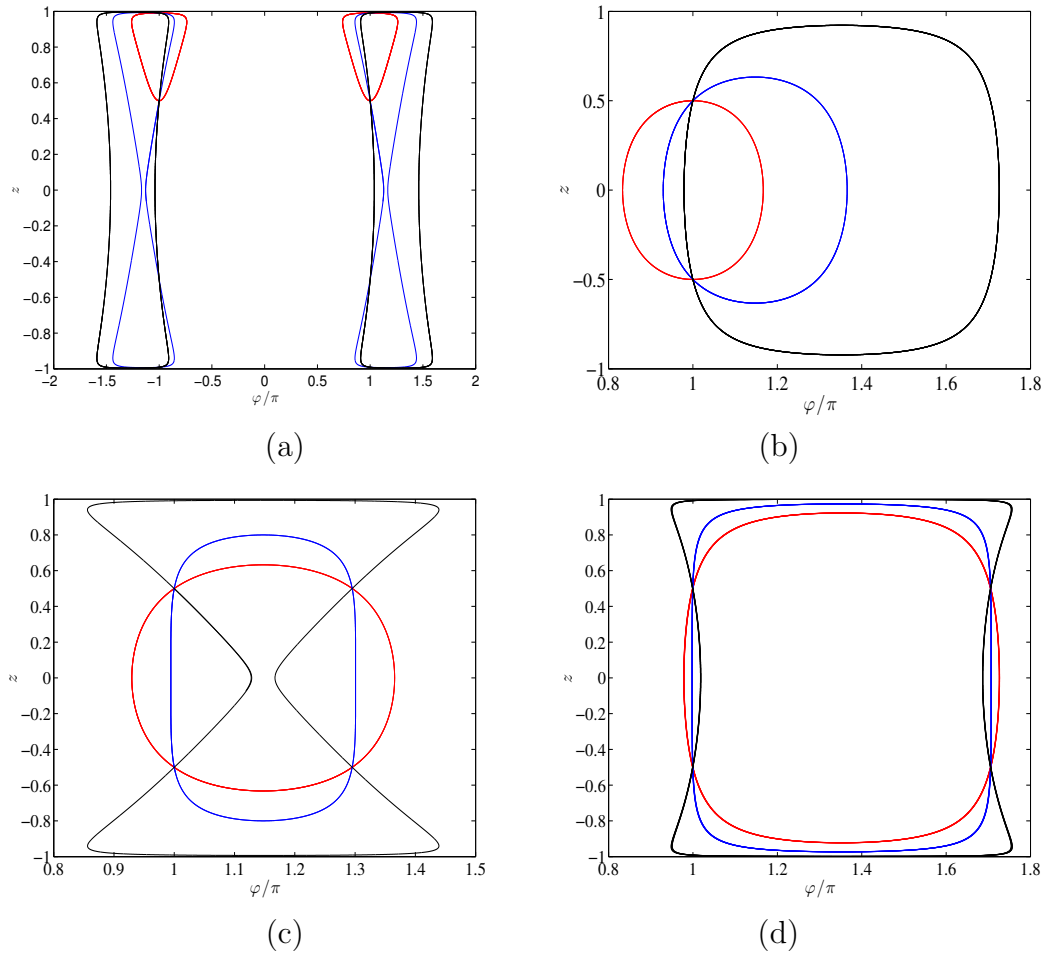

Figure 6.4: Lines of constant energy, with z versus φ. The initial conditions were $z(0) = 0.5$ and $\varphi(0) = \pi$ for (a)-(d). Figure (a) shows the numerical solutions to equations (6.4.6) and (6.4.7) with $\Lambda = 2$, while in (b) $\Lambda = 0$. The smallest to largest curves in each figure correspond to $\gamma_1 = \{0, \frac{1}{2}, 2\}$, respectively. For figures (c) and (d) the parameter $\gamma_1 = \frac{1}{2}$ for (c) and $\gamma_1 = 4$ for (d). The smallest through largest curves are then plotted for the values $\Lambda = \{0, 1, 2\}$ respectively [162].

$$H_0[z(0), \varphi(0)] = \frac{\Lambda z(0)^2}{2} - \sqrt{1 - z(0)^2}\cos(\varphi(0) - \varphi_0) > 1. \tag{6.4.10}$$

This condition allows us to determine the critical value Λ_c. When the parameter Λ exceeds this value, the population is said to become self-trapped, which is defined as $\langle z \rangle \neq 0$. Thus, the critical value is obtained from equation (6.4.10) as

$$\Lambda_c = \frac{2(1 + \sqrt{1 - z(0)^2}\cos(\varphi(0) - \varphi_0))}{z(0)^2}. \tag{6.4.11}$$

Let us consider the lowest energy configurations of equation (6.4.8). The ground state is obtained by the choice $z = z_g = 0$ and $\varphi = \varphi_g = 2\pi n + \varphi_0$, where n is an integer. The ground state energy is $E_g = -R$. The next state is given by $z = 0$ and $\varphi = \varphi_0 + (2n + 1)\pi$, with energy $E = +R$.

6.5 Summary

In this chapter it was shown how a continuum one-dimensional mean-field theory describing density-dependent gauge fields can be cast into a discrete two-site tight binding model, using a symmetric double-well potential. It was seen that this discrete formulation also features a current operator as well as the usual on-site interactions that appear in the standard Bose-Hubbard model. Finally, a phase-space analysis was presented, by way of the nonlinear Josephson equations. It was found that a classical Hamiltonian can be written down that describes the motion of a non-rigid pendulum, with an initial angular offset that depends directly on the strength of the density-dependent gauge potential.

Chapter 7

Summary and Outlook

In this thesis the concept of artificial gauge fields for ultracold atoms was discussed. It was shown how gauge potentials can be optically generated using the adiabatic theorem for these multi-level atoms. The first two chapters gave an introduction to the physics of cold atoms and the theory of gauge fields, respectively. It was explained how the dressed states of multi-level atoms can be used to construct artificial gauge fields, including the important concept of the dark state.

The third chapter develops these ideas further to consider the role that disorder plays for a spin-orbit coupled Bose-Einstein condensate. In particular, it was shown that for a particular choice of laser geometry an equation of motion can be generated for the condensate that exhibits a Dirac cone structure. This novel system was investigated to understand in particular how the localization properties of the system change as the strength of the spin-orbit coupling is varied. It was found that there is a crossover from Anderson localization to an 'anomalous' (non-localised) state as the strength of the spin-orbit coupling is increased from the Schrödinger to Dirac limit. The localization length of the spin-orbit coupled system was also calculated, and it was observed that this increases as one approaches the Dirac limit, in agreement with the numerical simulations presented in the first part of the chapter. In the final part of this chapter, the density of states (DoS) was calculated numerically, and it was shown that there is a peak at the Dirac point reminiscent of a Dyson singularity.

To truly simulate a gauge theory, one must be able to construct gauge fields that are dynamical variables. To this end, the fourth chapter details one method to create interacting gauge fields for the condensate. It was described how interacting gauge

fields can be formed by introducing perturbed dressed states, where it was assumed that the light-matter coupling (parametrized by the Rabi-frequency Ω) is stronger than the inter-particle scattering. This naturally leads to an effective Hamiltonian where the momentum is coupled to the density of the gas, such that one has density dependent gauge potentials. Interestingly, when one obtains the Gross-Pitaevskii like equation by minimising the associated energy functional, an extra term is obtained proportional to $\mathbf{a}_1 \cdot \mathbf{j}$, where $\mathbf{j}$ is the current operator and $\mathbf{a}_1$ parametrizes the strength of the gauge potential. This is an example of an anomaly, where the classical and quantum symmetries of a model differ. Historically, it was believed that the π^0 particle (pi meson) did not decay. However, a form of chiral anomaly explained how in fact the pion could decay into two photons [166].

The second part of this chapter explores the one-dimensional physics of this model. In particular it was shown that the expansion of such a condensate exhibits an unusual asymmetry. This scenario was further explored using a variational ansatz. In particular, the condensate was seen to experience a drift in the centre of mass. Next, a condensate in a ring was described. By calculating the eigenstates of this system using a plane wave (vortex) ansatz, it was found that the lowest angular momentum state changes at a critical density that depends on the particular angular momentum state given by the quantum number q. This unusual nonlinear system was explored further in the last part of this chapter, where it was shown that exact propagating soliton solutions can be constructed. These solutions are different to the Gross-Pitaevskii solitons, as they have a preferred direction, i.e. they are chiral. Mathematically, this is due to the strength of the nonlinear term being proportional to the velocity of the soliton, while physically the origin of the chiral soliton is from the lack of Galilean symmetry in the microscopic formulation of the theory. The concept of a chiral soliton was demonstrated by propagating the (initially) confined solution towards a hard wall. When the wave packet was reflected, the velocity changes and the soliton was no longer confined.

As an extension of the concept of a density dependent gauge potential, Chapter 6 of the thesis considers the effect of placing this model on a two site lattice. As such, it was shown how a modified form of the Hubbard model can be derived that includes the extra terms resulting from the one-dimensional continuum model presented in the previous chapter. The model was subsequently studied by looking at the population oscillations between the two wells for a variety of initial phase conditions. Interestingly, it was found that there are population dynamics even when the initial phase difference between the two wells is zero. This model was further analysed by drawing an analogy with a nonrigid pendulum. It was seen that the

effect of the extra terms in the underlying model cause the pendulum to undergo an angular offset that depends on the strength of the gauge potential. In the final part of this chapter, the nonlinear Josephson equations are solved numerically. The resulting phase-space trajectories show in particular that increasing the strength of the gauge potential causes two effects: the angular offset described above, and also an increase in the size of the obtained curves. This effect is no doubt linked to the increased population oscillations observed at larger values of the $\mathbf{a}_1$ parameter described in the first part of that chapter.

The work presented in this thesis has a number of natural extensions. The two chapters concerning density dependent gauge fields offers a new avenue to explore nonlinear phenomena with cold gases. It is expected that this model will offer many new usual effects. Particular attention should be focused on two-dimensions, where the structure of the vortex lattice will provide insight into the superfluid response of the system. As well as this, one can also study the excitation spectrum of the cloud, which would provide further insight into the gas, for both one and two-dimensional cases.

There are also opportunities at the single particle level. As an extension to the work considered in the third chapter, there is also the possibility to generate 'random' gauge fields. Here, one would use the notation of the perturbed dressed state at the single particle level in order to create a random gauge potential via the Berry's phase method. Such a situation would require one to work with dark states again, as the extended lifetimes of these dressed states would be required in an experiment to observe the associated localization effects. Alternately, one could use the Raman schemes discussed in the third chapter of this thesis, where a random detuning is used to generate the gauge potential.

To conclude, this work demonstrated experimentally feasible schemes for studying artificial gauge theories with gases of ultracold atoms at both the single and many particle level. In particular optical setups were described that would allow the generation of said potentials, and the relevant experimental parameters were described that would allow the observation of the effects associated with these potentials.

Appendix A

Numerical calculation: Disorder dynamics

The dimensionless Schrödinger equation (equation (4.6.1) of section 4.6) that we wish to discretise is

$$i\frac{\partial}{\partial\tau}\mathbf{\Psi} = -\frac{\hbar\Gamma}{2mv_D^2}\frac{\partial^2}{\partial\xi^2}\mathbf{\Psi} - i\cos\theta\hat{\sigma}_x\frac{\partial}{\partial\xi}\mathbf{\Psi} + \tilde{\Delta}(\xi)\hat{\sigma}_z\mathbf{\Psi}, \tag{A.0.1}$$

where $\mathbf{\Psi} = (\psi^+, \psi^-)^{\mathbf{T}}$. The taylor expansion of $\psi^{\pm}(\xi)$ around ξ is given by

$$\psi^{\pm}(\xi) = \sum_{n=0}^{\infty}\frac{(\xi-\xi_i)^n}{n!}\frac{d^n\psi^{\pm}}{d\xi^n}\bigg|_{\xi=\xi_i}, \tag{A.0.2}$$

from which the following expressions for the derivatives appearing in equation (A.0.1) can be obtained

$$\frac{d\psi^{\pm}}{d\xi}\bigg|_{\xi=\xi_i} = \frac{\psi^{\pm}_{i+1}-\psi^{\pm}_{i-1}}{2\Delta\xi} - \frac{\Delta\xi^2}{6}\frac{d^3\psi^{\pm}}{d\xi^3}\bigg|_{\xi=\xi_i}, \tag{A.0.3}$$

$$\frac{d^2\psi^{\pm}}{d\xi^2}\bigg|_{\xi=\xi_i} = \frac{\psi^{\pm}_{i+1}-2\psi^{\pm}_{i}+\psi^{\pm}_{i-1}}{\Delta\xi^2} - \frac{\Delta\xi^2}{12}\frac{d^4\psi^{\pm}}{d\xi^4}\bigg|_{\xi=\xi_i}, \tag{A.0.4}$$

where we define the spatial integration step $\Delta\xi = \xi_{i+1} - \xi_i$. Equations (A.0.3) and (A.0.4) constitute the central difference method, with error $\mathcal{O}(\Delta\xi^2)$. Inserting these expressions into equation (A.0.1), we obtain the finite difference equation

$$\begin{aligned}\frac{i}{\Delta\tau}(\psi^{\pm}_{i,n}-\psi^{\pm}_{i,n-1}) = &- J_S(\psi^{\pm}_{i+1,n}-2\psi^{\pm}_{i,n}+\psi^{\pm}_{i-1,n}) \\ &- iJ_D(\psi^{\mp}_{i+1,n}-\psi^{\mp}_{i-1,n}) \pm \tilde{\Delta}_i\psi^{\pm}_{i,n},\end{aligned} \tag{A.0.5}$$

where $\Delta\tau$ is the time step, the constants $J_S = \hbar\Gamma/2mv_D^2\Delta\xi^2$ and $J_D = \cos\theta/2\Delta\xi$, $\{i, n\}$ labels discrete points in space and time respectively and the $\pm$ superscripts refer to the two spin components of $\mathbf{\Psi}$. Equation (A.0.5) can also be written in terms of the discrete Hamiltonian

$$\hat{H} = \left(\begin{array}{c|c} A^+ & B \\ \hline B & A^- \end{array}\right) \tag{A.0.6}$$

and the wave function is given by $\Psi^T = (\Psi_1^+, \Psi_2^+, \cdots, \Psi_N^+, \Psi_1^-, \Psi_2^-, \cdots, \Psi_N^-)$. The blocks $A^\pm$ and B are then given by

$$A^\pm = \begin{pmatrix} 2J_S \pm \tilde{\Delta}_1 & -J_S & 0 & 0 & 0 \\ -J_S & 2J_S \pm \tilde{\Delta}_2 & -J_S & 0 & 0 \\ \vdots & \ddots & \ddots & \ddots & \vdots \\ 0 & 0 & 0 & -J_S & 2J_S \pm \tilde{\Delta}_N \end{pmatrix}, \tag{A.0.7}$$

$$B = \begin{pmatrix} 0 & -iJ_D & 0 & 0 & 0 \\ iJ_D & 0 & -iJ_D & 0 & 0 \\ \vdots & \ddots & \ddots & \ddots & \vdots \\ 0 & 0 & 0 & iJ_D & 0 \end{pmatrix}. \tag{A.0.8}$$

To generate the normally distributed pseudo random numbers per equation 4.4.1, $(\tilde{\Delta}_i)$ we use the Box-Muller transformation [167]. The transformation states that given two independent random variables U_1, U_2 drawn from the same rectangular density function on the interval $(0, 1)$, then

$$\tilde{\Delta}_1 = \sqrt{-2\ln U_1}\cos(2\pi U_2) \quad \text{and} \quad \tilde{\Delta}_2 = \sqrt{-2\ln U_1}\sin(2\pi U_2) \tag{A.0.9}$$

will be a pair of independent random variables with zero mean and unit variance. To connect the discrete model to the continuum model in section 4.4, we integrate both sides of equation 4.4.1 over ξ to obtain

$$\int_{-\infty}^{\infty} d\xi \overline{\tilde{\Delta}(\xi)\tilde{\Delta}(\xi')} = 1. \tag{A.0.10}$$

The quadrature of this expression gives us the following relationship

$$\sum_{i=1}^{N} \overline{\tilde{\Delta}_i\tilde{\Delta}_j} = \frac{1}{\Delta\xi}. \tag{A.0.11}$$

The numerical simulations were performed with FORTRAN 90, the integration step was taken as $\Delta\xi = 2.5\text{x}10^{-2}$ and for the time step $\Delta\tau = 2.5\text{x}10^{-4}$. The discrete

wave functions comprised $N = 10^4$ points for each component ψ^+ and ψ^-.

References

[1] R. P. Feynman. Simulating physics with computers. *Int. J. Theor. Phys.* **21**, 467 (1982).

[2] Y.-J. Lin, R. L. Compton, A. R. Perry, W. D. Phillips, J. V. Porto, and I. B. Spielman. Bose-Einstein Condensate in a Uniform Light-Induced Vector Potential. *Phys. Rev. Lett.* **102**, 130401 (2009).

[3] Y. J. Lin, R. L. Compton, K. Jimenez-Garcia, J. V. Porto, and I. B. Spielman. Synthetic magnetic fields for ultracold neutral atoms. *Nature* **462**, 628 (2009).

[4] Y. J. Lin, K. Jimenez-Garcia, and I. B. Spielman. Spin-orbit-coupled Bose-Einstein condensates. *Nature* **471**, 83 (2011).

[5] T. D. Stanescu, B. Anderson, and V. Galitski. Spin-orbit coupled Bose-Einstein condensates. *Phys. Rev. A* **78**, 023616 (2008).

[6] L. J. LeBlanc, K. Jiménez-García, R. A. Williams, M. C. Beeler, A. R. Perry, W. D. Phillips, and I. B. Spielman. Observation of a superfluid Hall effect. *P. Natl. Acad. Sci. USA* **109**, 10811 (2012).

[7] M. C. Beeler, R. A. Williams, K. Jimenez-Garcia, L. J. LeBlanc, A. R. Perry, and I. B. Spielman. The spin Hall effect in a quantum gas. *Nature* **498**, 201 (2013).

[8] M. Merkl, F. E. Zimmer, G. Jūzeliunas, and P. Öhberg. Atomic Zitterbewegung. *EPL* **83**, 54002 (2008).

[9] J. Ruseckas, G. Juzeliūnas, P. Öhberg, and M. Fleischhauer. Non-Abelian Gauge Potentials for Ultracold Atoms with Degenerate Dark States. *Phys. Rev. Lett.* **95**, 010404 (2005).

[10] I. Bloch, J. Dalibard, and W. Zwerger. Many-body physics with ultracold gases. *Rev. Mod. Phys.* **80**, 885 (2008).

[11] M. Greiner, O. Mandel, T. Esslinger, T. W. Hansch, and I. Bloch. Quantum phase transition from a superfluid to a Mott insulator in a gas of ultracold atoms. *Nature* **415**, 39 (2002).

[12] J. Struck, C. Ölschläger, R. Le Targat, P. Soltan-Panahi, A. Eckardt, M. Lewenstein, P. Windpassinger, and K. Sengstock. Quantum Simulation of Frustrated Classical Magnetism in Triangular Optical Lattices. *Science* **333**, 996 (2011).

[13] S. M. Barnett. *Quantum Information*. Oxford University Press, 2009.

[14] L. J. Garay, J. R. Anglin, J. I. Cirac, and P. Zoller. Sonic Analog of Gravitational Black Holes in Bose-Einstein Condensates. *Phys. Rev. Lett.* **85**, 4643 (2000).

[15] I. Aitchison and A. Hey. *Gauge Theories in Particle Physics: A Practical Introduction*. IOP Publishing, Bristol, 1989.

[16] P. A. M. Dirac. The Quantum Theory of the Electron. *Proc. Roy. Soc. (London)* **A117**, 610 (1928).

[17] A. J. Leggett. *Quantum Liquids*. Oxford University Press, 2006.

[18] S. N. Bose. Plancks Gesetz und Lichtquantenhypothese. *Z. Phys.* **26**, 178 (1924).

[19] A. Einstein. Quantentheorie des einatomigen idealen Gases. *Sitzungsber. Kgl. Presuss. Akad. Wiss.* , 261 (1924).

[20] O. Penrose and L. Onsager. Bose-Einstein Condensation and Liquid Helium. *Phys. Rev.* **104**, 576 (1956).

[21] F. London. On the Bose-Einstein Condensation. *Phys. Rev.* **54**, 947 (1938).

[22] N. Bogoliubov. On the theory of superfluidity. *J. Phys. (USSR)* **11**, 23 (1947).

[23] J. Bardeen, L. N. Cooper, and J. R. Schrieffer. Theory of Superconductivity. *Phys. Rev.* **108**, 1175 (1957).

[24] D. J. Wineland, R. E. Drullinger, and F. L. Walls. Radiation-Pressure Cooling of Bound Resonant Absorbers. *Phys. Rev. Lett.* **40**, 1639 (1978).

[25] W. Neuhauser, M. Hohenstatt, P. Toschek, and H. Dehmelt. Optical-Sideband Cooling of Visible Atom Cloud Confined in Parabolic Well. *Phys. Rev. Lett.* **41**, 233 (1978).

[26] C. E. Hecht. The possible superfluid behaviour of hydrogen atom gases and liquids. *Physica* **25**, 1159 (1959).

[27] M. H. Anderson, J. R. Ensher, M. R. Matthews, C. E. Wieman, and E. A. Cornell. Observation of Bose-Einstein Condensation in a Dilute Atomic Vapor. *Science* **269**, 198 (1995).

[28] K. B. Davis, M. O. Mewes, M. R. Andrews, N. J. van Druten, D. S. Durfee, D. M. Kurn, and W. Ketterle. Bose-Einstein Condensation in a Gas of Sodium Atoms. *Phys. Rev. Lett.* **75**, 3969 (1995).

[29] C. C. Bradley, C. A. Sackett, J. J. Tollett, and R. G. Hulet. Evidence of Bose-Einstein Condensation in an Atomic Gas with Attractive Interactions. *Phys. Rev. Lett.* **75**, 1687 (1995).

[30] S. Jochim, M. Bartenstein, A. Altmeyer, G. Hendl, S. Riedl, C. Chin, J. Hecker Denschlag, and R. Grimm. Bose-Einstein Condensation of Molecules. *Science* **302**, 2101 (2003).

[31] S. Inouye, M. R. Andrews, J. Stenger, H. J. Miesner, D. M. Stamper-Kurn, and W. Ketterle. Observation of Feshbach resonances in a Bose-Einstein condensate. *Nature* **392**, 151 (1998).

[32] J. Kasprzak, M. Richard, S. Kundermann, A. Baas, P. Jeambrun, J. M. J. Keeling, F. M. Marchetti, M. H. Szymanska, R. Andre, J. L. Staehli, V. Savona, P. B. Littlewood, B. Deveaud, and L. S. Dang. Bose-Einstein condensation of exciton polaritons. *Nature* **443**, 409 (2006).

[33] E. Gross. Structure of a quantized vortex in boson systems. *Il Nuovo Cimento Series 10* **20**, 454 (1961).

[34] L. P. Pitaevskii. Vortex lines in an imperfect bose gas. *Sov. Phys. JETP* **13**, 451 (1961).

[35] C. Pethick and H. Smith. *Bose-Einstein Condensation in Dilute Gases*. Cambridge, 2008.

[36] V. Ginzburg and L. D. Landau. On the theory of superconductivity. *Zh. Eksp. Teor. Fiz.* **20**, 1064 (1950).

[37] L. Onsager. *Nuovo Cimento* **6**, 249 and 281.

[38] R. Feynman. Chapter {II} Application of Quantum Mechanics to Liquid Helium. *Progress in Low Temperature Physics* **1**, 17 (1955).

[39] J. R. Abo-Shaeer, C. Raman, J. M. Vogels, and W. Ketterle. Observation of Vortex Lattices in Bose-Einstein Condensates. *Science* **292**, 476 (2001).

[40] J. Dalibard, F. Gerbier, G. Juzeliūnas, and P. Öhberg. *Colloquium* : Artificial gauge potentials for neutral atoms. *Rev. Mod. Phys.* **83**, 1523 (2011).

[41] D. L. Campbell, G. Juzeliūnas, and I. B. Spielman. Realistic Rashba and Dresselhaus spin-orbit coupling for neutral atoms. *Phys. Rev. A* **84**, 025602 (2011).

[42] I. B. Spielman. Raman processes and effective gauge potentials. *Phys. Rev. A* **79**, 063613 (2009).

[43] D. Jaksch and P. Zoller. Creation of effective magnetic fields in optical lattices: the Hofstadter butterfly for cold neutral atoms. *New. J. Phys.* **5**, 56 (2003).

[44] K. Jiménez-García, L. J. LeBlanc, R. A. Williams, M. C. Beeler, A. R. Perry, and I. B. Spielman. Peierls Substitution in an Engineered Lattice Potential. *Phys. Rev. Lett.* **108**, 225303 (2012).

[45] M. Aidelsburger, M. Atala, S. Nascimbène, S. Trotzky, Y.-A. Chen, and I. Bloch. Experimental Realization of Strong Effective Magnetic Fields in an Optical Lattice. *Phys. Rev. Lett.* **107**, 255301 (2011).

[46] G. Juzeliūnas and P. Öhberg. Slow Light in Degenerate Fermi Gases. *Phys. Rev. Lett.* **93**, 033602 (2004).

[47] G. Juzeliūnas, P. Öhberg, J. Ruseckas, and A. Klein. Effective magnetic fields in degenerate atomic gases induced by light beams with orbital angular momenta. *Phys. Rev. A* **71**, 053614 (2005).

[48] M. Fleischhauer, A. Imamoglu, and J. P. Marangos. Electromagnetically induced transparency: Optics in coherent media. *Rev. Mod. Phys.* **77**, 633 (2005).

[49] G. Juzeliūnas, J. Ruseckas, and P. Öhberg. Effective magnetic fields induced by EIT in ultra-cold atomic gases. *J. Phys. B-At. Mol. Opt* **38**, 4171 (2005).

[50] G. Juzeliūnas, J. Ruseckas, M. Lindberg, L. Santos, and P. Öhberg. Quasirelativistic behavior of cold atoms in light fields. *Phys. Rev. A* **77**, 011802 (2008).

[51] L. J. LeBlanc, M. C. Beeler, K. Jiménez-García, A. R. Perry, S. Sugawa, R. A. Williams, and I. B. Spielman. Direct observation of zitterbewegung in a Bose-Einstein condensate. *New. J. Phys.* **15**, 073011 (2013).

[52] G. Juzeliūnas, J. Ruseckas, A. Jacob, L. Santos, and P. Öhberg. Double and Negative Reflection of Cold Atoms in Non-Abelian Gauge Potentials. *Phys. Rev. Lett.* **100**, 200405 (2008).

[53] C. Salomon, J. Dalibard, A. Aspect, H. Metcalf, and C. Cohen-Tannoudji. Channeling atoms in a laser standing wave. *Phys. Rev. Lett.* **59**, 1659 (1987).

[54] J. I. Cirac, P. Maraner, and J. K. Pachos. Cold Atom Simulation of Interacting Relativistic Quantum Field Theories. *Phys. Rev. Lett.* **105**, 190403 (2010).

[55] K. G. Wilson. Confinement of quarks. *Phys. Rev. D* **10**, 2445 (1974).

[56] N. Metropolis, A. W. Rosenbluth, M. N. Rosenbluth, A. H. Teller, and E. Teller. Equation of State Calculations by Fast Computing Machines. *J. Chem. Phys.* **21**, 1087 (1953).

[57] K. Osterloh, M. Baig, L. Santos, P. Zoller, and M. Lewenstein. Cold Atoms in Non-Abelian Gauge Potentials: From the Hofstadter"Moth" to Lattice Gauge Theory. *Phys. Rev. Lett.* **95**, 010403 (2005).

[58] P. Würtz, T. Langen, T. Gericke, A. Koglbauer, and H. Ott. Experimental Demonstration of Single-Site Addressability in a Two-Dimensional Optical Lattice. *Phys. Rev. Lett.* **103**, 080404 (2009).

[59] A. Eckardt, C. Weiss, and M. Holthaus. Superfluid-Insulator Transition in a Periodically Driven Optical Lattice. *Phys. Rev. Lett.* **95**, 260404 (2005).

[60] Y.-A. Chen, S. Nascimbène, M. Aidelsburger, M. Atala, S. Trotzky, and I. Bloch. Controlling Correlated Tunneling and Superexchange Interactions with ac-Driven Optical Lattices. *Phys. Rev. Lett.* **107**, 210405 (2011).

[61] N. R. Cooper and J. Dalibard. Reaching Fractional Quantum Hall States with Optical Flux Lattices. *Phys. Rev. Lett.* **110**, 185301 (2013).

[62] N. R. Cooper. Optical Flux Lattices for Ultracold Atomic Gases. *Phys. Rev. Lett.* **106**, 175301 (2011).

[63] C. A. Mead. The geometric phase in molecular systems. *Rev. Mod. Phys.* **64**, 51 (1992).

[64] M. V. Berry. Quantal Phase Factors Accompanying Adiabatic Changes. *Proc. Roy. Soc. Lond. A. Mat* **392**, 45 (1984).

[65] A. A. Abrikosov. On the magnetic properties of Superconductors of the second group. *Sov. Phys. JETP* **5**, 1174 (1957).

[66] A. Bohm, A. Mostafazadeh, H. Koizumi, Q. Niu, and J. Zwanziger. *The Geometric Phase in Quantum Systems*. Springer, 2003.

[67] M. Born and R. Oppenheimer. Zur Quantentheorie der Molekeln. *Annalen der Physik* **389**, 457 (1927).

[68] F. Wilczek and A. Zee. Appearance of Gauge Structure in Simple Dynamical Systems. *Phys. Rev. Lett.* **52**, 2111 (1984).

[69] J. Moody, A. Shapere, and F. Wilczek. Realizations of Magnetic-Monopole Gauge Fields: Diatoms and Spin Precession. *Phys. Rev. Lett.* **56**, 893 (1986).

[70] C.-P. Sun and M.-L. Ge. Generalizing Born-Oppenheimer approximations and observable effects of an induced gauge field. *Phys. Rev. D* **41**, 1349 (1990).

[71] M. Cheneau, S. P. Rath, T. Yefsah, K. J. Günter, G. Juzeliūnas, and J. Dalibard. Geometric potentials in quantum optics: A semi-classical interpretation. *EPL* **83**, 60001 (2008).

[72] J. D.-R. C. Cohen-Tannoudji and G. Grynberg. *Photons & Atoms*. Wiley, 1997.

[73] M. D. Lukin. *Colloquium* : Trapping and manipulating photon states in atomic ensembles. *Rev. Mod. Phys.* **75**, 457 (2003).

[74] S. M. Barnett and P. M. Radmore. *Methods in Theoretical Quantum Optics*. Oxford University Press, 2005.

[75] A. Jacob. *Non-Abelian Atom Optics*. PhD thesis, Universität Hannover, 2009.

[76] V. Pietilä and M. Möttönen. Non-Abelian Magnetic Monopole in a Bose-Einstein Condensate. *Phys. Rev. Lett.* **102**, 080403 (2009).

[77] V. Pietilä and M. Möttönen. Creation of Dirac Monopoles in Spinor Bose-Einstein Condensates. *Phys. Rev. Lett.* **103**, 030401 (2009).

[78] S. Tung, V. Schweikhard, and E. A. Cornell. Observation of Vortex Pinning in Bose-Einstein Condensates. *Phys. Rev. Lett.* **97**, 240402 (2006).

[79] R. A. Williams, S. Al-Assam, and C. J. Foot. Observation of Vortex Nucleation in a Rotating Two-Dimensional Lattice of Bose-Einstein Condensates. *Phys. Rev. Lett.* **104**, 050404 (2010).

[80] A. Klein and D. Jaksch. Phonon-induced artificial magnetic fields in optical lattices. *Europhys. Lett.* **85**, 13001 (2009).

[81] J. Ruostekoski, G. V. Dunne, and J. Javanainen. Particle Number Fractionalization of an Atomic Fermi-Dirac Gas in an Optical Lattice. *Phys. Rev. Lett.* **88**, 180401 (2002).

[82] P. W. Anderson. Absence of Diffusion in Certain Random Lattices. *Phys. Rev.* **109**, 1492 (1958).

[83] M. Cutler and N. F. Mott. Observation of Anderson Localization in an Electron Gas. *Phys. Rev.* **181**, 1336 (1969).

[84] D. S. Wiersma, P. Bartolini, A. Lagendijk, and R. Righini. Localization of light in a disordered medium. *Nature* **390**, 671 (1997).

[85] R. Dalichaouch, J. P. Armstrong, S. Schultz, P. M. Platzman, and S. L. McCall. Microwave localization by two-dimensional random scattering. *Nature* **354**, 53 (1991).

[86] R. L. Weaver. Anderson localization of ultrasound. *Wave Motion* **12**, 142 (1990).

[87] A. A. Gogolin. Electron localization and hopping conductivity in one-dimensional disordered systems. *Phys. Rep.* **86**, 1 (1982).

[88] M. Fabrizio and R. Mélin. Coexistence of Antiferromagnetism and Dimerization in a Disordered Spin-Peierls Model: Exact Results. *Phys. Rev. Lett.* **78**, 3382 (1997).

[89] R. G. Unanyan, J. Otterbach, M. Fleischhauer, J. Ruseckas, V. Kudriašov, and G. Juzeliūnas. Spinor Slow-Light and Dirac Particles with Variable Mass. *Phys. Rev. Lett.* **105**, 173603 (2010).

[90] I. M. Lifshits, S. A. Gredeskul, and L. A. Pastur. *Introduction to the theory of disordered systems.* Wiley, New York, 1988.

[91] D. G. Shelton and A. M. Tsvelik. Effective theory for midgap states in doped spin-ladder and spin-Peierls systems: Liouville quantum mechanics. *Phys. Rev. B* **57**, 14242 (1998).

[92] L. Balents and M. P. A. Fisher. Delocalization transition via supersymmetry in one dimension. *Phys. Rev. B* **56**, 12970 (1997).

[93] A. J. Millis and H. Monien. Pseudogaps in one-dimensional models with quasi-long-range order. *Phys. Rev. B* **61**, 12496 (2000).

[94] L. Bartosch and P. Kopietz. Exact numerical calculation of the density of states of the fluctuating gap model. *Phys. Rev. B* **60**, 15488 (1999).

[95] F. J. Dyson. The Dynamics of a Disordered Linear Chain. *Phys. Rev.* **92**, 1331 (1953).

[96] L. Fleishman and D. C. Licciardello. Fluctuations and localization in one dimension. *J. Phys. C. Solid State* **10**, L125 (1977).

[97] G. Theodorou and M. H. Cohen. Extended states in a one-demensional system with off-diagonal disorder. *Phys. Rev. B* **13**, 4597 (1976).

[98] T. P. Eggarter and R. Riedinger. Singular behavior of tight-binding chains with off-diagonal disorder. *Phys. Rev. B* **18**, 569 (1978).

[99] E. R. Smith. One-dimensional X-Y model with random coupling constants. I. Thermodynamics. *J. Phys. C. Solid State* **3**, 1419 (1970).

[100] S.-L. Zhu, D.-W. Zhang, and Z. D. Wang. Delocalization of Relativistic Dirac Particles in Disordered One-Dimensional Systems and Its Implementation with Cold Atoms. *Phys. Rev. Lett.* **102**, 210403 (2009).

[101] R. Unanyan, M. Fleischhauer, B. Shore, and K. Bergmann. Robust creation and phase-sensitive probing of superposition states via stimulated Raman adiabatic passage (STIRAP) with degenerate dark states. *Opt. Commun.* **155**, 144 (1998).

[102] P. Strange. *Relativistic Quantum Mechanics.* Cambridge University Press, 1998.

[103] S. Das Sarma, S. Adam, E. H. Hwang, and E. Rossi. Electronic transport in two-dimensional graphene. *Rev. Mod. Phys.* **83**, 407 (2011).

[104] R. Gerritsma, G. Kirchmair, F. Zahringer, E. Solano, R. Blatt, and C. F. Roos. Quantum simulation of the Dirac equation. *Nature* **463**, 68 (2010).

[105] J. Billy, V. Josse, Z. Zuo, A. Bernard, B. Hambrecht, P. Lugan, D. Clement, L. Sanchez-Palencia, P. Bouyer, and A. Aspect. Direct observation of Anderson localization of matter waves in a controlled disorder. *Nature* **453**, 891 (2008).

[106] G. Roati, C. D'Errico, L. Fallani, M. Fattori, C. Fort, M. Zaccanti, G. Modugno, M. Modugno, and M. Inguscio. Anderson localization of a non-interacting Bose-Einstein condensate. *Nature* **453**, 895 (2008).

[107] D. Clément, A. F. Varón, J. A. Retter, L. Sanchez-Palencia, A. Aspect, and P. Bouyer. Experimental study of the transport of coherent interacting matter-waves in a 1D random potential induced by laser speckle. *New. J. Phys.* **8**, 165 (2006).

[108] L. Sanchez-Palencia, D. Clément, P. Lugan, P. Bouyer, G. V. Shlyapnikov, and A. Aspect. Anderson Localization of Expanding Bose-Einstein Condensates in Random Potentials. *Phys. Rev. Lett.* **98**, 210401 (2007).

[109] A. A. Ovchinnikov and N. S. Erikhman. Density of states in a one-dimensional random potential. *Zh. Eksp. Teor. Fiz.* **46**, 340 (1977).

[110] L. Pastur and A. Figotin. *Spectra of Random and Almost-Periodic Operators.* Spinger, New York, 1991.

[111] M. J. Edmonds, J. Otterbach, R. G. Unanyan, M. Fleischhauer, M. Titov, and P. Öhberg. From Anderson to anomalous localization in cold atomic gases with effective spin-orbit coupling. *New. J. Phys.* **14**, 073056 (2012).

[112] L. Karpa, F. Vewinger, and M. Weitz. Resonance Beating of Light Stored Using Atomic Spinor Polaritons. *Phys. Rev. Lett.* **101**, 170406 (2008).

[113] H. Wang, S. Li, Z. Xu, X. Zhao, L. Zhang, J. Li, Y. Wu, C. Xie, K. Peng, and M. Xiao. Quantum interference of stored dual-channel spin-wave excitations in a single tripod system. *Phys. Rev. A* **83**, 043815 (2011).

[114] C. M. et al. *Ultracold Gases and Quantum Information.* Oxford University Press, 2009.

[115] O. Klein. Die Reflexion von Elektronen an einem Potentialsprung nach der relativistischen Dynamik von Dirac. *Z. Phys.* **53**, 157 (1929).

[116] B. I. Halperin. Green's Functions for a Particle in a One-Dimensional Random Potential. *Phys. Rev.* **139**, A104 (1965).

[117] J. Bouchaud, A. Comtet, A. Georges, and P. L. Doussal. Classical diffusion of a particle in a one-dimensional random force field. *Ann. Phys-New York* **201**, 285 (1990).

[118] W. E. Thirring. A soluble relativistic field theory. *Ann. Phys-New York* **3**, 91 (1958).

[119] P. M. Chaikin and T. Lubensky. *Principles of condensed matter physics.* Cambridge University Press, 2000.

[120] M. Troyer and U.-J. Wiese. Computational Complexity and Fundamental Limitations to Fermionic Quantum Monte Carlo Simulations. *Phys. Rev. Lett.* **94**, 170201 (2005).

[121] D. Banerjee, M. Dalmonte, M. Müller, E. Rico, P. Stebler, U.-J. Wiese, and P. Zoller. Atomic Quantum Simulation of Dynamical Gauge Fields Coupled to Fermionic Matter: From String Breaking to Evolution after a Quench. *Phys. Rev. Lett.* **109**, 175302 (2012).

[122] D. Banerjee, M. Bögli, M. Dalmonte, E. Rico, P. Stebler, U.-J. Wiese, and P. Zoller. Atomic Quantum Simulation of $\mathbf{U}(N)$ and $\mathrm{SU}(N)$ Non-Abelian Lattice Gauge Theories. *Phys. Rev. Lett.* **110**, 125303 (2013).

[123] P. O. L. Tagliacozzo, A. Celi and M. Lewenstein. Simulations of non-Abelian gauge theories with optical lattices. *arxiv:1211.2704* (2012).

[124] T. Keilmann, S. Lanzmich, I. McCulloch, and M. Roncaglia. Statistically induced phase transitions and anyons in 1D optical lattices. *Nat. Commun.* **2**, 361 (2011).

[125] O. Dutta, A. Eckardt, P. Hauke, B. Malomed, and M. Lewenstein. Bose-Hubbard model with occupation-dependent parameters. *New. J. Phys.* **13**, 023019 (2011).

[126] F. Wilczek. Quantum Mechanics of Fractional-Spin Particles. *Phys. Rev. Lett.* **49**, 957 (1982).

[127] S. J. B. Rabello. 1D Generalized Statistics Gas: A Gauge Theory Approach. *Phys. Rev. Lett.* **76**, 4007 (1996).

[128] S. J. B. Rabello. 1D Generalized Statistics Gas: A Gauge Theory Approach. *Phys. Rev. Lett.* **77**, 4851–4851 (Dec 1996).

[129] U. Aglietti, L. Griguolo, R. Jackiw, S.-Y. Pi, and D. Seminara. Anyons and Chiral Solitons on a Line. *Phys. Rev. Lett.* **77**, 4406 (1996).

[130] P. Kok and B. W. Lovett. *Optical Quantum Information Processing.* Cambridge University Press, 2010.

[131] K. W. Madison, F. Chevy, W. Wohlleben, and J. Dalibard. Vortex Formation in a Stirred Bose-Einstein Condensate. *Phys. Rev. Lett.* **84**, 806 (2000).

[132] R. Dum and M. Olshanii. Gauge Structures in Atom-Laser Interaction: Bloch Oscillations in a Dark Lattice. *Phys. Rev. Lett.* **76**, 1788 (1996).

[133] P. M. Visser and G. Nienhuis. Geometric potentials for subrecoil dynamics. *Phys. Rev. A* **57**, 4581 (1998).

[134] J. Ye, H. J. Kimble, and H. Katori. Quantum State Engineering and Precision Metrology Using State-Insensitive Light Traps. *Science* **320**, 1734 (2008).

[135] A. Görlitz, J. M. Vogels, A. E. Leanhardt, C. Raman, T. L. Gustavson, J. R. Abo-Shaeer, A. P. Chikkatur, S. Gupta, S. Inouye, T. Rosenband, and W. Ketterle. Realization of Bose-Einstein Condensates in Lower Dimensions. *Phys. Rev. Lett.* **87**, 130402 (2001).

[136] F. Schreck, L. Khaykovich, K. L. Corwin, G. Ferrari, T. Bourdel, J. Cubizolles, and C. Salomon. Quasipure Bose-Einstein Condensate Immersed in a Fermi Sea. *Phys. Rev. Lett.* **87**, 080403 (2001).

[137] P. O. Fedichev, Y. Kagan, G. V. Shlyapnikov, and J. T. M. Walraven. Influence of Nearly Resonant Light on the Scattering Length in Low-Temperature Atomic Gases. *Phys. Rev. Lett.* **77**, 2913 (1996).

[138] M. Theis, G. Thalhammer, K. Winkler, M. Hellwig, G. Ruff, R. Grimm, and J. H. Denschlag. Tuning the Scattering Length with an Optically Induced Feshbach Resonance. *Phys. Rev. Lett.* **93**, 123001 (2004).

[139] K. Enomoto, K. Kasa, M. Kitagawa, and Y. Takahashi. Optical Feshbach Resonance Using the Intercombination Transition. *Phys. Rev. Lett.* **101**, 203201 (2008).

[140] D. J. Papoular, G. V. Shlyapnikov, and J. Dalibard. Microwave-induced Fano-Feshbach resonances. *Phys. Rev. A* **81**, 041603 (2010).

[141] E. Harikumar, C. Nagaraja Kumar, and M. Sivakumar. Chiral solitons in a current coupled Schrödinger equation with self-interaction. *Phys. Rev. D* **58**, 107703 (1998).

[142] D. R. Murray. *Vector potentials in Bose-Einstein condensates.* PhD thesis, University of Strathclyde, 2008.

[143] M. J. Edmonds, M. Valiente, G. Juzeliūnas, L. Santos, and P. Öhberg. Simulating an Interacting Gauge Theory with Ultracold Bose Gases. *Phys. Rev. Lett.* **110**, 085301 (2013).

[144] V. E. Zakharov and A. B. Shabat. Exact theory of two-dimensional self-focusing and one-dimensional self-modulation of waves in nonlinear media. *Sov. Phys. JETP* **34**, 62 (1972).

[145] P. Öhberg, E. L. Surkov, I. Tittonen, S. Stenholm, M. Wilkens, and G. V. Shlyapnikov. Low-energy elementary excitations of a trapped Bose-condensed gas. *Phys. Rev. A* **56**, R3346 (1997).

[146] D. R. Murray, S. M. Barnett, P. Öhberg, and D. Gomila. Elementary excitations of a Bose-Einstein condensate in an effective magnetic field. *Phys. Rev. A* **76**, 053626 (2007).

[147] M. R. Andrews, C. G. Townsend, H.-J. Miesner, D. S. Durfee, D. M. Kurn, and W. Ketterle. Observation of Interference Between Two Bose Condensates. *Science* **275**, 637 (1997).

[148] J. Javanainen and S. M. Yoo. Quantum Phase of a Bose-Einstein Condensate with an Arbitrary Number of Atoms. *Phys. Rev. Lett.* **76**, 161 (1996).

[149] J. Stenger, S. Inouye, A. P. Chikkatur, D. M. Stamper-Kurn, D. E. Pritchard, and W. Ketterle. Bragg Spectroscopy of a Bose-Einstein Condensate. *Phys. Rev. Lett.* **82**, 4569 (1999).

[150] J. Denschlag, J. E. Simsarian, D. L. Feder, C. W. Clark, L. A. Collins, J. Cubizolles, L. Deng, E. W. Hagley, K. Helmerson, W. P. Reinhardt, S. L. Rolston, B. I. Schneider, and W. D. Phillips. Generating Solitons by Phase Engineering of a Bose-Einstein Condensate. *Science* **287**, 97 (2000).

[151] A. Smerzi, S. Fantoni, S. Giovanazzi, and S. R. Shenoy. Quantum Coherent Atomic Tunneling between Two Trapped Bose-Einstein Condensates. *Phys. Rev. Lett.* **79**, 4950 (1997).

[152] M. Albiez, R. Gati, J. Fölling, S. Hunsmann, M. Cristiani, and M. K. Oberthaler. Direct Observation of Tunneling and Nonlinear Self-Trapping in a Single Bosonic Josephson Junction. *Phys. Rev. Lett.* **95**, 010402 (2005).

[153] S. Levy, E. Lahoud, I. Shomroni, and J. Steinhauer. The a.c. and d.c. Josephson effects in a Bose-Einstein condensate. *Nature* **449**, 579 (2007).

[154] B. Juliá-Díaz, J. Martorell, and A. Polls. Bose-Einstein condensates on slightly asymmetric double-well potentials. *Phys. Rev. A* **81**, 063625 (2010).

[155] B. Juliá-Díaz, J. Martorell, M. Melé-Messeguer, and A. Polls. Beyond standard two-mode dynamics in bosonic Josephson junctions. *Phys. Rev. A* **82**, 063626 (2010).

[156] R. Gati and M. K. Oberthaler. A bosonic Josephson junction. *J. Phys. B-At. Mol. Opt* **40**, R61 (2007).

[157] R. Qi, X.-L. Yu, Z. B. Li, and W. M. Liu. Non-Abelian Josephson Effect between Two $F = 2$ Spinor Bose-Einstein Condensates in Double Optical Traps. *Phys. Rev. Lett.* **102**, 185301 (2009).

[158] M. Lewenstein, A. Sanpera, V. Ahufinger, B. Damski, A. Sen(De), and U. Sen. Ultracold atomic gases in optical lattices: mimicking condensed matter physics and beyond. *Adv. Phys.* **56**, 243 (2007).

[159] P. Krüger, X. Luo, M. W. Klein, K. Brugger, A. Haase, S. Wildermuth, S. Groth, I. Bar-Joseph, R. Folman, and J. Schmiedmayer. Trapping and Manipulating Neutral Atoms with Electrostatic Fields. *Phys. Rev. Lett.* **91**, 233201 (2003).

[160] T. Schumm, S. Hofferberth, L. M. Andersson, S. Wildermuth, S. Groth, I. Bar-Joseph, J. Schmiedmayer, and P. Kruger. Matter-wave interferometry in a double well on an atom chip. *Nat. Phys.* **1**, 57 (2005).

[161] G. J. Milburn, J. Corney, E. M. Wright, and D. F. Walls. Quantum dynamics of an atomic Bose-Einstein condensate in a double-well potential. *Phys. Rev. A* **55**, 4318 (1997).

[162] M. J. Edmonds, M. Valiente, and P. Öhberg. On the Josephson effect in a Bose-Einstein condensate subject to a density-dependent gauge potential. *J. Phys. B-At. Mol. Opt* **46**, 134013 (2013).

[163] S. Raghavan, A. Smerzi, S. Fantoni, and S. R. Shenoy. Coherent oscillations between two weakly coupled Bose-Einstein condensates: Josephson effects, π oscillations, and macroscopic quantum self-trapping. *Phys. Rev. A* **59**, 620 (1999).

[164] K. W. Mahmud, H. Perry, and W. P. Reinhardt. Quantum phase-space picture of Bose-Einstein condensates in a double well. *Phys. Rev. A* **71**, 023615 (2005).

[165] T. W. B. Kibble and F. H. Berkshire. *Classical Mechanics.* Imperial College Press, 2004.

[166] A. Zee. *Quantum Field Theory in a Nutshell.* Princeton University Press, 2003.

[167] G. E. P. Box and M. E. Muller. A Note on the Generation of Random Normal Deviates. *Ann. Math. Statist.* **29**, 610 (1958).